UNIVERSITÀ DEGLI STUDI DI PADOVA

SCHOOL OF SCIENCES

Department of Geosciences

MASTERS THESIS IN GEOPHYSICS FOR NATURAL RISKS AND RESOURCES

THE GEOTHERMAL SYSTEM OF VULCANO ISLAND: NEW INSIGHTS FROM INTEGRATED GEOPHYSICAL METHODS AND LABORATORY DATA

Supervisor: Prof. Antonio Galgaro
Co-supervisor: Dr Luca Peruzzo

Student: Denise Makoura Guilavogui

Academic Year 2023-2024

Acknowledgments

First of all, I am grateful to the Lord for his love and grace in bringing me to this point.

My heartfelt thanks go to Professor Antonio Galgaro for having accompanied me in the realization of this project. His guidance and support were unfailing.

I would also like to thank Ms. Maria Giulia di Giuseppe from the INGV of Naples for her invaluable help in obtaining the data and software.

I would also like to thank Dr. Luca Peruzzo for his assistance with laboratory measurements.

Additionally, I would like to express my gratitude to Prof. Jacopo Boaga and Dr. Mirko Pavoni for their help with data processing.

Many thanks to Mohaman Dan Azimi and Anna Mocerino for their availability and collaboration.

I am incredibly grateful to my parents, for their support and undeniable contribution to the person I have become.

Finally, thanks to all those who, in a way or another, have contributed to the realization of this project.

Abstract
The Aeolian Islands, located in the southern Tyrrhenian Sea on the western coast of Italy, like several other volcanic islands, confront challenges when it comes to electricity and water supply, dependant on the surrounding mainlands at high expenses.

Yet, several geoscientific surveys and drillings have confirmed the presence of geothermal systems, that could turn this situation around.

Previous research on the geothermal resource of Vulcano, one of the seven islands making up the Aeolian archipelago, did not produce conclusive results as to the feasibility of its power production plant project, although the reported temperatures from existing exploratory wells, were sensibly high (198° C ~236 m in Vu2bis well).

In order to detect the most advantageous site to realize a geothermal power plant, it is fundamental to know the permeability distribution across the island of Vulcano.
Recent studies evidenced heterogeneities between in-depth and lateral permeabilities, implying a discontinuous and complex hydrogeological network; making it difficult to localise the pathways through which hydrothermal fluids ascend to the surface.

The aim of this work is to target the most suitable potential drilling spots by detecting hydrothermal fluid upwelling paths, linked to higher temperatures at shallower depths, essential for implementing the future geothermal power plants cogenerating electricity and energy for seawater desalination on the island.

To achieve this objective, a multidisciplinary approach is adopted, including geophysical methods, notably Electrical Resistivity Tomography (ERT) coupled with Magnetotellurics (MT). Moreover, are measured and analysed the thermal conductivities, electrical resistivities, and elastic moduli of eleven (11) outcropping rock samples, representative of the encountered lithologies in the VP1 and IV1 wells, drilled in the 1980s.

Geophysical data allowed to localize hot fluid ascension paths, coinciding with the main areas of fumarolic activity between Baia di Levante and Faraglione, crossed by the
NNE-SSW tectonic lineament.
The laboratory data, on the one hand, provided us with information on rocks' physical properties useful for drilling operations, and on the other hand, complementary elements for the interpretation of geophysical data.
The integrated analysis of geological, geophysical and laboratory data delivered a better understanding of the structural framework of our investigated area, presenting lava flows as the potential drilling target with sufficient spatial coverage and modest physical properties.

These results do not only represent another step forward in our knowledge of the superficial part of Vulcano's geothermal system, but can also serve as a reference for the exploration of neighbouring islands, and even other volcanic islands elsewhere in the world.

However, they pave the way to questions concerning the influence of mineralogical composition and geological context of rock samples and their representativeness of in-situ conditions.

Therefore, the mineralogical analysis of samples and well logging in the study area are recommended for a better constrain of these findings.
Additionally, a tailored ecological operational scheme for geothermal energy extraction is proposed, in particular considering closed-loop borehole heat exchangers operating under Organic Rankine Cycle (ORC) systems.

Keywords: Geothermal energy exploration, ERT, MT, thermal conductivity, electrical resistivity, elastic moduli.

Content **Pages**

List of tables and figures **page**

Introduction

It is now a common knowledge that fossil fuel energy generation is a source of pollution through the release of greenhouse gases in the atmosphere.

Moreover, the depletion of these energetic resources makes it more urgent than ever to transition to renewable energy sources.

As one of the pioneers in geothermal energy production, Italy, through the PEARS 2030 (Piano Energetico Della Regione Siciliana), plans to extend its geothermal energy production to Sicily, including the Aeolian Islands. This energetic plan aligns with the goals of "Clean Energy for EU Islands"secretariat and its partners, which aim to promote the switch from fossil fuels to sustainable energy sources on over 1400 minor European islands by 2030, with a focus on 30 islands, including the Aeolian islands. [1].

The Aeolian islands are the scenery of hydrothermal manifestations, suggesting their volcanic origin and the presence of probable high enthalpy geothermal systems.

The scientific interest in these islands, particularly in geothermal resources, dates back to the 1920s. However, it is only in the 1950s that the company Vulcano s.pa (AGIP), realized the first exploratory wells on the island of Vulcano. [2]

One of the wells (VU2 bis) produced fluids composed of 90% of steam, with temperatures reaching 198°C at a depth of ~ 236m.

With the limited resources available at the time, these temperatures, although more than sufficient today, were considered to be of lesser interest for electricity production. As a result, the research was abandoned.

Nowadays, with technological advances in methods of converting energy into electricity, Vulcano's geothermal resource cannot be ignored; especially considering its difficult electricity supply.

In fact, the Aeolian Islands rely mostly on imported energy and potable water, which turns out to be costly and may be delayed by adverse weather conditions. [3] [4].

Exploiting these resources will not only generate clean electricity, but also the energy needed to desalinate seawater to meet the island's water needs, rendering the island self-sufficient, while at the same time preserving its environment, which in itself contributes to the growth of its economy.

The main problem holding back the implementation of a geothermal power plant that would co-generate electricity and drinking water, is the uncertainty surrounding the location of the upwelling paths of the hydrothermal fluids. The preliminary studies have shown that the shallow geothermal system of Vulcano has a complex permeability. [5][2]

In this work, we intend to detect those upwelling hydrothermal fluid paths, thus reduce the perimeter of possible drilling targets, aimed at intercepting these fluids in the northern part of the island of Vulcano.

Geothermal reservoirs generally occur at depths of several kilometres. Consequently, drilling remains the most reliable means of gathering first-hand information on these reservoirs.

Nevertheless, due to the high expenses of drilling, indirect approaches, notably geophysical methods, are generally utilized to gain some prior knowledge and increase the chances of success.[6]

We will therefore make use of the geophysical data collected in Vulcano by the INGV (Istituto Nationale di Geofisica e di Vulcanologia), which has been operating in the region for decades, mainly in the field of volcanic activity monitoring.

Although being a reference in non-invasive exploration of natural resources, the question of the quantitative and qualitative interpretation of geophysical data remains delicate.

To overcome this shortcoming, we will integrate Electrical Resistivity Tomography data with Magnetotelluric data of the same site in Vulcano Island.

Furthermore, the thermal conductivity, electrical resistivity and elastic moduli were determined on eleven (11) outcropping samples. Each sample represents a lithology present on the stratigraphic columns of IV1 and VP1 wells realised in the 1980s; allowing to some extent the correlation of their physical properties.

Restricting the prospective drilling zone involves more than figuring out the routes by which hydrothermal fluids reach the surface.

Wells are certainly designed to catch these heated liquids, but understanding the mechanical characteristics of the rocks that will be encountered is equally crucial to guaranteeing the drilling system's structural integrity and longevity.

The elastic moduli show the ability of rocks to resist deformations induced by drilling activities. In addition, their knowledge is important in modeling the reservoir's dynamic evolution in response to heat extraction, allowing to control production rates and prevent premature cooling of the reservoir.

Shedding light on the strength of the formations to be drilled is essential in the selection of the drill bit, the drilling mud density and the drilling technique (rotary and /or percussive), to avoid borehole instability.

knowing these properties could help in mitigating events such as hot plumes around the wellbores and heat depletion by:

i. Strategically placing the wellbores, near faults, aquifers or permeable and thermally conductive formations where the extracted heat can be replenished by heat conduction or convection from surrounding rocks and fluid flow;
ii. And drilling in sufficiently robust rocks to prevent blowouts and subsidence that can originate from stress redistribution, thermal expansion and thermal contraction, due to heating and cooling cycles in the reservoir.[52] [58]

In the first and second chapters, we will briefly introduce geothermal systems and overview the geoscientific studies carried out in the Aeolian Islands, with particular emphasis on the island of Vulcano. In the third chapter, the principles of the ERT and MT methods are exposed, along with some examples of geophysical methods application in geothermal exploration in volcanic contexts. Finally, the fourth chapter is dedicated to our methodology of data

acquisition, processing and inversion, while the fifth chapter delves into depicting the results and their significance.

Chapter 1: Geothermal Systems and the Aeolian Islands

This chapter discusses the origin of geothermal energy and the different types of geothermal systems, as well as the geological contexts in which they are found.

After this overview of the occurrence of these natural systems, the Aeolian islands, including Vulcano, the subject of our study, are presented in their geographical and geological aspects.

1.1 Origin of geothermal systems and their geological settings:

The geothermal energy comes from the residual heat generated during the formation of the earth and from the radioactive decay of isotopes in the crust. This heat has been stored in the earth thanks to its low thermal conductivity. [7]

The average thermal conductivity of the earth is λ =3.2 $Wm^{-1}K^{-1}$[8]

In the subsurface, heat is predominantly transferred by conduction according to Fourier's law of conduction:

$$Q = \lambda A \frac{d\theta}{dz}$$

Where Q is the heat flow (W), A the cross-sectional area (m^2), θ the temperature

(°C or°K), Z the depth(m);λ the thermal conductivity ($Wm^{-1}K^{-1}$)

For rocks with a good hydraulic content, heat is transported by convection, attracting more thermal energy towards the surface. Heat may also be transported by advection under gravity forces, as it is often the case in sedimentary basins. [9].

At a temperature of 600°C, heat begins to move by radiation in most polycrystalline materials, and becomes effective around 1200°C. However, for monocrystalline rocks and glassy materials as obsidian, radiation becomes important at lower temperatures (200-400°C) [9]

Given that the lithosphere is not homogeneous, some spots are closer to heat sources where hot materials rise towards the surface, making heat more accessible. They are:

a-Extensional plate margins: At these margins, magma ascends from the asthenosphere through the fissures caused by rifting. They are generally mid –ocean ridges (i.e., Iceland, Azores) or proto-rifts (i.e., Great rift valley of central and eastern Africa, the Rhine graben) The geothermal field around Reykjavik, Iceland is an example. [8]

b-Convergent plate margins: High pressure and temperature causes the partial melting of the sinking lithospheric slab, triggering the rise of molten rocks to form mountains chains and volcanic Islands on the overriding slab where intense volcanism occur, and geothermal fields develop. [8]

c-Below some tectonic Plates: these are areas where the upwelling of molten materials is seemingly not related to a nearby plate margin; they are referred to as mantle plumes. Their origin and mechanism are still object of research and scientific debate. The Hawaiian Island, the Yellowstone volcanoes and geothermal fields are examples of plume activity.

Out of these particular tectonic settings, there some modest geothermal anomalies in hot sedimentary basins where reservoir temperatures range between(50-150°C), covering large

areas (50 to >500km2). The Paris basin in France, the Beijing Basin in China are good examples. [10]

It is also believed that the dynamics of the earth through crustal uplift could bring hot rocks towards the surface. [8]

Another source of heat is granitic rock bodies with high internal radioactivity. It is also important to mention that deep faults near heat sources may allow groundwater to rise by advection to the surface. [8]

For the geothermal field to be economically viable, three (3) fundamental conditions have to be met: a heat source, a fractured or permeable rock, and a circulation fluid to allow

heat extraction in the production wells. [11]

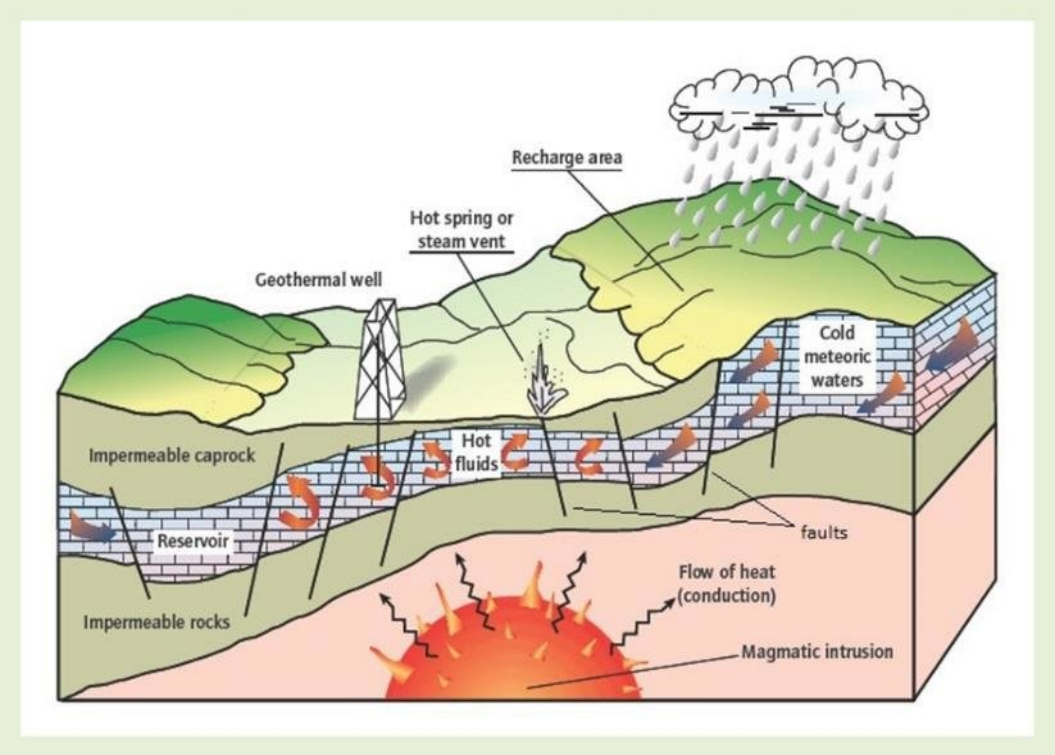

Fig1.1: Schematic representation of a typical Geothermal system, modified from (Bertani, 2010) [A review of geothermal mapping techniques using remotely sensed data, Aliyu Ja'afar Abubakar1, 2, Mazlan Hashim1, Amin Beiranvand Pour1 and Kabiru Shehu3]

As one might expect, these conditions are not always met, we then speak of conventional and unconventional geothermal systems.

Conventional geothermal systems:

Are called conventional, the ones that possess high underground temperatures, the presence of fluid to ensure the heat transfer and a fractured or permeable rock to facilitate heat extraction

processes. They are systems that are being in commercial use for several years and consequently, are well Known.

Among the conventional resources we distinguish:

Liquid-dominant hydrothermal resources:

The temperatures can reach 360°C and are kept constant all over the reservoirs through convective flows, resulting in a much higher thermal gradient than conduction would allow(>100°C/Km) [7] [11]. The wells may produce mixtures of hot water and steam or even dry steam because of phase changing caused by the change in pressure and temperature conditions while reaching the surface. [8]. The Brady, East Mesa in the United States, (Aydin, Buharkent) in Turkey, are of this Category.

Steam-dominant hydrothermal resources:

These types of resources are rare; the temperatures are close to 230°C and the wells may produce dry or superheated steam.

Their advantage lies in the fact that the dry steam that they produce is directly usable to run the turbines. For this reason, they are considered as the highest-grade geothermal resources. The Geysers, USA (850 MWe) and Lardarello, Italy (594 MWe) are some examples [10]

Unconventional Geothermal systems:

This term is used to designate those resources that are still being investigated and have not known big commercial success. they include:

Hot dry rocks: sometimes referred to as Enhanced geothermal systems or engineered geothermal system (EGS), they represent an important source of energy made of granitic rocks. Yet, the absence of heat transfer fluids and the poor permeability of these rocks, require the permeability of the system to be enhanced. A power generation facility is found at Soultz-sous-Forêts in France. [8] [11]

Supercritical deep volcanic systems: With an important power potential (50-70) MWe, drilling these systems is not without risks. In fact, at around 4 to 5 km depth, temperatures could reach 450 to 600°C and pressures are elevated. As it is in Iceland, with the deep drilling project (IDDP), the well IDDP-1 was drilled, reaching the magma at around 2km of depth. Acidic condensate and corrosive steam damaged the well casing. Despite those challenges, the supercritical deep volcanic systems are still to be explored. [11]

Geopressurised systems: They are sedimentary aquifers under high pressure with dissolved gases within their water. The main gases are methane (CH_4), nitrogen (N_2) , Carbone dioxide (CO_2), hydrogen sulphide (H_2 S). In some cases, the sedimentary sequence is overlying a granite which generates heat by radioactivity. (i.e. Cooper basin, Australia) [11]

It exits the possibility of a co-production of heat and methane gas from these reservoirs. However, the high pressure within the reservoir and operating well head pressure (WHP) with the associated environmental risks, make their commercial development hazardous. [11]

All These systems mentioned above, may be classified based on a number of criterions such as: the geological circumstances, enthalpy, the reservoir's temperature, the level of geological knowledge etc.

The classification may help in selecting the exploration strategy, the extraction technology in comparison to similar systems. At different stages of a project life, each of these classifications may be useful. These classifications are made possible as the knowledge of the field increases; a temperature classification is possible from early stages of exploration and are crucial in planning next exploration strategies. After the first drillings, a classification of the resource based on the fluid properties could be done. [11]

Geothermal Resources	Muffler and Cataldi 1978	Hochstein 1988	Benderitter and Cormy 1990
Low enthalpy	< 90°C	< 125°C	<100°C
Intermediate enthalpy	90-100°C	125-225°C	100-200°C
High enthalpy	>150°C	>225°C	>200°C

Table1.1: Temperature Classification of geothermal resources [11]

One should keep in mind that enthalpy and temperatures are closely related, but sometimes the enthalpy is not necessarily considered in this temperature classifications.

1.2 The Aeolian Islands

Located in the southern Tyrrhenian Sea on the western coast of Italy, the Aeolian islands represent the immerged portions of subaerial volcanic edifices, and several seamounts.

The archipelago comprises seven mainlands that could be divided in three sectors, according to their geographical positions and tectonic trends:

-Alicudi and Filicudi in the western sector,

-Vulcano, Lipari and Salina in the central sector.

-Panarea and Stromboli in the eastern sector. [12]

Vulcano is the closest island to the mainland of Milazzo, on the Northeastern cost of Sicily. [13]

The archipelago knows not only touristic interest but also scientific interest. The specific features of the still active volcanoes of Stromboli and Vulcano, have earned them the so called "strombolian" and "Vulcanian" eruption types in Vulcanology.

The last volcanic eruptions on the Islands occurred respectively in 1888/1890 and july 2024 in Vulcano and stromboli.

An important fumarolic activity from the seafloor in Panarea was observed in 2002, with consistent flux up to 2003-2004. [14]

Regarding Salina, Alicudi and Filicudi, there are considered extinct, while Lipari is considered dormant. [15]

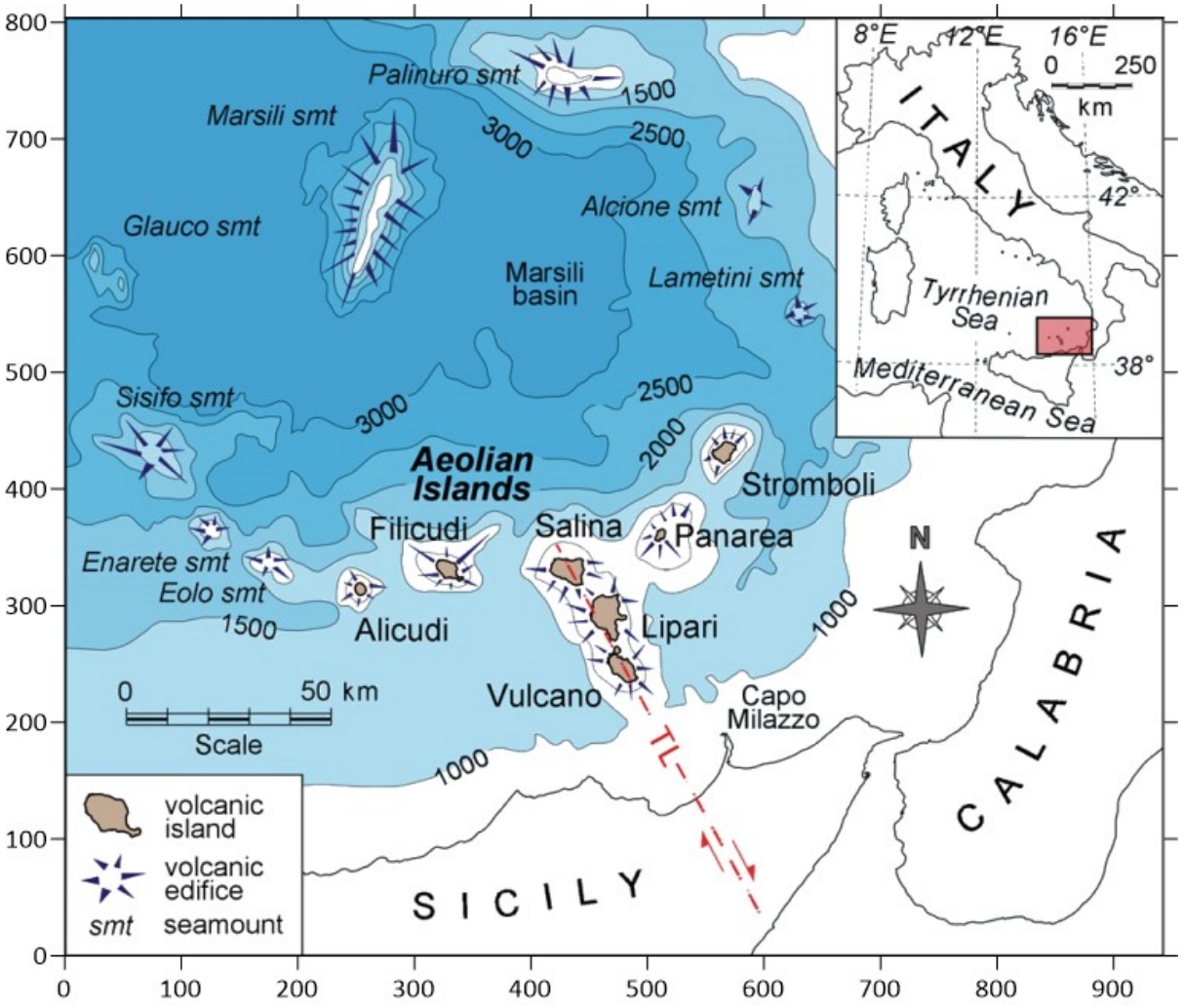

Fig 1.2: Sketch bathymetry of the southern Tyrrhenian Sea and the Aeolian Islands. The main Tindari–Letojanni (TL) fault system is shown. Depth contour lines in metres below sea level, modified from [15]

1.2.1 Geomorphology

The current landforms present on the Aeolian islands are the result of recurring volcanic activities, volcano-tectonic and sedimentary processes, that commenced during the quaternary around 1.3Ma in the submarine areas; and around 270-250 ka for the emerged portions. [16]

In fact, the emerged edifices display either constructional or destructional surfaces.

Constructional landforms:

They are lava flows and domes, having a relatively smooth surface, the Rocce rosse rhyolitic coulée of Lipari, rich in obsidian is an example.

Pyroclastic cones and fissures:

They usually have a subcircular or elongated shape and are formed after explosive eruptions. The Monte Guardia (Filicudi), San Vincenzo (stromboli) are scoria cones with lava flows.

Stratocones and composite volcanoes: they are characterized by stratified pyroclastic successions, sometimes with some lava flows. Due to a pronounced steepness and some unconsolidated layers, these stratocones are unstable and susceptible to collapse especially when local gravity is associated to shallow seismicity. [15] la Fossa cone (Vulcano)and Fossa Felci (Filicudi), Pizzo di Corvo (Salina) are some examples.

Eroded landforms:

They represent remains of eroded stratocones , and are mainly lava neck and dykes. As example, one can cite: the canna (Filicudi) and Strombolicchio(Stromboli)Lava necks.

Volcano-tectonic collapses led to the formation of calderas and lateral collapses.

The sea floor displays some morphogenic features such as canyons, valleys and hummocky surfaces. Hummocky surfaces are circular in shape with 100 to 150 m of height, are more likely derived from landslides of volcanic edifices. They are found in the eastward offshore from Salina, and north eastwards from Vulcano.

Good examples of valleys and canyons are the submarine extension of Sciara del Fuoco in Stromboli, the Canneto canyon eastward offshore from Lipari.

The submarine abrasion platforms with scarps ranging from 20° to 30°, are the evidence of quiescence periods or low volcanic activity on the Islands.

The geomorphic features reflect the tectonic trends in the region.

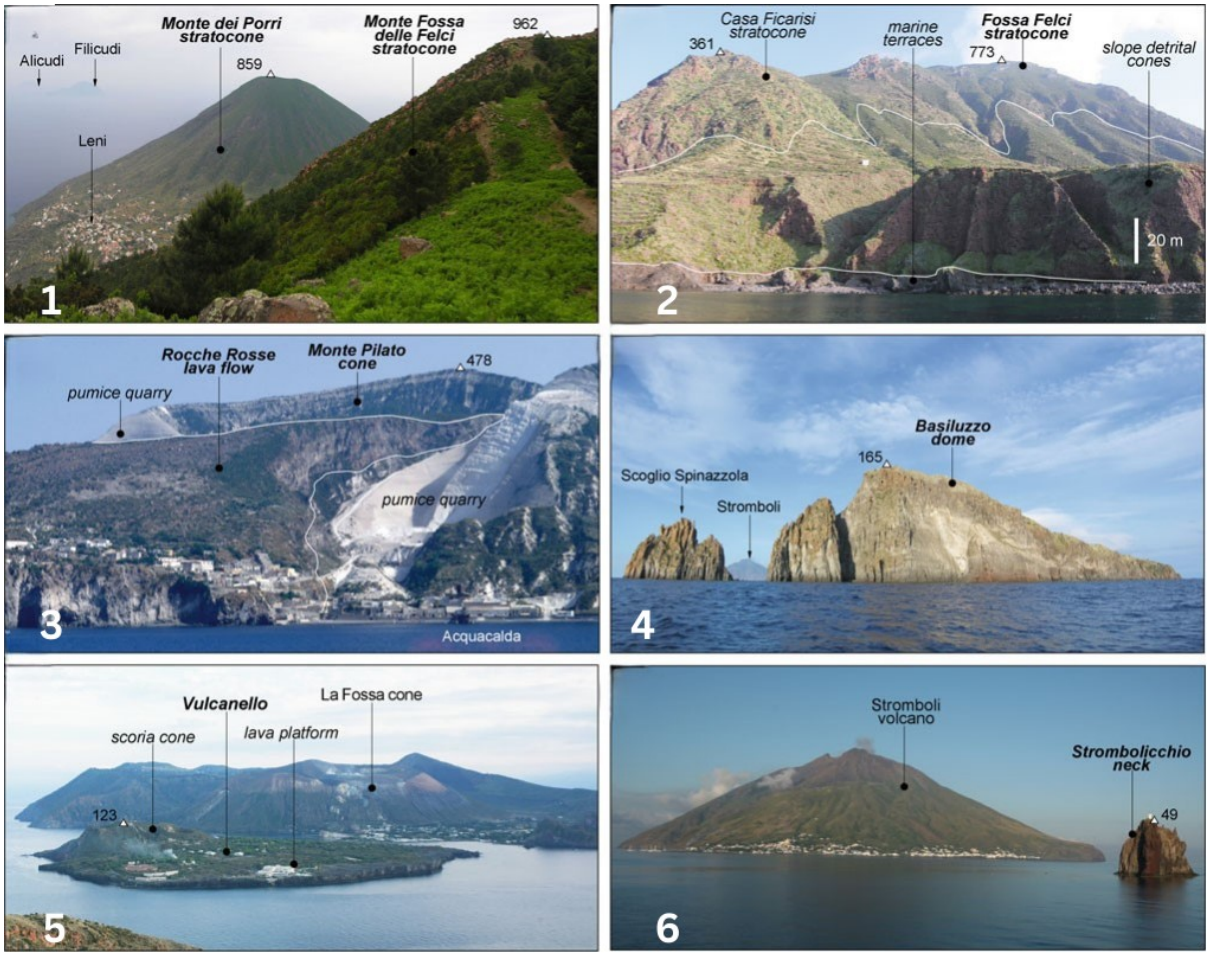

Fig1.3: Some volcanic landforms in the Aeolian Islands. Numbered points in the figures indicate metres a.s.l. 1) Monte dei Porri and Monte Fossa delle Felci stratocones in Salina. 2) Northern side of the Fossa Felci and Casa Ficarisi stratocones on Filicudi. 3) Northern view of the Rocce Rosse obsidian coulee originated from the rim of the Monte Pilato pumice cone (Lipari). 4) Basiluzzo endogenous dome,in the NE of Panarea. 5) Vulcanello lava platform and composite scoria cone in the northern sector of Vulcano. 6) Strombolicchio lava neck, NE of Stromboli (Stromboli in the background).[15]

1.2.2 Geological context and tectonics

Standing between 2000 and 3000m a.s.l, the aeolian archipelago is a volcanic arc located in the Mediterranean Basin. [15]

The subduction involving the African plate and the Eurasian plate, gave rise to the Calabrian arc followed by the roll-back of the Ionian slab (African margin), that subsequently, caused the rifting of the Tyrrhenian Sea, allowing a back-arc volcanism from which, the Aeolian Islands originate. [15] [13]

The volcanism in the region started in the quaternary,1.3Ma ago, first in the submarine areas, then on the mainlands between 270-250 Ka. [15] It is associated to the strain release by the slab detachment beneath the Calabrian arc . [17]

The regional tectonic events are dominated by the Tyrrhenian Sea opening from late Miocene to Pleistocene. [18]

As mentioned above, the archipelago is composed of three tectonic domains, that are dominated each by fault systems striking in some principal directions.

The eastern sector /domain including Stromboli and Panarea is a 45 Km volcanic belt with principal striking direction NE-SW, to NNE SSW.

The Central sector/domain (Vulcano, Lipari, and Salina) extends on a NW SE to NNW, SSE volcanic belt controlled by the tindari-letojanni fault system (TLF). [19] [20]

The western sector, Alicudi and Filicudi is mainly aligned on the WNW ESE directions, which corresponds to the main structural lineament of the sisifo-Alicudi faulting system, [20]

The TLF is the most important tectonic lineament, running from the Salina -Lipari-Vulcano bloc to the Malta escarpment. It separates the islands in two distinct tectonic domains: an extensional regime along and east to it, while a compressional regime prevails at the west of it. [19]

As a result, active or dormant volcanoes are located along and at the northeast (Stromboli, Panarea) of the TLF system, causing a deep seismicity (550Km). In the western sector, it is rather a compressional regime that prevails. [21]

The crustal thickness beneath the Aeolian arc varies from 15 to 25 km, increasing westwards [19]

This variation of crustal thickness supports the hypothesis according to which there are different types of basement rocks across the islands:

-the calabro-peloritano basement rock in the central-eastern sectors, and the

-accretionary prism rocks under the western islands. [19]

The oldest rocks (ca 1.3Ma) are from calc-alkaline to High K calc-alkaline composition, and are present all over the Aeolian archipelago, with predominance at Alicudi, Filicudi, Salina and Lipari. Shoshonites are found and in the central –eastern parts (Vulcano, Panarea, Stromboli).

Similarly, the seamounts (Marsili, Eolo, Enarete, Sisifo, Lametini, Alcione, Palinuro...) are also of calc-alkaline mafic to intermediate composition, except in Marsili where it has been identified an affinity to basaltic andesitic composition [19] [22]

Records from Stromboli and Vulcano show that melts transitioned from high k calc-alkaline to shoshonites and K alkaline magmas over time.

Calk-alkaline rocks have comparable composition to shoshonites that have higher amounts of phosphorus P and incompatible elements.

Some shoshonites are undersaturated in silica while calc-alkaline rocks are saturated to oversaturated in silica.

These differences in composition are attributed to heterogeneities in the mantle wedge, to its contamination by sediments and aqueous inflow from the subducting Ionian crust.

These hydrous melts triggered a metasomatism of low temperature (700-800°C).

The mafic enclaves in felsic magmas are evidence of magma mixing while ascending to the surface. The Pollara depression and Porri lava flow in Salina, la fossa cone at Vulcano; Monte Guardia and Monte Pilata in Lipari, illustrate this phenomenon. [23]

It also occurred that during their journey towards the surface, the melts were contaminated by crustal walls(assimilation), different amounts of crustal rocks being incorporated by basaltic or andesitic magmas, the latter being less affected by assimilation. An example is observed at Alicudi, where evolved andesites where less affected by assimilation and consequently shew more primitive isotopic compositions. [19]

The recuring chemical composition of rocks throughout the Aeolian archipelago are Basalts, andesites, dacites, rhyolites, shoshonites ,trachytes, latites. Most rocks are rich in calc alkaline (CA), High K elements. Thus, they are enriched in these elements and may present intermediate compositions like CA basalts to basaltic andesites, high-k andesites, high-k dacites to rhyolites, shoshonitic basalts, latites to trachytes, CA to high k basaltic andesites ,trachy-andesites,etc.

In some places the deposits are hydrothermally altered, as in the case of the formations of fossa di Faurdo in Lipari,Grotta del Tabacco in Panarea, L'Omo in stromboli.

The erupted products are in the form or lava flows or coulée, and the observed rocks are:

Tuffaceous breccias, lapilli tuffs, massive tuffs, scoriaceous tuff-breccias, brown tuffs, pumices, grey tuffs, obsidian fragments coarse ashes, etc. Conglomerates are also abundant, usually laying on marine eroded surfaces. The encountered textures are typical of volcanic rocks including: the aphyric to subaphiric texture, the porphyritic texture, the vesicular texture...Some xenoliths and metamorphic xenoliths are also abundant all over the Islands. [24][25][26][27][28][29][30]

The following chronostratigraphic units make up the vulcano volcanic edifice:

Vulcano primordial (120-100ka) and the Piano Caldera (100-23ka) in the south: this strato andesitic complex consists of alternating lava flows and pyroclasts;

Mastro Minico-Lentia(28-13ka): predominantly of rhyolitic compostion,it seems to be partly buried under la Fossa Caldera in the north west;

La fossa cone: was formed by successive phases including the Caldera collapse between 6 ka and 1890 AD; and

Vulcanello(183 BC- 1550 AD): this peninsula in the north of Vulcano is mainly composed of shoshonitic and latitic lava flows. [23] [5]

Chapter2: Geothermal explorations in Vulcano and in the Aeolian Islands

This chapter summarizes the geoscientific studies carried out in the Aeolian archipelago, with particular emphasis on the island of Vulcano.

2.1Geothermal explorations in Vulcano:

The scientific interest in the Aeolian Islands, particularly in geothermal energy dates to the 1920s[2]; It is only in the 1950s that the company Vulcano s.pa (AGIP), realized the first exploratory wells on the Island of Vulcano.

The «Vulcano» project of AGIP-ENEL, was intended for electricity and potable water production. Still in the 1950s, the steam-liquid reservoirs were considered of limited interest for energy production, compared to the dry steam resources, as the one of Larderello.

The SCIA (societa Carburanti Italiani Azionaria), that was relpaced by «Vulcano-SPA», obtained a research permit for "Vapore Naturale" (Natural steam). Vulcano SPA and AGIP-Attività mineraria SPA and affiliated realized the first boreholes VU1 and VU2 near Faraglione di Levante between 1950 and 1951.

The VU1 pit was 234m long, cased but not cemented and produced a wet steam between 195 and 234m at an estimated rate of 150t/h, with geyser eruptions that reached a height of 300m approximately. Between 4-5 m, a temperature of 101°C was also encountered as in Vu2bis. Mud absoprtions were also observed between 137 and 146m.

The second borehole VU2 bis was drilled after the abandonment of VU2, the drilling of which could not go beyond 14m of depth, because of a hard underlying formation.

The VU2 bis was 76m distant from VU1 and was cased and properly cemented. The planned depth to reach was 300-350m, but finally the total depth reached was of 236m.

Given the limitations in terms of technology at that time, the borehole was executed by core drilling and was continually under surveillance.

However, a stratigraphic profile as well as fluid analysis and 64 thermal profiles were carried out.

The VU2 bis allowed to detect three characteristic levels:

The first level: between 7 and 14 m deep, a temperature of 101°C, the pressure being atmospheric, some fumarolic manifestations and mud absorptions were observed.

The second level: this level was located between 90-100m of depth, with a temperature of 136°C and 10 atm of pressure. The extracted fluid had a temperature of 104°C under a pressure of 1.2atm and a flow rate of 0.35t/h. the fluid was almost a dry steam.

The third level: corresponds to depths laying between 185 and 236m, temperatures varying from 194 and198°C, and 19 atm of pressure. The produced fluid was composed of 90% of steam at a rate of 1t/h at 140°C. After 2 years of production, the temperature dropped at 161°C,

the pressure at 7 atm, the observed flow rate was 6.6t/h and the percentage of dry steam went from 90% to 33%.

The VU2 bis showed a limited permeability compared to the VU1, this was interpreted as mud absorption during drilling operations. This hypothesis of mud invasion seems to have been confirmed by the subsequent increase in production.

The encountered lithologies were:

Alternances of ashes, volcanic tuffs and breccias, lapillis boiling or compacted lava flow and volcanic sands. An alteration zone was observed, and the concerned formations were pyrite and anhydrite successively at 0-16m,36-96m, and 122-236m.

An argillitic zone made of chlorite and sericite was observed as well.

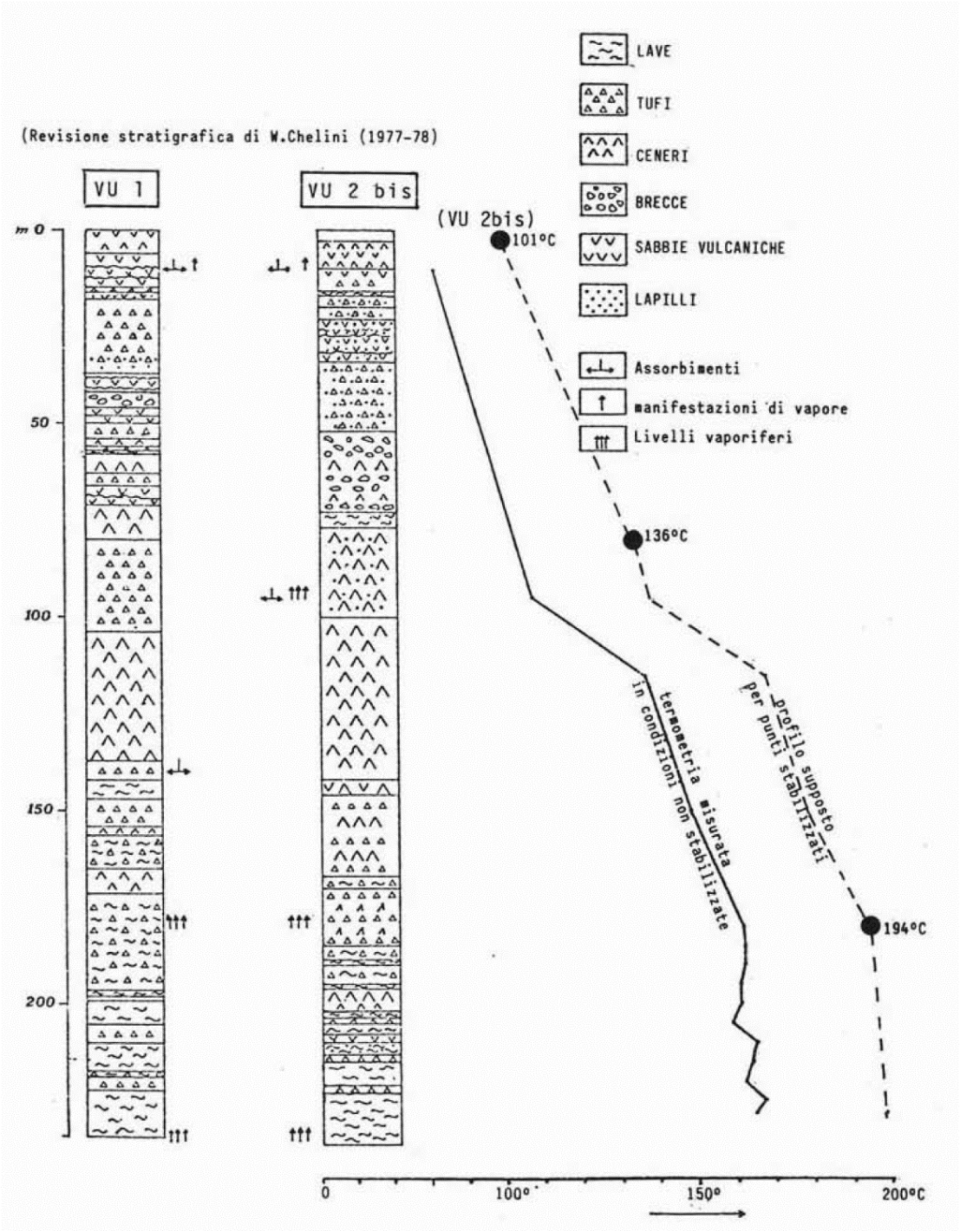

Fig 2.1 Stratigraphy and thermal profiles of the VU1 and VU2bis wells. The full line represents the thermal profile measured in unstable conditions, while the dotted line represents the supposed thermal profile in stabe conditions.[2]

The geothermal research was abandoned in favor of the Larderello large geothermal field. The VU2 bis well had been entrusted to another company that was planning to produce alum and boric acid.

This project was not realized and AGIP was then requested to close the borehole.

The geothermal exploratory wells of the 1950's laid the foundation upon which the future exploration works were elaborated.

Thanks to them, we came to know about the existence of a geothermal system of moderate commercial interest at a depth of about 200m, with possible electric production and associated substances such as boric acid.

Assumptions on a geothermal system at a greater depth (around, 600m) were emitted, and an exploration beyond 600m in the crystalline basement was proposed.

A superficial hydrothermal model heated up by marine and magmatic fluids and the absence of a specific sedimentary cover at some places of the Island were evidenced. [2] [5]

A new project of drilling a deeper well of 600m on the lineament "la fossa –forgia vecchia-faraglione-vulcanello "was considered. This NNE-SSW volcanic pathway, between faraglione and vulcanello , close to the sulfuric emissions was the preferred profile. [2]

[31] Subsequently, AGIP, ENEL and EMS pursued research in Vulcano and analyzed the data collected during the1979 fumarolic activity. An estimation of the volume, and depth of the identified geothermal reservoir by analyzing the fumarolic output was provided.

The composition of fumarolic gases was determined by a couple of methods such as:

The Aether condenser method to determine the gas /H_2O ratio.

The fumarolic gases absorption in a solution of NH_4OH containing $AgNO_3$ was used to determine the H_2S and SO_2 quantities.

The quantity of gas emanating per unit surface was calculated through this equation:

$$Q = \sum_{1}^{n} i\ A_i \phi_i$$

Where Q=the total mass emanated per unit of time

A_i =emanating surface of the i^{th} fumarole,ϕ_i=average output of the i^{th} fumarole per unit surface.

The emanating quantity of water per day was calculated as well.

$$Q = \frac{V\,A}{S\,T} \times 86400\ s$$

V=volume of the collected condensate

A= the measured surface of the emanating area of the fumarole

S=the intercepting area of the device in which the condensate was collected

T=the time in seconds in which the condensate is collected

86400 the number of seconds in a day.

The producible energy was also estimated through the two gas species forming 98% of the total output: water and carbon dioxide.

The total energy output was estimated to be about 11.5MW, from which 8.4MW is from the crater rim, and the remaining from fumaroles near the crater and the seaside.

The volume of the reservoir was also determined as approximately 0.1Km^3 . By considering the temperature of the boiling aquifer (340° and a pressure of 180± 20atm) as the same in the bottom of the reservoir, a depth of 1.6-2 km was obtained.

According to experience in similar geothermal fields, the energy output of 11.5 MW was then considered as only 1/5 to 1/10 of the total energy flux towards the surface. As a result, the available geothermal energy in Vulcano is much greater and would be near 100MW. [31]

[32 A The role of permeability and porosity in the evolution of Vulcano's hydrothermal system was done thanks to the physical modelling of a two-phase fluid circulation in a cylindrical domain. The system's initial and boundary conditions were defined on the base of the available preliminary studies.

Two more wells were drilled in Vulcano by the AGIP-ENEL-EMS: the IV1 in 1983-1984, SW to the active cone, and the VP1 in 1987, north to the cone.

The data from these wells, and the direct analysis of superficial manifestations allowed to have a better insight on the hydrothermal system of Vulcano.

The relatively low thermal gradient in the first 600m(50-60°C), suggests that the hydrothermal system benefits from a meteorological inflow of water. Also, the presence of both high temperature and low temperature minerals, supports the fact that the hydrothermal activity occurred at different temperatures throughout time, and had different intensities. The higher temperatures might have had a deep source.

The boreholes IV1 and VP1 were unproductive because of their low permeability. This may be due to the mineral deposition by hydrothermal alteration in the fractures and pores, causing their so-called self-sealing. The seismic activity also could have caused a rearrangement of fluid pathways and increase in pore pressure, leading to a continuous variation in the permeability of rocks.

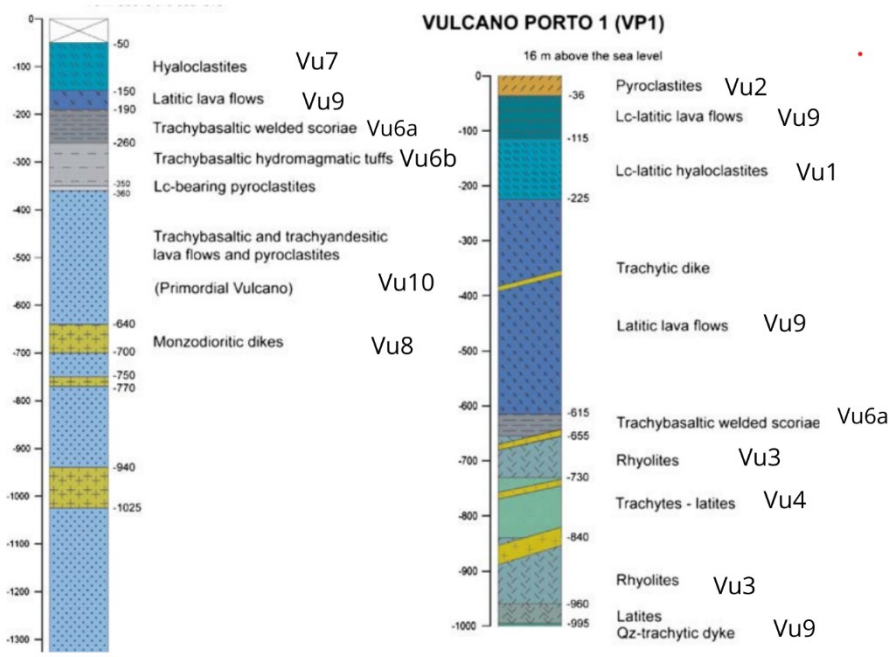

Fig2.2: Stratigraphic profiles from IV1(at the left) and VP1 wells and corresponding sample outcrops. (Modified from, Blanco-Montenegro, I., De Ritis, R. & Chiappini, M. Imaging and modelling the subsurface structure of volcanic calderas with high-resolution aeromagnetic data at Vulcano (Aeolian Islands, Italy). *Bulletin of Volcanology* **69**, 643–659 (2006)).

The shallow hydrothermal field of Baia di Levante beach (water-rich), and the deeper field at the crater (carbon dioxide –rich), though presenting different compositions, are believed to be connected at depth by a common source. In fact, the variations in temperature, salinity, and chemical composition are interpreted as seasonal and caused by different inputs from the hydrothermal system.

Permeability controls the external water input as well as fluid circulation. The deep fractures would enable to reach higher temperatures, while at shallow levels, there would be a cold fluid inflow, thus a mixing and temperature variation.

The numerical simulations performed to understand the permeability distribution and its impact on the observed thermal gradient were done with TOUGH2, a geothermal simulator, on the base of the heat and pure water transport in a cylindrical domain.

The cylinder had a depth of 1500m and a radius of 500m.The temperature and pressure were fixed at 300°C and $1.5.10^7$ Pa at the base of the cylinder and 30°C under atmospheric pressure at the top. The initial conditions were fixed as follows:

Temperature =30°C, pressure: hydrostatic rock density 2800 Kg/m^3 ; specific heat capacity:800 J/kg°K , thermal conductivity :2.5 W/m°K.

Three permeability distributions were considered: uniform, layered and channeled under the no flow condition.

In the first simulation, the domain is heated from below, creating two convective cells. heat and fluids are discharged from the top, and the increase in temperature favors a two-phase fluid zone.

The second simulation involved a more permeable (0-600m) zone overlaying a less permeable zone which goes from about 600 to 1500m. In this last interval, the pressure is higher, and the fluids are less mobile. The heat discharge gets important when approaching to the surface. When the system stabilizes, the thermal gradient becomes steeper at depth(0.25°C), consistent with those observed in VP1.The fluid and heat flows are up to two orders of magnitude lower than in the first case (uniform).

In the channeled case, the fluid, still heated from below, induced a development of a superficial two- phase zone. The fluid flow from the top is not very important.

Some more simulations were carried out, considering other boundary conditions such as free flow at the vertical boundary. This condition being more representative of the free access of seawater to the hydrothermal system near the beach.

The results provided relevant information on the role of permeability in the fluid circulation in a volcanic hydrothermal system.

Two permeable zones were observed:

A permeable zone from 0 to about 600m, where the cold fluid has access, and a less permeable zone around 600m to 1500m, irrespective of the permeability distribution.

This confirms the fact that permeable layers overly less permeable layers.

The variation in permeability around the 600m is interpreted as the result of fluid –related seismic events with high pressures causing the decrease in permeability.

An increase of pressure is localized around the zone where the cold water is injected and decreases towards the surface.

At steady state, in the uniform system, the pressure exceeds the hydrostatic pressure, whereas in the layered case, hydrostatic pressure is observed in the shallow permeable zone.

The high permeability zones are associated to the area around the la fossa cone

The temperature profiles obtained correlates with those collected in shallow wells for water supply, also with the data from geothermal wells.

In the layered permeability, the changes in temperatures occurring at depth either by fluid injection or a change in porosity, are not perceived at the top in the short run; it takes more time for these effects to be visible towards the surface. The setting of a permeable channel below a layered channel supports that rock fracturing at depth could trigger important changes in the temperature and fluid discharge at the top. This implies that changes at depth are not necessarily felt at the surface.

The highest permeability was seen in the uniform and channeled systems, where an important discharge of high enthalpy fluids was present at the top. This situation could be associated to the hydrothermal systems at the beach and at the crater. These places are characterized by high temperatures up to 100°C and high flow rates of fluids.

The free flow condition is best represented at the beach, where connections between the hydrothermal system and the seawater is more likely to exist.

Overall, the results of these simulations were promising, consistent with the knowledge from previous studies, even though the gases and dissolved salts effect on permeability and porosity, were not considered.[32]

[5] The project «Vapore Naturale» implemented by Vulcano-AGIP in the 1950's on the island of Vulcano, was resumed in the 1980s with the objective of finding geothermal fluids for energy and potable water production.

In order to get more relevant results, several methods were involved such as: geophysics, geochemistry,etc.

A geoelectric survey was carried out in 1981, to better characterize the subsurface formations found in the well VU2 bis.

One of the profiles near the VU2bis revealed the presence of a conductive at the depth of 160m approximately. Beyond that depth, a resistive body, interpreted as lava underlying superficial deposits filled with marine water, was found.

The profile in the vicinity of the crater only reached a 100 m of depth, with a resistive body in the first 10s of meters.

Discontinuities, interpreted as faults were found as well: mainly with N-S and E-W trends.

The magnetometry survey of the year 1982 confirmed the N-S discontinuity previously evidenced by the geoelectric survey. The survey also revealed a WNW-ESE discontinuity separating the north to the south. In the north, bodies with high magnetic susceptibility were found, most probably lava flows or pyroclastic deposits. In the southern part, no high magnetic signal was detected; the reason might be the absence of lava flows or an indication of an intense hydrothermal alteration.

Airborne magnetometry data collected by in 1977 and integrated to those of Sicily by AGIP in 1976 were interpreted, and made possible the realization of magnetic maps and their interpretation maps of the central part of the Aeolian archipelago.

The magnetic anomalies are presented as follows:

Positive anomalies are important in Salina and Vulcano, with an extension on the western edge of Lipari.

South of Vulcano, the anomalies tend to attenuate as the volcanic events become scarce.

Lipari appeared less magnetized probably because of the dacite and rhyolitic composition of rocks originating from a relatively recent volcanism, unlike Vulcano and Salina where the andesite-basaltic composition is predominant.

In 1985, another magnetic survey, aiming at removing topographic effects for the localization of deeper anomalous bodies was undertaken.

This survey allowed three important magnetic susceptible bodies to be found in Vulcano:

Two of them were located near the sea on the coast, opposite to M. lentia and the zone of il piano in the south. This anomaly is interpreted as an extension of the monzodioritic intrusion intercepted by the IV1.

The third body being of smaller intensity was located north-east of Vulcanello.

The NNW-SSE and E-W discontinuities going from Lipari to Vulcanello ,up to la Fossa crater coinciding with fractures and superficial manifestations, confirm the tectonic trends evidenced by the previous geophysical surveys.

In the south of Vulcano, the discontinuities are more likely to be at the limits of big susceptible bodies (lava accumulation or intrusions) following the costal trend and overlying deep north – south trending faults. The east-west discontinuity could be related other than susceptible bodies, to secondary faults.

In 1983, a marine gravimetric survey was carried out in the Aeolian archipelago with terrestrial stations in Vulcano, Lipari and Salina.

An anomaly map of Bouguer at the scale of 1:50 000 with a 2.6g/cm^3 for calculations using the Nettleton method was elaborated.

The large positive anomalies between Filicudi and Salina, up to 10 km beyond at the east are all associated to metamorphism at the base of volcanic edifices.

A remarkable fault in front of the metamorphic complex seems to be responsible for the intense gravimetric gradient that attenuates towards the southern coast of Sicily.

The gravimetric map displayed a depression zone, visible on magnetic data, interpretated as a graben with faults at both sides. This could explain the volcanism in the area.

The gravimetric anomalies are presented as follows:

-A high gradient in the south, most likely because of the primitive volcanic products of Trachy andesites and Trachy basalts in composition,

-A decreasing gradient as we move towards the north, the depleting volcanic products could be the reason.

-The NNW-SSE discontinuities recognized at Vulcanello, la fossa crater, and central part of Piano, while the E-W discontinuities were on the Lentia-Fossa-Piano lineament.

pyroclastic deposits and compact tuffs at la fossa with 1.4g/cm^3 and 2.0g/cm^3 respectively, were identified.

The la Caldeira lava flow had a density of 2.2 g/cm^3 , whereas the sub intrusive monzodioritic body intercepted by the vulcano 1 well, had a density of 2.75g/cm^3

The densities in the south ranged in the interval of 2.7 to 2.8g/cm^3 . Such densities are hypothesized as those of the metamorphic basement extended below the archipelago and emerging towards Sicily.

In august 1983, a marine reflection seismic survey was directed on the island of Vulcano. Five profiles of 59.5Km in total had been investigated, and a reflector at the south was identified.

In the light of the gravimetric data, the identified reflector could be a dense body (2.7-2.8g/cm^3) , more likely an intrusion or the metamorphic basement. The reflector was evaluated to be at a depth of 1500m near the coast of Vulcano.

The seismic sections were not of best quality because of multiple lateral reflections from the surroundings.

A remote sensing campaign that took place in 1980-1981, to research thermal anomalies occurring along the faults, allowed to distinguish hot and saline waters from marine water at the beach.

The hydrogeological network of Vulcano could be represented in characteristic units as follows:

-La fossa crater with radial fluxes,

-The Piano with fluxes-oriented NNW towards Rio Grande torrent.

-Vallonazzo Porto oriented from north to south with respect to la fossa crater. The northern fluxes flow towards the sea.

Three types of permeable terrains have been recognized: permeable terrains by fractures composed of lavas and pyroclastic deposits,

porous permeable rocks: vulcano-clastic deposits or unconsolidated deposits such as tuffs, ashes, pumice, sands.

Less permeable rocks: the porosity of these rocks have been reduced by clayey deposits.

At Porto di Levante(Vulcano port), the discovered phreatic aquifer is often contaminated by thermal fluids and has shallow temperatures in the range of 90 to 100°C.

At depth around 600m to 700m, the temperatures vary from 50 to 60°C as revealed by the wells IV1 and VP1.

This low thermal gradient at such depths, led to hypothesizes the presence of a fractured aquifer around 250 –600m.the aquifer is believed to be heated up by thermal fluids from deep sources or from crater activity.

A geochemical prospection for the recognition of gases at ground level (especially helium), was carried out to highlight permeable and fractured areas.

The first samples were collected in 1982 then in 1983 at Piano, between Vulcanello and Grotta dei palazzi. The most anomalous helium concentrations were found in the NW-SE (Grotta dei palazzi, Vallonazzo, Piano), NE-SW(Vulcanello,Gelso), and N-S (Cugni di Molinello) tectonic lineaments.

Other than Helium, the carbone dioxide (CO_2) was spread all over the island, with predominance in the south around the crater and at Vulcanello. The carbone dioxide was almost absent where there was less Helium. The hydrogen was found in the crater zone and surroundings, whereas methane (CH_4) remained almost undetectable.

It is important to note that all these are linked to superficial manifestations thus to the ascension pathways of fluids at the surface.

Later in 1984, hydrous samples were collected in the wells and along the cost of Vulcano, to discover the nature of fluids and their temperature distribution. The collected samples were alkaline in composition; the samples from the port showed higher ratios of carbonate acid/sulphate.

The elevated concentration in magnesium was an indication that the aquifer had not had a long time of residence, because hydrothermal waters tend to be rich in lithium and poor in magnesium.

Though boric acid and ammonium were found in some samples, it was not possible to link that fact to gaseous emissions since boric acid is normally abundant in marine water as well. It was therefore suggested that the boric acid was coming from the condensate flux of the la fossa crater.

The ammonium anomalies with modest temperatures are thought to be associated to a mixture of fluids with hypothermal waters, whereas the anomalies of higher temperatures are assumed to be directly mixed with vapors.

As a support to the geochemical data, an isotope survey took place in Vulcano and Lipari in March 1985.

The following elements were found:

D(deuterium), ^{18}O, in meteoritic waters, springs and fumarolic condensates,

^{13}C in both CO_2 and CH_4 in gaseous manifestations and ^{18}O in CO_2 .

From these findings, the origine of carbone was deducted and seems to be mainly from thermal decomposition of marine carbone.

By considering the isotopic equilibrium condition between CH_4 and CO_2, it was possible to estimate a temperature ranging from 395°C (Vulcano Porto) and 430°C(Lipari).

The waters and condensates could be considered of meteorologic origin with marine water contribution in some cases, this is supported by the presence of ^{34}S in sulphurs in the fumaroles at the crater, different from their typical content in marine water.

Estimations on the thermal energy flux in the zone of piano, and crater-capo secco lineament was done. The quantity of phreatic water entering from piano and exiting towards the Vulcano port along with the geothermic flux was estimated. The flux was 50-100 h.f.u,incompatible with the one observed in the well vulcano1(7.6 h.f.u).

At piano, the terrigenous waters, samples along the cost have similar temperatures from the ones at the sea. Some samples reached 45°C. the phreatic aquifer at piano is estimated to be at a depth of 200m, with a thermal flux of 2-3.5 h.f.u .

The thermal and geochemical (ammonium in particular) anomalies delineate a zone comprising the southern edge of Caldeira della Fossa and the central portion of Caldeira del piano.

Colder waters are predominant in the south, probably due to the abundance of permeable formations that would allow ascension of hot fluids from below. Yet, gaseous emissions in the uttermost south supports the facts that there should be a thermal source at depth.

With a total depth of 2050m, the IV1 borehole encountered a monzodioritic intrusion at 1360m of depth.

The VP1 was drilled down to a depth of 1000m. An argillitic hydrothermal alteration profile was recognizable with predominance of montmorillonite. A deep thermometamorphism and metasomatism in subvolcanic bodies gave birth to deposits of minerals in fissures such as biotite, amphiboles, clinopyroxenes, garnet, pyrite, epidote...

The first well, Vulcano 1, referred to as IV1 above, is located 2 km south from the port, and SSW to the crater. A depth of 1448m was reached in a first place, and then extended from 1448 to 2050m. Temperatures of 60°C(238m) to 305°C(1820m) and beyond 419°C at 2050m were obtained from the formation fluid sampling analysis.

The well revealed to be impermeable and for this reason, a deviation was executed to find more favorable lithologies.

The deviation had an angle of 30°C and went from 697 to 2180m. The final depth was 1700m, which corresponds to a vertical depth of 1578m.

Still, there were no fluid manifestations as expected. The temperatures varied from 245°C at 1420m corresponding to 1338m vertically, to 350°C at 1700m corresponding to a vertical depth of 1578m.

In both cases, vertical and deviated wells, the stratigraphy remained similar, with pyroclastic deposits in the first 350m roughly, and with Trachy basaltic to Trachy andesitic lava flows and intrusions in the remaining interval.

The second well Vulcano port 1 (VP1) drilled in 1987, at Vulcano port reached a depth of 1000m and presented high temperatures but no gaseous manifestations. From 600m and beyond, a shift in temperatures was observed, going from around 62.2°C at 600m to a maximum of 168°C at 970m.The well was permeable up to 600m and decreased drastically beyond that depth, which led to the drilling of a deviation well to research a possible reservoir towards Faraglione where the 1950s wells were drilled.

With an angle of 30° and a depth of 975m (902.8 m vertical), the deviation well was drilled in 1987; some samples were retrieved, and Schlumberger temperature logs were registered along the drilling operations.

At 550m (543m vertical), the max temperature was 58.5°C and 242°C around 900m

A fractured zone between 370 -400m and 500-600m with low temperatures, overlying an impermeable lava with a high geothermal gradient (5°C/10m) was identified.

The encountered lithologies in both vertical and deviated wells were similar and are mainly Trachy andesitic lavas and tuffs. From 450m down to the bottom of the well, a moderated hydrothermal profile and thermometamorphism were observed. the hydrothermal deposits along the fractures were: calcite, anhydrite, silice, pyrite, etc.

Number of hypotheses concerning the geothermal system of Vulcano were emitted thanks to the fumarolic composition at the crater and at Baia di Levante.

One of them supports that an aquifer of an unknown thickness and geometry would be laying between the magmatic chamber of la Fossa and the surface, absorbing the convective thermal flux from depth; and the fluid mixture would escape from the fractures or would remain in depth, causing changes in their chemical composition. The fumaroles at Baia di Levante have similar composition to those at the crater, with the difference of marine water input. Martini (1979)

Carapezza (1984-1985), thanks to the geochemical data, hypothesized on the presence of a spring of unknown extension was hypothesized in the subsurface of the whole island, with temperatures between 250°C and 300°C based on the analysis of gaseous emissions.

According to another hypothesis, there would be an important rock volume at high temperature in degassing phase, heating up the marine water that infiltrates through permeable zones. The super-heated water vaporizes and mixes with fluids from the hot rocks degassing. Then, the authors of this last proposition (Cioni and D'Amore) added the possibility that the vapors could originate from discontinued aquifers or from marine water.

In 1981, Valette and Picot proposed another« dry model», where a magmatic chamber at around 2000m to the north of Vulcano, would heat up meteorologic and sea waters transported through fractures. The hot waters vaporize with magmatic gases (HCL, HF, H_2),exit towards the surface by volcanic route.

From petrographic studies of the wells (Barberi,1984), it was noticed that the subsoil of la Fossa up to around 300m of depth, is affected by fluid circulation of high temperature(250°-300°C), most probably due to the presence of a nearby intrusion.

This was noted by the hydrothermal mineral veins of calcite, anhydrite, quartz, and pyrite mostly. Then the lava series under la Fossa are refreshed by marine water invasion, leading to an argillification up to the self-sealing above the intrusive body.

Of all the proposed models, the dry model by Cioni and D'Amore was considered as preferable because the presence of an aquifer would suggest a reservoir of high permeability, and the temperature variation would imply a rapid evolution of the hydrologic equilibrium of the aquifer, which is less probable. Still according to the authors, the presence of SO_2 is better explained by such a model.

In conclusion, the multidisciplinary geothermal exploration of the 1980's allowed to have new insights on the geothermal system of Vulcano and supported most of the previous knowledge.

Both wells Vulcano 1(IV1) and Vulcano port 1 (VP1) revealed the presence of a conductive body with high gradient under a superficial cover of 600m approximately. The Vulcano 1 showed temperatures above 420°C at 2050m, indicating an increasing gradient from the top of the monzodioritic intrusion, whereas the Vulcano Porto 1 had a temperature of 240°C around 1000m. These considerations indicate the presence of a conductive body extended up to 2000m in the crater, delivering heat at the surface.

The low thermal gradient encountered in both IV1 and VP1 in the first 600m suggests a fractured zone with cold water inflow.

The magnetic data exhibits a probable intrusive body under the Piano, similar to the one encountered in the well Vulcano 1.

The important thermal flux all over the island implies the presence of a spring in the subsoil with temperatures ranging between 250° and 300°C as already emitted by Carapezza (1984-1985).

The geochemical data conclude that the superficial thermal waters could not be considered as coming from an aquifer of long time of residence, because hydrothermal waters with long time of residence are rich in lithium and poor in magnesium, which is not the case for the retrieved samples in Vulcano.

The results tend to favor a geothermal dry model, supplied by marine heated water that circulates through fractures. The thorny issue remains to detect the location of those fractures and intercept the hot fluids.

[33]

A magnetotelluric survey was conducted in Vulcano to monitor the volcanic risks intensified by the physico-chemical changes in the superficial manifestations and increase in gas emission rate mainly at the crater rim and at Baia di Levante. In fact, the INGV, through its Napolitan section directed this campaign that took place in October 2021 with the aim of elaborating a 3D electrical resistivity model up to 2.5km below the la fossa caldera.

Such a model provides new insights on the previous knowledge on the shallow geothermal system of Vulcano by allowing to characterize the subsurface regarding the geometrical structure of the caldera, the tectonic discontinuities, the fluid circulation patterns and even the nature of fluids.

The main resistive horizons, referred to as Greek letters here, are the following:

-α, an anomaly of hundreds of Ωm, corresponds approximately to la Fossa crater, extended to a depth beyond 2.5 km; this anomaly acts as a conduit for the ascension of magmatic fluids to the surface.

-the β anomaly, confined in the first 500m, gets thick westwards up to reaching 1000m approximately. It represents a conductive layer, laying on top of the α anomaly. The transition interface between both anomalies knows a shift in permeability. This characteristic is consistent with the VP1 well's data that showed a more permeable interval in the first 600m.

Thus, the α anomaly might represent a fluid channel trough which hot fluids rise towards the surface, and β the shallow geothermal system of Vulcano.

-A series of shallow resistivity anomalies (γ) along the N-S direction, present the highest resistivities and coincides with La Forgia Vecchia and Baia di Levante degassing structures located N-NE in the crater sector.

-A more superficial anomaly α_2 coincides with the maximum degassing areas such as grotta Palizzi, Camping Sicilia, Baia di Levante which are along faults or fault intersections.

The α -α_2 anomalies with their similar resistivities lead to hypothesize on the presence of a clay cap of hydrothermally altered rocks at the top of the volcanic conduit (α). The relatively high resistivity of the supposed clay cap (α_2) is explained by the dry environment in which it is assumed to be. A perturbation in the hydrothermal system by a deep input of hot fluids,

altered the pressure, temperature and fluid circulation in the surrounding rocks, causing a fracturing in the upper cap rock leading to a diffuse soil degassing and fumarolic vents.

To sum up, the heat source of the Vulcano's geothermal system would be an important intrusive volume of rock laying at depth (~ 2000m) below the crater, with temperatures around 420°C as revealed by the IV1.

The first 600m represents its shallow geothermal system that is more permeable than the underlying formations.

The relatively low temperatures in this transition zone (50-60°C) suggests the presence of a fractured aquifer in the interval of 250 and 600m, supplied by marine and meteorological water.

The unproductivity of the wells beyond 600m supports the dry model presented by Cioni and D'amore [5].

The hydrothermal alteration zones encountered around 450m in VP1 plays in favor of the interpretation provided by the 3D magnetotelluric survey according to which, there is a fractured clay cap sealing the volcanic conduit.

The fumarolic vents would come from the clay cap that was fractured by changes in temperature and pressure.

The fluid circulation is controlled by some principal strike directions:

Radial fluxes of La fossa crater, making the surroundings of the cone more permeable, [5]

The fluxes at Piano are oriented in the NNW direction, while the Vallonazzo Porto fluxes are oriented in N-S direction with respect to la Fossa.

2.2 Geoscientific data on the rest of the Aeolian archipelago:

Just like Vulcano, the rest of the Aeolian archipelago has been the subject of geoscientific campaigns aimed at increasing the knowledge of both its geology and the natural resources it contains, particularly geothermal resources. An overview of the data that we were able to access is provided below.

Lipari

[34]

A geothermal exploration survey was performed at Fossa di Fuardo and Terme di San Calogero in Lipari, both scenery of hydrothermal activity.

An integrated geophysical approach was applied for a better characterization of the subsurface. The employed methods were: micogravity,2D geoelectric, seismic reflection and seismic refraction.

In Fossa di Fuardo, the survey zone is affected by hydrothermal alteration, characterized by a high CO_2 flux. Those fluxes suggest that thermal hot water infiltrates shallow aquifers and mixes with cold groundwater.

A first layer of about 10 to 20m thick was recognized, with a low seismic velocity $V_p <$ 600 m/s, a very low resistivity $\rho < 5\ \Omega m$,and a density of 1.6 g /cm^3 . This layer was considered as the lower limit of an hydrothermally altered outcrop.

A second layer, that corresponds to a clay deposit, characterized by an average seismic velocity of $V_p = 800$ m/s, a density of 1.8 g/cm^3 and a resistivity of $\rho < 5\ \Omega m$, was identified.

A third layer of 40m thick with similar characteristics to the second layer, except for the resistivity that was high, was recognized. This layer is considered to be the upper portion of the second layer, made of dry pyroclastic deposits, the bottom of which outcrops at the sea level, about 400m SW from the survey profiles.

A fourth layer, displaying characteristics of the basement, thus with higher seismic velocity and density (2.6 g/cm^3) , was also found. This layer is most likely of basalt –andesitic composition.

The limit between the two last layers, 3rd and 4th ,represents a sharp increase in seismic velocity and density, and is therefore interpreted as the top of the old basalt -andesitic lava with an approximate thickness of 60m. These lava outcrop near the seashore at ~ 400m from the survey area.

It is important to mention that the seismic data highlighted some fractures, not all visible at the surface and confirmed by the geoelectrical data. One of the fractures is near to the hot spring and the ENE trending fault.

At Terme di San Calogero, microgravity and geoelectric surveys were carried out. Near the profile, there is a hot spring of sodium-bicarbonate-sulphate composition and a neutral PH. The spring's temperature went on decreasing from 90°C to 60°C in the period 1906-1972, to reach 47°C at the time of these surveys.

The gravity data shows an ENE fault in the southeastern part of the investigated profile, a 2.5g/cm^3 body interpreted as Mt Mazza Caruso lava flow and a less dense body overlying this lava flow most probably lacustrine deposits.

An outcropping lava flow formation of 10-20m thick, of density 2.5g/cm^3 was detected.

The geoelectric records exhibit a low resistive (0.7-10 Ωm)body of 60 to 80m thick and 150m wide, probably in which there is hydrothermal circulation given its position centered on the fault plane. Deeper in this zone, there is high resistive rocks (300-500 Ωm) also close to the fault plane.

Even though there is no evidence of geothermal fluid upraising, this possibility cannot be discarded because the horizontal geoelectrical resolution is only 20m.

Such fluids may rise within or beyond that resolution field and spread through the shallow formations along the fault plane and be mixed with cold infiltration waters, which would explain the important CO_2 fluxes in the site.

For the localization of the exact rising point of deep fluids, it is convenient to plan further subsurface investigations along the ENE trending fault.

The most important outcomes of the geophysical surveys in Lipari may be summarized as follows:

The fractured pyroclastic lava banks detected at Fossa di Fuardo may represent a low-enthalpy geothermal reservoir,

The two overlying layers of altered and lacustrine deposits of low permeability act as a sort of cap rock, preventing important heat fluxes towards the surface, except through the few unsealed fractures.

In Terme di San Calogero, the subsurface fluid circulation is mainly along the ENE trending fault in the southeastern side near the hot spring, and the geothermal fluid circulation pattern is still to be investigated.

Salina

A low altitude aeromagnetic data collected in 2003 and 2005, reveals the inner structure of Salina's volcanoes and marine regions nearby.

Measurements of magnetic susceptibilities and natural remanent magnetization were carried out.

Due to a limited paleomagnetic data on Salina, those of the neighboring Lipari Island were considered for data obtained on rocks of similar age and chemical composition.

The results indicate two main periods of volcanism that developed along specific tectonic trends:

The basaltic-andesitic volcanism of age 168-100 ka, developed along the N-S and NE-SW trends;

Andesitic and rhyolitic volcanism (100-13 ka) are related to the NW-SE faulting system.

Some regional negative anomalies were interpreted as related to sedimentary basins, whereas shorter-wavelength anomalies are linked to volcanic and tectonic structures.

The NW-SE linear positive anomalies appear to highlight towards the southeast dyke-like structures in the la Fossa delle Felci and Pollara marine region.

On the NE-SW trends, is aligned the Rivi-Capo volcanic complex originating from early volcanic activities(168Ka).

La Fossa delle Felci,Porri (43-108Ka), and Pollara vents (13-30 ka) developed mainly in the TLF trend and some other NW-SE striking structures. [35]

Panarea

Located in the northeastern part of the Aeolian archipelago, Panarea island has recently known a submarine gas eruption that led its volcanism to be reconsidered, until then considered extinct. [36]

The submarine eruption started in November 3,2002 and affected the islets of Lisca Bianca, Bottaro, Lisca Nera, Dattilo and Panarelli, which are 2.5km east of Panarea mainland.

The eruption went on progressively decreasing to a degassing state by July 2003, and lasted up to 2004. The degassing was mainly in the NE and NW, NNE-SSW to NW-SE tectonic lineaments. The Panarea volcano had been undergoing an active subsidence estimated at a rate of 1.87mm/year for the last 2000 years, with continuous exhalative fumarolic activity, both on land and offshore. In the islet area, a WNW shortening trend in the order of

10^{-6} $year^{-1}$,estimated between 2002-2007, causing the closing of NNE fractures, was observed. [14] [36].

A sudden displacement occurred in June 2005 in Lisca Bianca, probably related to aseismic spreading of crack closure or migration of pressurized fluids. [36]

The 2002-2004 degassing activity triggered a series of effusive activity in Stromboli (10 NM to NNE), an offshore earthquake between Palermo and Ustica island, and eruption at Mont Etna. [36] A multidisciplinary investigation was then conducted in the active area of Panarea, for volcanic surveillance including visual inspections and sampling by divers and ROV (remotely operated vehicles), GPS networks, oceanographical measurements, magnetic and gravimetric surveys, multichannel reflection seismic, etc. [14]

The composition of the gases and their isotopic signatures suggested their origin from hydrothermal/geothermal reservoir, fed by magmatic fluids and seawater. [36]

The gaseous emissions were found to be a carbone dioxide-dominated emulsion with suspended sediments, colloidal sulphur and dissolved acids (SO_2 ,HCL,HF).[14]

Still in the frame of volcanic risk hazard surveillance, the GPS velocity field of episodic site observations from 1995 to 2007 is analyzed. [36]

The degassing intensity and distribution are strongly influenced by geophysical and geochemical changes within the hydrothermal /geothermal system. The variations may be due to changes in the regional field stress. [36]

The maximum strain contraction axes are located on the N-S trend away from Sicily and in the Western portion of the Aeolian islands, and a minor NW-SE extension in the eastern part. A prevailing NNE to NE trends affects Panarea and Stromboli that are on the active eastern portion of the Aeolian arc. [36]

Gravimetric and magnetic measurements display a positive anomaly between the islet of basiluzzo and Panarea island. This anomaly seems to be related to the main tectonic trends. [36] [14] A decreased magnetization was observed in exhalative areas because of hydrothermal alteration affecting the seafloor. [36]

The seismic survey provided useful information on the plio-quarternary sediment thickness. Strong PH anomalies were reported, reflecting the seawater acidity. [36]

The proposed hydrothermal geothermal reservoir model is supplied by a mixture of volcanic fluids and marine water. In the model, the NW portion of Panarea is represented by coherent rocks, whereas the SE portion of Panarea and islets are represented by highly fractured and permeable rocks. [36]

Stromboli

Few months prior to the 2002 volcanic activity, causing sector collapses in the submarine and aerial parts of Stromboli, a set of geophysical measurements including geoelectric, temperature and CO_2 ground concentration surveys were carried out.

The surveys were intended to determine the structural apparatus and determine the crater limits and pathways for hydrothermal fluids up flow.

The survey profiles were placed in a way to cross the Fossa(crater) area, comprising the Pizzo crater. The Fossa is surrounded by the topographic rim called Pizzo crater, which contains the large Fossa crater(280m). The large Fossa crater in its turn hots the small Fossa crater(150m).

The small Fossa crater is characterized by low temperature values and no anomalous carbone dioxide concentrations. This implies that the small crater is sealed with respect to the underlying hydrothermal system by an impermeable layer, impeding the raising of hot hydrothermal fluids and CO_2 at the surface. Fluids pathways were identified both around large and small craters and are thus subject to temperature, carbone dioxide and self-potential anomalies extending on tens of meters.

Low electrical resistivities were found on the two profiles, associated with permeable zones and fluids escaping routes. In this way, a large contrast was noticed between surrounding rocks and the supposed hydrothermal reservoir which contains saline water.

Temperature and CO_2 measurements showed an important geothermal gradient in the first decimeters in the subsurface :25° to 90°C around 30m of depth.

The combination of all these data demonstrates the presence of an aquifer inside the small Fossa crater, laying at 20m of depth approximately, and, at about 100m away from the magmatic conduits. [37]

A high-resolution 3D velocity model of Stromboli's Volcanic edifice down to 4 km b.s.l was made from seismic data collected in 2006-2007.

The V_p and V_p /Vs values allowed to locate the position of magma storage, the geometry of the shallow volcanic plumbing system. Subvertical pipe-like bodies were identified, one for instance was found beneath Strombolicchio , and represents the plumbing system of this old eruptive center. [38]

A coastal groundwater body, present in the northeastern side of Stromboli is studied to evaluate its potential in potable water supply. In fact, potable water is supplied from mainland by tankers or desalinization plants, both options being costly and not eco-friendly.

The aquifer presents quite constant temperatures with a slightly acidic P^H and dissolved salts, its chemical isotopic composition reflects its interaction with magmatic gases which, with the salinity render the aquifer's water unsuitable for consumption.

A continuous groundwater temperature monitoring for volcanic surveillance revealed the Physico-chemical temperatures of samples collected from eleven thermal wells.

The temperatures spanned between 22.8 and 47°C, and P^H ranging between 6.3 and 7.2. these observations are thought to be the result of volcanic gases being mixed with meteoric infiltration waters.

The rainfall infiltration causes a decrease in the groundwater temperature, suggesting that vertical discontinuities (fractures) of the San Vincenzo eruptive center play and important role in groundwater circulation.

The measurements of monthly effective precipitations permitted to estimate the groundwater availability and demonstrated that the actual infiltrating volume of rainfall during wet months, is one order of magnitude higher than the consumption during dry touristic months. [4]

Chapter3: Geophysical methods

This chapter focuses on the geophysical methods employed in this study. We begin with a concise overview of their fundamental physical principles, followed by a detailed discussion of data acquisition, processing, and inversion techniques.

3.1 The magnetotelluric method:

The magnetotelluric (MT) surveys are intended to represent the spatial distribution of electrical resistivity or conductivity with respect to the induced Electromagnetic waves generated naturally. The signals are generated by thunderstorm activity (for frequencies higher than 1Hz) and ionospheric currents for (frequencies lower than 1 Hz)..[39] [33]

These fluctuations of the earth's electromagnetic field create the so-called telluric currents. The magnetic properties of near surface rocks create variations in the strength and direction of the earth's magnetic field.

Tikhnov and Cagniard discovered in 1950 and 1953 respectively that if the fluctuations of the electric and magnetic fields in orthogonal directions at the earth's surface are measured simultaneously, then impendences, describing the electromagnetic field's penetration in the earth can be derived.

The penetration depth of EM fields depends on the sounding period and on the subsurface electrical conductivity. The investigation depths achieved by this method are in the range of several tens of Kilometers. For this reason, they have become a standard method in geothermal exploration, usually applied for regional reconnaissance. Hydrothermal alteration in geothermal fields causes an interesting contrast between reservoir and surrounding rocks, these contrasts are evidenced in MT profiles. [39] [40]

The skin depth is a representation of the penetration scale. It is given by:$P(T) = (T/\pi\,\mu\,\overline{\sigma})^{\frac{1}{2}}$ where: $P(T)$ is the electromagnetic skin depth in meters given at period T, μ is the magnetic permeability, $\overline{\sigma}$ is the average conductivity of the medium.

This relation can be approximated as given below:

$P(T) \approx 500\sqrt{T}\rho_a$, ρ_a being the apparent resistivity or the average resistivity of an equivalent uniform half-space.

At the skin depth, the amplitude of the incident electromagnetic field attenuates by a factor $1/e$.

The relationship among the horizontal and orthogonal components of the electric field E and magnetic field B is represented by a complex impedance tensor.

$$\begin{pmatrix} Ex \\ Ey \end{pmatrix} = \begin{pmatrix} Zxx & Zxy \\ Zyx & Zyy \end{pmatrix} \begin{pmatrix} Bx/\mu_0 \\ By/\mu_0 \end{pmatrix}$$

Z is a complex number composed of a magnitude and a phase which is imaginary. The apparent resistivity ρ_a and phase ϕ are then derived

$$\rho_a, ij(\omega) = \frac{1}{\mu_0 \omega} \left| Z_{ij}(\omega) \right|^2 \qquad \phi_{ij} = \tan^{-1}\left(\frac{Im\{Z_{ij}\}}{Re\{Z_{ij}\}}\right)$$

μ_0 is the magnetic permeability and ω the frequency.

As they penetrate through the earth, the electromagnetic waves are not only attenuated, but a phase lag also occur, due to the time required for them to reach a certain depth.

The impedance tensor also contains information about dimensionality.

In the 1 D case, the electrical conductivity varies only with depth, the diagonal elements Z_{xx} and Z_{yy} ,coupling the parallel electric(E) and magnetic (B) field components, are equal to zero. The off-diagonal component of E and B are equal and opposite in sign, $Z_{xy} = -Z_{yx}$.

In 2D, the electrical conductivity varies not only with depth, but also in a perpendicular direction. $Z_{xx} = -Z_{yy}$ and $Z_{xy} \neq Z_{yx}$. [41]

The 2D case is the most assumed situation in the MT data processing. The electrical resistivity changes with depth and with respect to the geological/electrical strike direction, two polarization modes are then distinguished: the transverse electric mode (TE), when the electrical field is parallel to the strike direction and the magnetic field is perpendicular,

and the transverse magnetic mode, when the magnetic field is parallel to the strike direction and the electric field is perpendicular. [39]

Depending on the measurement frequency, the Magnetotelluric (MT) method is named differently:

Magnetotelluric within the frequency range of 10^{-6} and 1Hz,

Audiomagnetotellurics (AMT) for frequencies going from 1 to 105 Hz. A controlled electromagnetic source (CSMAT) is often used for higher frequencies for a better signal-to-noise ratio. In the frequency range of 15 to 250 KHz,the method is referred to as audiomagnetotellurics (RMT). [39]

A typical MT station for data acquisition comprise 2 pairs of electrodes of lengths between 50 and 100m, set up in orthogonal directions, and 3 magnetometers (fluxgates or induction coils) also settled in orthogonal directions.

The two dipoles measure the electric field variations in the horizontal directions from the potential difference between them, and the magnetic field fluctuations are measured in the three spatial directions through the induced currents in the magnetometers.

The stations may be placed at hundred meters or tens of kilometers from each other, depending on the targeted resolution and depth. The surveys may be performed on the ground or through an aircraft.

Signals get attenuated (vary in strength) with time. therefore, the recording period has to be long enough for a quality data. For instance, a period of 100s would sound depth around 1 to 2 km and the acquisition may last a day, while a 10000s period would reach 100km for several weeks of acquisition.

From the recorded time series of electric and magnetic fields, the apparent resistivity and phase versus frequency are retrieved. [39]

A crucial step to data processing is noise removal, which are induced by cultural, pipelines, railway lines, thunderstorm activity, wind, etc. [39] This suggests that the source of magnetic anomalies is not solely restricted to the subsurface magnetic susceptibility.

In fact, the geomagnetic field of the earth has three components, all contributing to the recorded signals. The main field from the inside (earth's core), a smaller field compared to the main one, with external origine, and local magnetic anomalies in the near subsurface of the crust that are targeted in geomagnetic surveys. [42]

Generally, the near-subsurface rocks get their magnetic properties from their content of magnetite $Fe_3\ O_4$ and hematite $Fe_2\ O_3$ mainly.

Basic and ultrabasic rocks have the highest magnetic susceptibilities, while acidic igneous and metamorphic rocks have intermediate to low susceptibilities, and sedimentary rocks have low susceptibilities in general. [43]

The rocks with magnetic minerals will have both induced and remanent magnetization.

The induced magnetization comes from the earth's current magnetic field, and the remanent magnetization from the rock magnetic history. Below 40 km of depth, the temperatures are above 550°C, rocks lose their magnetization: it is the curie temperature. [44] [42]

As seen above, the magnetic field has contributions other than that of the subsurface magnetic sources; some corrections need to be applied to the data. Such corrections may include diurnal variation correction, terrain correction, etc. Even though complex, especially for highly susceptible terrains, the latter may be needed for a detailed survey.

The effects of latitude have also to be considered; the earth's field varies from 25000nT(nanotesla) at the magnetic equator to 69000nT at the poles. Survey data can be obtained at any location, by subtracting the theoretical field value from the international geomagnetic reference filed from the measured value. [43]

The noise problem in the collected data could be addressed by referring to a remote reference site outside of the influence of the local signal. This technique resulted in in improving significantly the data quality where cultural noise is high. Such a site is located on the island of Jeju, for Japan and South Korea, another one is in the Aegean Sea off west coast of Italy, four sites in Tuscany or larderello for example. [39]

Noise effect can manifest in the form of telluric or static shift due to the complexity and heterogeneity of the earth. This phenomenon may be caused by: 1) voltage distortion, when the electric field depends on the resistivity of the measuring dipoles domain. For example, if the resistivity is lower near the dipoles, the electric filed tends to reduce, and if the resistivity is higher near the dipoles, the electric field would be stronger. 2)current channelling or current distortion occurs when, the flowing current encounters anomalies. if the anomaly is more conductive than the surroundings, the current is deflected inside the anomaly. In the opposite case, if the anomaly is less conductive than the surroundings, the current is then deflected outside of it. Static shift is a vertical displacement of apparent resistivity curves while the phase angle remains unchanged. It usually occurs in terrains with heterogeneous resistivities near the electric dipoles, as it is often the case in volcanic regions, and less often in sedimentary layers. [39] [41]

The time domain electromagnetic survey (TDEM) is often realized on the same MT station as correction to the static shift.

The goal of data processing is to describe the relationship that exists in the frequency domain between electric and magnetic field components represented in the impedance tensor. The data is then submitted to an inversion process which will provide the most likely apparent resistivity distribution of the subsurface either in 1D,2D or 3D.

Despite the significant improvements of data processing, inversion algorithms, numerical modelling, in MT application, data interpretation remains difficult. Consequently, geological data must confirm data interpretation.

3.2 Electrical methods:

[43] [40]

If we inject in a cylinder, a direct current *I* between two current electrodes A and B, the difference of potential that is build up can be measured by two other electrodes M and N called potential electrodes as described by Ohm's law:

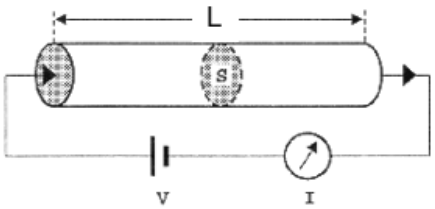

Fig 3.1: current through a cylindrical domain [47]

$\Delta V = R.\ I$,

$\overline{J} = \sigma \overline{E}$ (vectorial form of Ohm's law)

J is the current density, σ the conductivity, E the electric field.

$\sigma = \frac{1}{\rho}$

The conductivity is the inverse of the resistivity measured in [s/m],

ΔV is the potential difference, R is the resistance of the cylinder to the current flow, and I the current intensity.

The resistance is expressed by:

$$R = \frac{\rho\, L}{A}$$

ρ Is the resistivity [Ωm] , L the length of the medium [m], A is the cross-sectional area of the cylinder [m^2]

The current density J is the current divided by the area over which the current is distributed.

By considering that J is the current divided by the area, and considering a hemisphere of area $2\pi r^2$, we can write:

$\frac{\delta V}{\delta r} = -\rho J$, $\frac{\delta V}{\delta r}$ being the electric field,

$\frac{\delta V}{\delta r} = -\rho \frac{I}{2\pi^2 r}$ represents the difference of potential across an hemisphere.

The voltage (potential) at a point r from a current point source would be:

$$V_r = \int \delta V = \frac{\rho\, I}{2\pi r}$$

For a quadrupole (two current electrodes A-B, and two potential electrodes M-N), implanted at the surface of the semi-sphere, the difference of potential is given by:

$$\Delta V = \frac{\rho\, I}{2\pi}\left[\left(\frac{1}{AM} - \frac{1}{MB}\right) - \left(\frac{1}{AN} - \frac{1}{NB}\right)\right]$$

$$K = 2\pi\left[\left(\frac{1}{AM} - \frac{1}{MB}\right) - \left(\frac{1}{AN} - \frac{1}{NB}\right)\right]^{-1} \quad [43]$$

K is the geometric factor, accounting for the anisotropy of the medium.

For a homogeneous semi-sphere, of resistivity ρ , a single electrode planted at its surface will propagate radially into current lines from the injection point, equipotential lines cutting them at right angles.

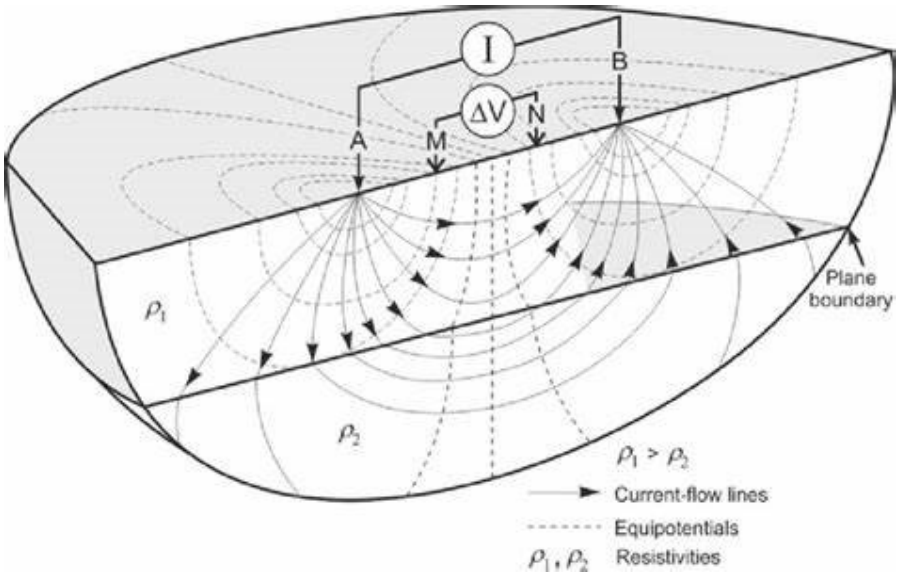

Fig3.2: Current lines propagating in a semi-sphere [47]

Because the earth is not homogeneous, the measured resistivity values are called apparent resistivity.

$$\rho_a = \frac{V}{I} K$$

3.2.1 Electrical Resistivity tomography (ERT):

Electrical resistivity tomography is a geophysical method used in geothermal exploration to image the subsurface electrical resistivity distribution. Most dry rocky materials are poor conductors; therefore, their resistivity depend on their fluid content and temperature.

Temperature could increase the bulk conduction of a rock up to one order of magnitude at around 200°C. [39]

The contribution of fluids in increasing the conductivity depends on the amount of dissolved solids; the surface conductivity becomes important with clay minerals.

Smectite(montmorillonite), has the strongest effect in increasing the conductivity. Less pronounced effects are observed for kaolinite, alunite, sericite and chlorite. [40]

The relationship describing the interdependency between resistivity and fluid characteristics is given by Archie's law.

$\rho = \alpha\, \phi^{-m}\, S^{-n}\, \rho_w$, where:

ρ is the resistivity of the formation, ϕ the porosity, S the water saturation, α the tortuosity, m the cementation factor, and n the saturation index. [39]

The ERT data is acquired along electric cables by installing electrode quadrupoles in a specific array configuration, depending on the targeted resolution and depth of investigation. The electric cables are connected to a resistivity meter and a computer.

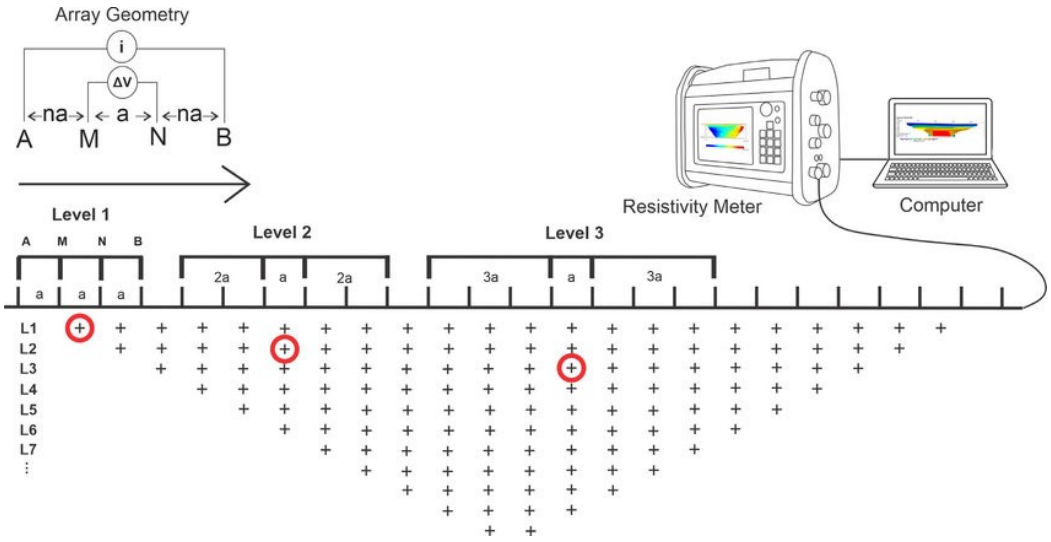

Fig3.3: ERT acquisition array geometry [45]

A power generator is used to inject the current in square waves, to avoid polarization effects. Electrodes need to have a good galvanic contact with the ground. [46]

There are several kinds of array configurations among which: the dipole-dipole, Schlumberger, Wenner, pole-pole, etc.

The depth of investigation depends on the array length.

Depth of investigation=1/5 array length [47]

The investigated depths by ERT usually stands in the range of 0-200m, very few experimental works were able to reach depths of approximately 500m.

In order to achieve a greater depth, the spacing between electrodes needs to be increased. This increase in spacing requires the use of longer electric cables, for which the installation is time consuming and present greater risks of current induction. [46]

The data processing consists mainly of noise removal, resolution of technical problems such as electrodes galvanic contact, estimation of the amplitude of the useful signal. [46]

The inversion process intends to turn the apparent resistivity pseudo sections in sections of true resistivity. The apparent resistivity represents the spatial average of resistivity of volumes of rocks surrounding the electrode array. Thus, inverting the data will provide a true resistivity

distribution of the subsoil by breaking down the set of apparent resistivities (Which are averages) into smaller specific true resistivity values. [48]

Another approach is to create a forward model of the subsurface based on a priori information on the site, then find a good fit of that model with the observed data. [48]

Data interpretation remains challenging; especially in complex environments.in fact, the resistivity is influenced not only by local variations in conductivity caused by weathering for example, but also by the topography. The current flow gets dense in valleys and dispersed beneath a hill. This phenomenon can cause false anomalies; finite-element numerical modelling is more suitable in matching such irregular boundaries. [42]

3.2.2 Application examples of geophysical methods in volcanic geothermal sites:

Ulubelu, Sumatra, Indonesia:

The Ulubelu site occupy a 50km^2 area in Sumatra; and is known for its surface manifestations, evidence of its internal hydrothermalism. Being in a volcano-tectonic depression, the surface manifestations comprise hot springs, fumaroles, etc. The site exploration started in 1989 and involved geological, geophysical, geochemical campaigns and exploration wells.

The reservoir was categorized as liquid-dominated with 210°C as highest temperature.

Electrical resistivity, magnetotelluric and gravimetry were applied as geophysical methods.

The Electrical resistivity and magnetotelluric allowed to map the top conductive layer sealing the geothermal reservoir as well as an alteration zone. Both methods probed respectively depths approximating 400m and 1.1km. moreover, the drilling points were determined by the outcome of these two methods.

Two (2) of the three (3) wells that were realized, detected temperatures of >210°C with resistivities ranging between 45-75ohm.m under the conductive layer of <15ohm.m the third well was not permeable enough.

The gravimetry highlighted a negative anomaly extending over ~ 7km, interpreted as a trench, formed by volcano-tectonic collapse, filled with pyroclastic deposits, not confirmed by drilling data. [44]

Karaha Telaga Bodas:

The Karaha Telaga Bodas geothermal field is located east to Java in Indonesia in a volcanic rift. This prospect has been investigated and revealed to be a vapor dominated system with temperatures as high as 350°C, extending from the active chimney of Kawah Galunggung at the south, up to Kawah karaha at the north.

Geological, geophysical geochemical surveys and drillings were conducted to characterize the reservoir. The main rock types are tuffs, breccias and andesitic lavas. Detailed Magnetotelluric (MT) and gravity surveys were carried out.

In 1996 and 1997, 180 MT surveys were realized as well as TDEM for the static correction.

From the MT, a precise map of the conductive argillitic layer, at the base of which the resistivity went on increasing due to increasing amount of vapor, was obtained. A positive gravity anomaly of 20 mGal interpreted as a granodioritic intrusion and heat source of the system was discovered. The granodioritic intrusion in fact is a sill laying at 2400m of depth, thick of 425m of wide of 1600m. this geometry was confirmed by drillings.

Leyte Island:

The Leyte geothermal field, situated at the center of Leyte Island in the Philippines, at the intersection of the volcanic arc and the Philippines' fault, is one of the largest liquid-dominated reservoirs in the world. [6] [44]

The volcanic arc formed after the collision of the Philippines' plaque and the Sonde bloc. The field surveys started in the 1950's by the Volcanology service completing a geothermal feasibility study that led in the 1970's to develop the geothermal resource. Leyte production field is composed of two distinct hydrothermal systems: Togonan to the north and Mahanagdong to the south, separated by the low permeable Mamban block.

Commercial operation started in 1983 with Togonan-1 Power plant 112.5 MW of power. The Togonan resource was further increased by commissioning additional power plants in Malitbog (232MW) and upper Mahiao (132MW) in 1996-1997. [6] [44]

Detailed electrical resistivity, micro-seismicity, gravimetric and GPS surveys were realized on the site. Gravity and GPS surveys were intended to follow mass movement at depth and monitor crustal deformation.

The electrical methods were those of direct current, using Schlumberger array. The most significant outcome of the resistivity survey is the NW-SE 1D interpretational resistivity profiles down to 500m of depth. Resistivity range of 10 to 200 ohm.m were found in Mahaio, Sambaloran Bao and Malitbog. The 10 ohm.m resistivity coincide with the 300°C isotherm, while < 20 ohm.m anomaly corresponds to a decreasing thermal gradient zone. The anomalies are aligned on the NW-SE and central parts of the Philippines' fault. Two district resistivity zones were distinguished: the cover (7-40 ohm.m) and underneath the cover (100-3600 ohm.m). [44]

The analysis of microearthquakes was made possible by the installation of a permanent station since 1980 and five (5) temporary stations that worked from time to time in 1981,1982 and 1987. The microearthquakes were focalized along the fault zone and hypocenters reached up to 15km.

A network of 18 remote stations, five (5) 3D sensors and eighteen (18) vertical seismometers were installed in 1996 and 1997 by the "Institut de Physique du globe" of Paris in collaboration with institutions in the Philippines. This network was designed to monitor the micro seismicity associated with injections during testing in Upper Mahiao and Malitbog fields; and hydraulic simulation intended to increase injection rate. After injection, seismic events were not only distributed along the faulting zone, but also in the testing area.

A tomographic inversion of velocities allowed to obtain a distribution model of P wave velocities in 3 D from an initial model of 3.75Km/s, reaching a depth of 1500m.

Moreover, gravity data allowed to constraint structures further confirmed by drillings.

Chapter 4: Geophysical and Laboratory data

This chapter covers the methodology used to obtain our results.

4.1 Electrical Resistivity Tomography data acquisition, Processing and Inversion:

The study area is Vulcano Island, where several geoscientific investigations have been conducted from the 1950's, whereby first hypothesis on its geothermal system were emitted. [2] [5] [32]

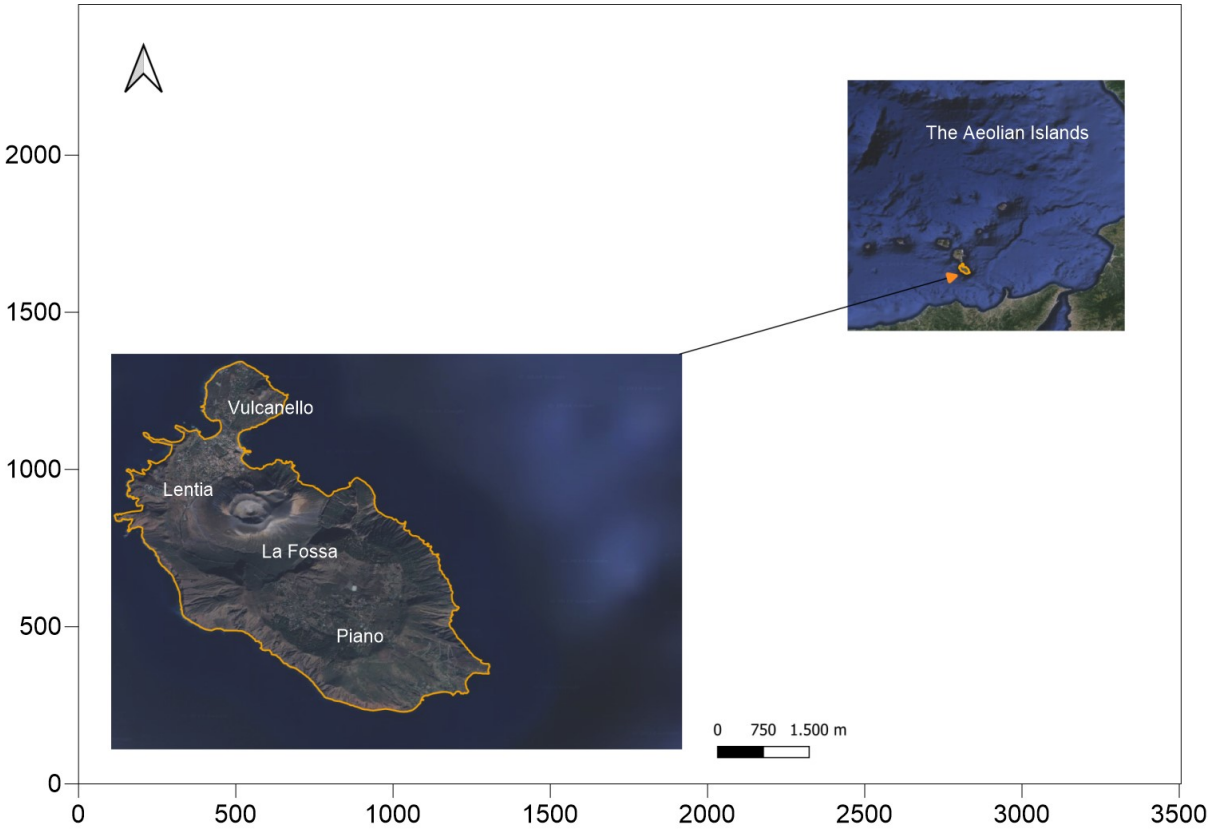

Fig4.1: Vulcano Island with respect to the Aeolian Islands

The Electrical Resistivity Tomography, was used to characterize in detail the first ~ 200m of the subsurface. These data will support the recent magnetotelluric data that provided crucial information on the geothermal system of Vulcano. [33].

In this work, two survey lines are taken into consideration: ERT3 and ERT4.

The ERT3 goes from Porto di Levante to Vulcanello in via delle provinciale; and ERT4 from via lentia,crossing Vulcano Porto up to via dei Villini in Vulcanello.

The wells VU1 and VU2bis are close to the profiles as seen on the image below.

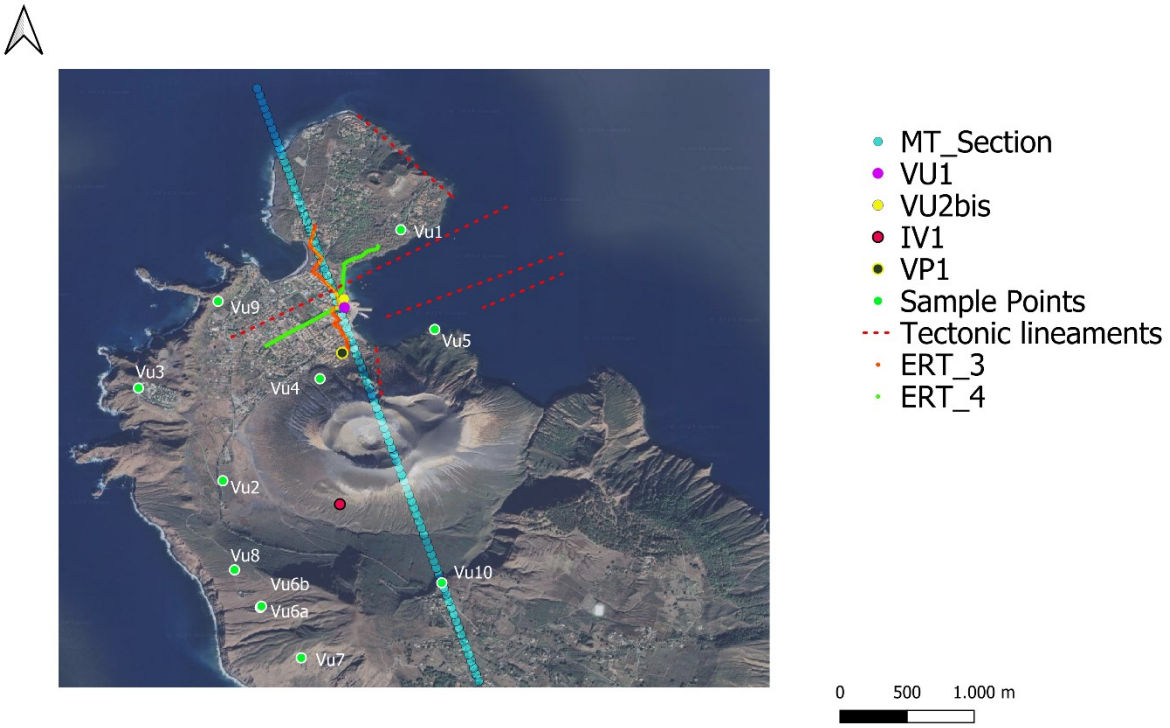

Fig4.2.ERT profiles, MT section, well locations, tectonic lineaments and rock sampling points.

The electrical resistivity data acquisition in Vulcano that spanned from the 28th to the 30th of November 2023, was carried out under the volcanic surveillance framework of the INGV operating in the Aeolian archipelago for several years.

Along with the Syscal Pro resistivity meter, the acquisition system was composed of a battery, 3 cables of 24 electrodes layouts each, 72 electrodes, a computer and connectors.

Fig 4.3 ERT acquisition near Baia di levante.

The cables are laid on the ground, connected between them to achieve the desired length, and stainless-steel electrodes are planted in the ground at regular intervals (20m) and connected to the cables through connectors. Measurements are conducted at different depth levels as shown in figure 3.3.

At each level, the current electrodes separation increases by a fixed multiple *a,* allowing to reach a greater depth at every level. [45]

The multichannel measuring system allowed relatively rapid measurements. Thanks to the real-time graphical pseudo-section display of apparent resistivity, some first improvements in data quality were performed: enhancing the ground-electrode galvanic contact, reconnecting disconnected electrodes to the cables and enhancing ground conductivity by pouring some salty water on the electrodes.

GPS coordinates were acquired for each electrode position.

Unfavorable weather and topographic conditions, such as wind and rain, had a significant impact on the collected data quality.

In order to minimize these effects, we filtered the data using the demo version of the res2dinv software, which allows to visualize the acquisition profile and eliminate undesirable points. Further filtering was performed with ResIPY.

After this first operation, the triangular meshing, surface topography integration and inversion were all done in ResIPY with a final RMS error of <2% for both profiles.

ResIPY is an open-source software written in Python, with finite element source codes: R2, cR2 for inversion/forward modelling, and Gmsh for mesh generation, available on https://gitlab.com/hkex/pyr2. The software handles importing, filtering, forward and inverse modelling of DC resistivity and IP data. Thanks to its graphical interface (GUI), it provides pre-processing and post processing tools. It is capable of reading many different file formats including Res2dinv files. [49]

4.2 Magnetotelluric data integration:

The magnetotelluric method provides models of the subsoil at depths up to several kilometers, capable to image large scale structural features such as the heat source or the geothermal reservoir, while ERT offers high-resolution at shallower depths, a few hundred meters.

Integrating both types of data will ensure a more comprehensive subsurface picture. ERT will complement MT by detecting small-scale resistivity contrasts in the near subsurface.

Overlapping anomalies will reinforce confidence in the model, reducing ambiguity in interpretation.

In this work, the MT data are from the INGV, the same that were used to produce a 3D model of Vulcano's geothermal system. [33]

The section that we used is in the N-W to S-E direction almost coinciding with the ERT3 profile.

An interpolation of both ERT3 profile and the MT section is performed using Surfer 10, a mapping software.

To realize this operation, the inverted data are retrieved and prepared for gridding by Kriging method. The grided data is the input file to produce contour maps that allow a direct comparison an analysis of MT and ERT data.

To perform gridding, the input file should be formatted in X, Y and Z format. The columns represent generally the X Y and Z coordinates.

For the ERT file, X represents the inversion mesh nodes coordinates, Y the elevations and Z the corresponding resistivities.

Similarly, the MT file is organized in the same format, where the column Z consists of impedances.

4.3 Laboratory data:

Integrating data from various sources is a way of reducing uncertainty in interpretation.

Laboratory results are precise, obtained in controlled conditions of properties such as temperature, pressure, moisture, etc. The change of one or more of these properties leads to changes in the results, allowing to elaborate a relationship between the measured and the samples physico-chemical conditions.

Even though the samples are poor representative of the in-situ heterogeneity and geomechanical conditions, validation from geological and geophysical sources minimize these aspects.

In this work, Electrical resistivity measured in the field is correlated with Laboratory measured electrical resistivity on eleven (11) outcropping rock samples from Vulcano Island, representative of the lithologies found in IV1 and VP1 wells drilled in the 1980s.

The thermal conductivities on the same samples are also determined.

Moreover, elastic properties are calculated; they are: the P and S wave velocities, the poissons' ratio, the shear modulus, the lamé first parameter, the Bulk and young's moduli.

The borehole stability is strictly related to these mechanical properties of rocks. Mechanically weak or strong formations respond differently to drilling activities.

Weak formations are prone to plastic deformations, and temperature alteration, leading to further weakening. Caving and mud cake formation are common.

However, compared to weak rocks, strong rocks resist better to deformation and the drilling equipment is more stable. But fractures within them, have the potential to spread and create instability.

All these factors demonstrate the importance of mechanical properties, knowledge of which can enable us to select the density of the drilling mud, the drill bit and the drilling systems (rotary and /or percussive) in order to avoid drilling-related inconveniences.

Thermal conductivities are obtained both in dry and saturated conditions and the elastic moduli in dry conditions.

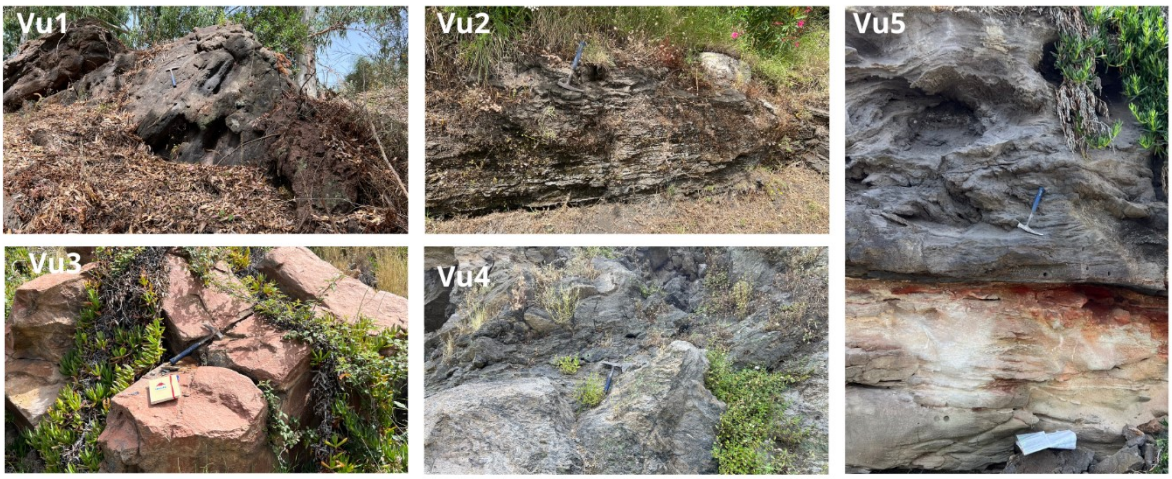

Fig 4.4: Outcrops of some samples.

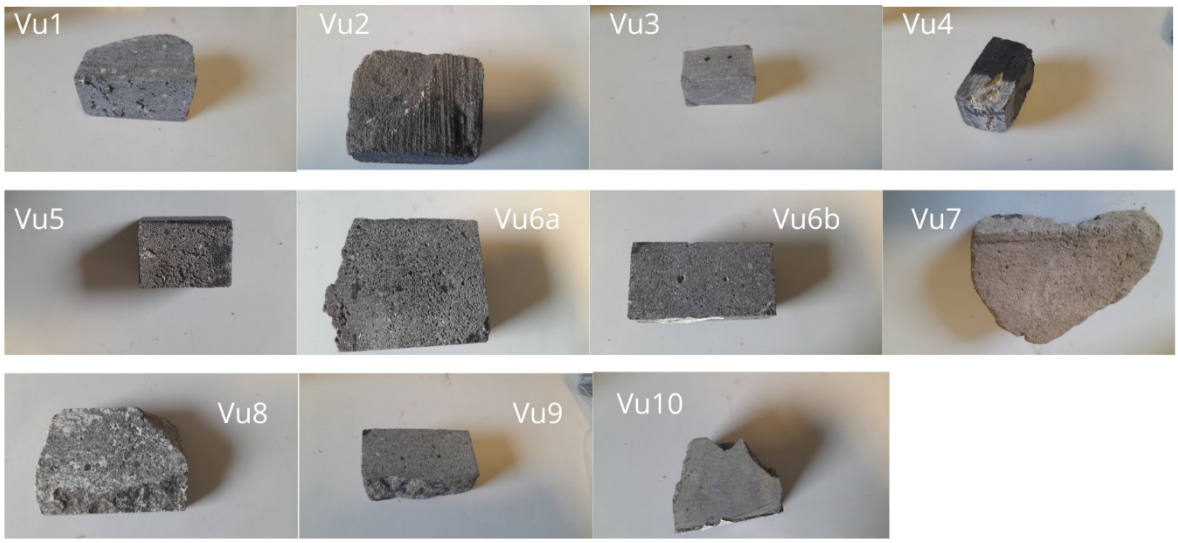

Fig4.5: Rock samples used for laboratory analyses.

4.3.1 Thermal conductivity:

The thermal conductivity is the ability of a material to transmit heat. It plays an important role in the development of a geothermal project; from exploration to the operational phase.

For instance, it is essential for heat flow modelling, drilling operations, the selection of constituting materials of the power plant such as: heat exchangers, turbines, cooling systems.

Thermal conductivity measurements were run with an instrument called “Trident”, built on C-therm thermal conductivity fourth generation technology.

It combines 3 industry measurements techniques, allowing to measure high performance materials heat transfer properties:

The Modified Transient Plane Source (MTPS), the Flex Transient Plane Source (Flex TPS) and the needle transient line source (TLS).

In our case, the MPTS is the employed method. Before running the actual measurements, a calibration is needed by a reference test material. The material for the reference test is chosen according to its thermal conductivity that should be the closest to the expected thermal conductivity of our sample. Here, the pyroceram is used; calibrated on ceramics with a thermal conductivity of ~ 4.11W/m°K, close to the one of rocky materials.

The device also measures the thermal diffusivity which links the thermal conductivity (λ), the specific heat capacity (Cp) and the density (Q)

$$Q = \frac{\lambda}{Cp\ Q}$$

The MTPS technique uses a single-sided, factory-calibrated sensor to evaluate a material's thermal conductivity. Of the three approaches, the MTPS method is the simplest to apply and is also the most accurate and sensitive.

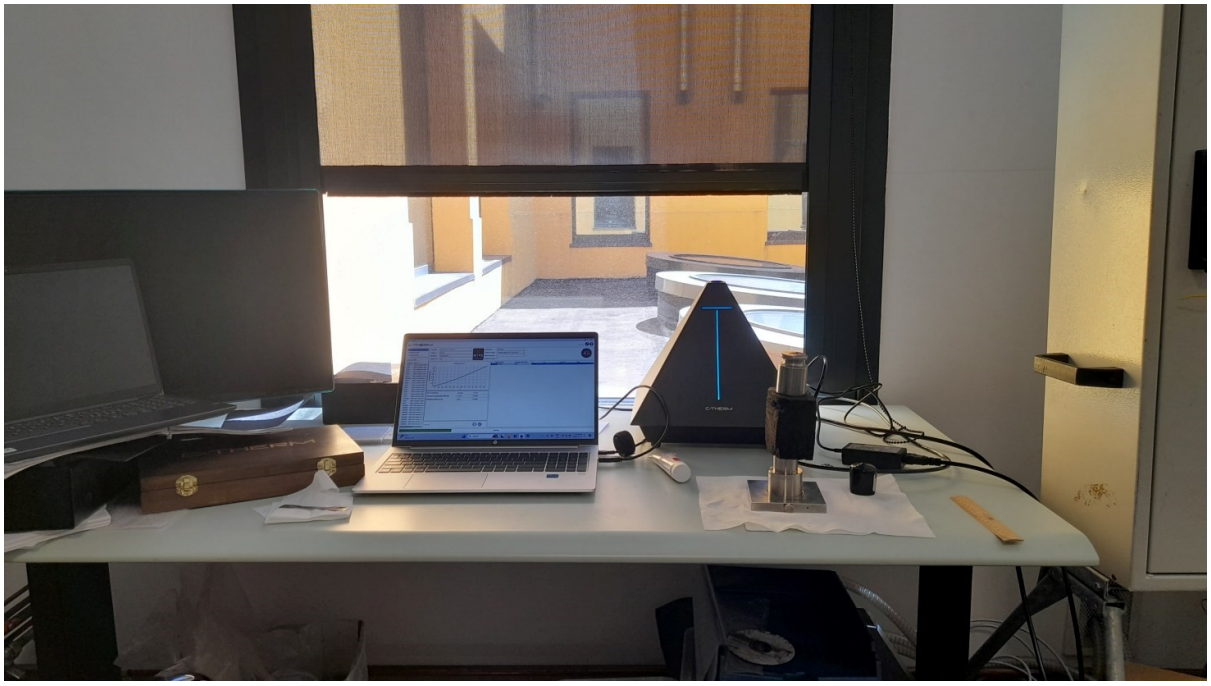

Fig4.6: C-therm ongoing measurement.

Three drops of water are used to ensure the contact between the pyroceram and the sensor.

The reference test is validated if the thermal conductivity value falls in the range expected for the specific reference material, in our case pyroceram.

Afterwards the actual test is run, and the measurements are displayed on a sheet as in **(table4.1)**

C-THERM

MTPS GUARD RING TECHNOLOGY

Test Details

Instrument:	**C-Therm Trident**	Test ID:	**MTPS-Polymers-2024-05-17-01:27:00P**
Instrument Serial:	**TR92-23-00323**	Test Date:	**2024-05-17 13:27**
Sensor Serial:	**H1153**	Project:	**Denise**
Calibration Date:	**2024-01-22**	Material:	**Hyaloclastites**
Calibration Name:	**Polymers**	Sample ID:	**Vu7**
Contact Agent:	**Thermal Paste**		

Measurement Results

Average Conductivity:	**0.7035** W/mK	Average Effusivity:	**1052.7** Ws½/m²K
Conductivity RSD:	**0.5966** %	Effusivity RSD:	**0.3708** %

Measurement Data

#	k (W/mK)	Effusivity (Ws½/m²K)	R²	1/m	Temperature (°C)
1	0.6953	1045.1	0.9999	34.4	23.4
2	0.7070	1056.0	0.9999	34.6	23.4
3	0.7046	1053.7	0.9999	34.6	23.5
4	0.7044	1053.6	0.9999	34.6	23.4
5	0.7061	1055.2	0.9999	34.6	23.4

Table4.1: Example of C-therm result sheet.

Measurements are run several times and then averaged. It is recommended to run five to ten measurements. A good contact between sensor and the sample is critical; environmental stability such as temperature may affect the results. Invalid results appear as red cells and are mostly due to a poor sample-sensor contact or an inadequate calibration.

The samples Vu2, Vu5, Vu7, and Vu4 required the use of the polymer's calibration with the Pyrex material; because of their nature: more porous, and sometimes less compact. A thermal paste was used as contact agent with the sensor.

4.3.2 Electrical Resistivity:

The samples' electrical resistivities are determined in two steps: the resistances are measured, and the resistivities retrieved by applying Ohm's law. The Wenner array configuration is used, where a set of four electrodes is placed horizontally and equally spaced at the surface of the samples. A DC current is injected through electrodes A and B, and the resulting voltage drop is measured between the remaining electrodes M and N.

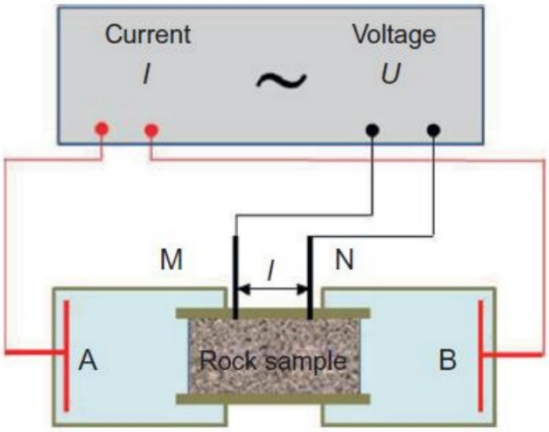

Fig 4.7: Electrical resistance measurement of a rock sample in a Wenner array.[52]

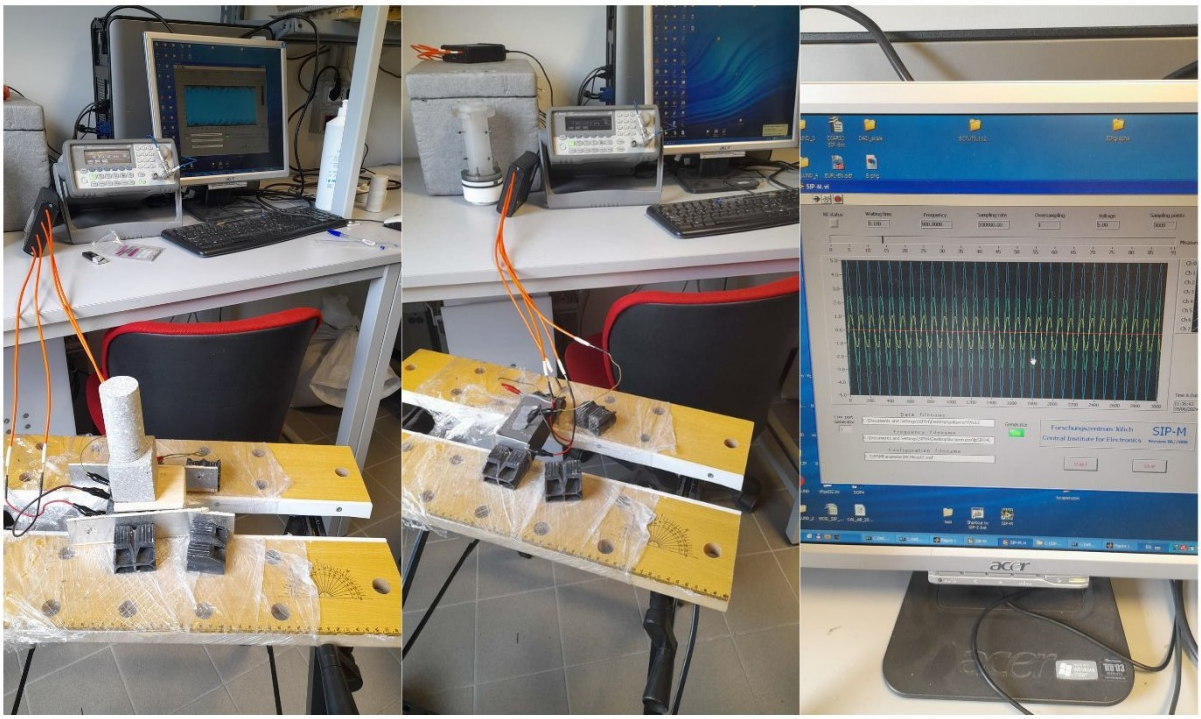

Fig 4.8: Resistance measurement with Agilent 33220A

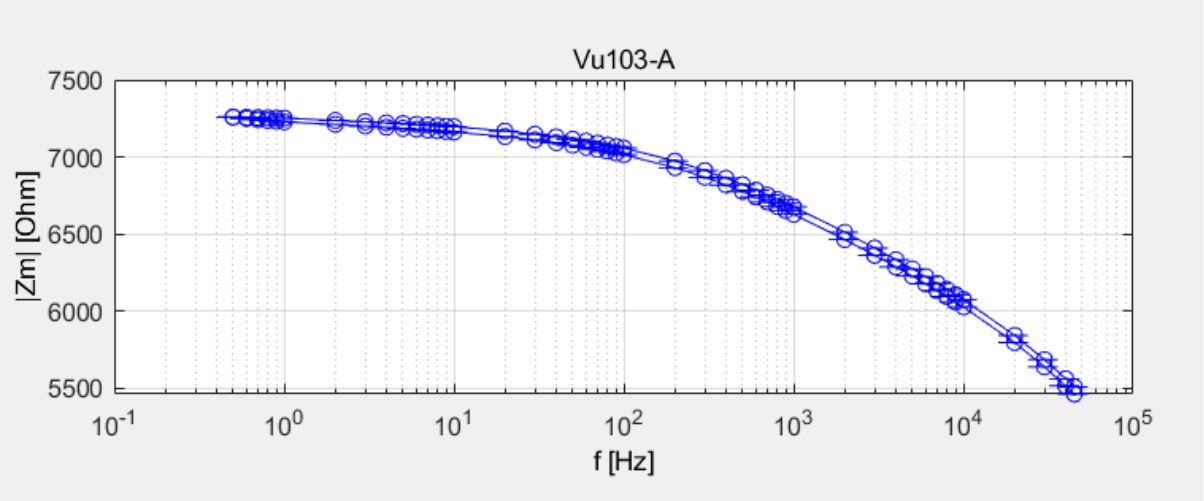

Fig 4.9: Example of a resulting resistance plot in function of frequency.

Ohm's law:

$R = \frac{\rho.l}{A} \rightarrow \rho = \frac{R.A}{l}$

R is the resistance [Ω], ρ is the resistivity [Ωm], A the area in [m^2] and l the spacing between electrodes in [m].

The resistivity depends on the resistance and the dimensions of the samples that should be as regular as possible.

Here, the resistance is measured with the Agilent 33220A, that generates various types of waveforms for testing and measurement purposes. It can generate standard waveforms such as sine, square, ramp, and pulse, as well as arbitrary waveforms, with frequencies up to 20 MHz for sine and square waves.

Two main shapes were retained for area calculations: the rectangular parallelepiped and rectangular trapeze.

Area of a rectangular parallelepiped:

$$A=2(h \times l + L \times l + L \times h)$$

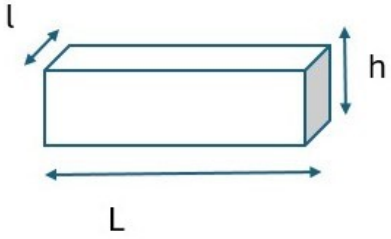

Rectangular trapeze

$$A = (L+l) \times h / 2$$

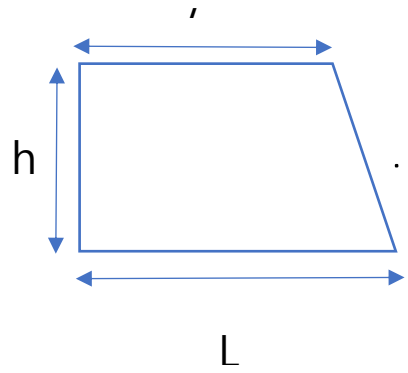

4.3.3 Elastic Properties: P and S waves velocities, poisson's ratio, lamé first parameter, shear modulus, young's and bulk moduli

For loading times less than 10^5 seconds, under moderate temperature and pressure conditions, rocks can be assimilated to elastic materials. [50]

Their elastic properties tell us about their ability to resist mechanical changes when subjected to various stress conditions.

In geothermal applications, especially drilling operations, the elastic properties of rocks are essential to ensure the wellbore's structural integrity and longevity. They help in selecting the appropriate drill bit, optimize mud weight and casing to minimize risks of fracturing and blowouts.

Moreover, the analysis of these properties provides valuable insights regarding porosity and pore fluids of rocky materials.

The *P and S waves velocities* of the eleven (11) samples were determined both in dry and saturated conditions at room temperature using the EPOCH 600.

The EPOCH 600 is a Digital Ultrasonic Flaw Detector from Olympus' industry. It offers the convenience of being portable and intuitive instrument, with the possibility to adjust parameters from the keypad.

An ultrasonic pulse is emitted and the travel time between the transmitter and the receiver is measured. An oscilloscope displays the received signal and the travel time in microseconds.

Knowing the distance between the transmitter and the receiver (the thickness of the sample), the wave velocity is determined by V=X/T. X is the thickness of the sample, and T is the signal's travel time across the sample.

Fig 4.10: Elastic wave propagation time measurement with Epoch 600.

The detection of each wave type (P and S) requires the use of a specific type of gel as coupling agent between the sample and the sensors.

(EPOCH 600 Ultrasonic Flaw Detector (olympus-ims.com)

From the *ratios Vp/Vs*, it is possible to determine the *Poisson's ratio* which is the ratio between transverse strain (et) and longitudinal strain (el) under elastic loading as ν = -et/el [51]

$$\nu = \frac{1}{2} \cdot \frac{(Vp/Vs)^2 - 2}{(Vp/Vs)^2 - 1}$$

The Poisson's ratio is a good indicator for compressibility, because it is mainly controlled by the rock type and pore fluids. For isotropic materials, ν must satisfy $-1 \leq \nu \leq 1/2$.

For most incompressible materials such as liquids and rubbers, $\nu \rightarrow ½$, while it is 0 for gases. [51] [52]

To calculate the other elastic moduli such as the Lamé parameters, knowing the *density* is necessary. To do so, we proceeded by the water displacement method as most of the samples are irregularly shaped. Water is poured in a beaker in which the sample is submerged. The sample will displace water by a quantity equivalent to its own volume. For sample Vu8, the initial water volume was 600ml, and the final volume after submersion of the sample was 675ml, the volume of the sample is equal to the difference between the two volumes which is 75ml=75 cm3 . **(see fig4.11)**

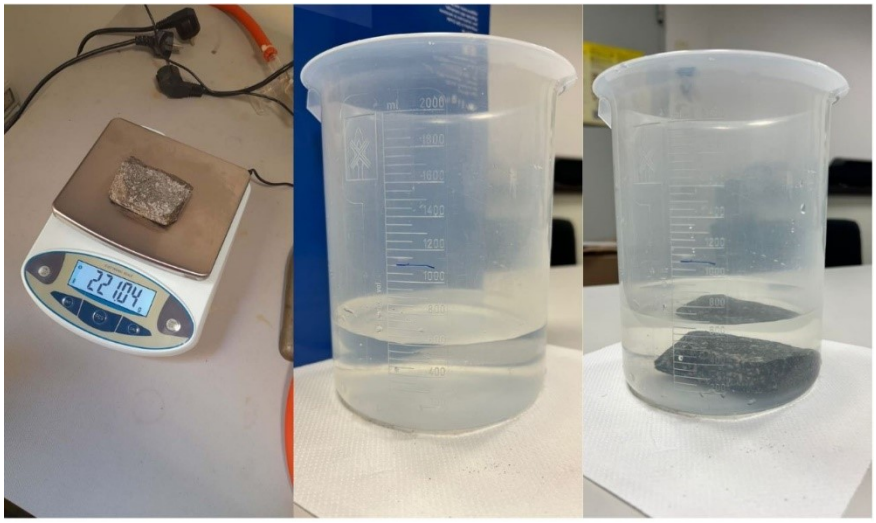

Fig 4.11: Mass and Volume measurements.

Afterwards, the bulk density is calculated through the formula: D=M/V

M being the weighted mass of the sample and V the volume.

lamé parameters λ and μ respectively compressibility and shear modulus, which are intrinsic rock elastic properties, describe the resistance of an elastic material to a change in volume caused by a change in pressure. [53]

$\lambda = \rho \cdot (Vp^2 - 2 \cdot Vs^2)$

$\mu = \rho \cdot Vs^2$, where ρ is the density.

The *bulk and young's moduli* were calculated respectively through the following expressions:

$$K = \frac{E}{3.(1-2v)}$$

$$E = 2\mu(1+v)$$

The bulk modulus measures a material's resistance to isotropic compression. It is an indication of the material's compressibility under a given amount of external pressure;

While the Young's modulus measures a material's stiffness or rigidity, indicating how much it will deform under an uniaxial stress.

Chapter 5: Results and discussions

5.1 Electrical resistivity tomography results:

The profile lines cross a NNE-SSW tectonic lineament and present some transitions from resistive to conductive anomalies. In the bigger picture, those abrupt shifts are located in Baia di Levante and Faraglione. From the deepest parts of the sections, the resistive bodies are intersected by conductive conduits raising up to the surface in some intervals.

Both survey lines cross the Vulcanello 1b formation, seashore deposits, the urbanised area, colluvial deposits and the faraglione formation which is close to fumarolic vents of Baia di Levante.

The Vulcanello 1b formation is a 30m thick deposit, consisting essentially of massive scoriaceous lava flows (shoshonites).

The faraglione formation is a highly fumarolized deposit building the Porto di Levante stack. Bedded pyroclasts with relicts of dense scoriaceous bombs and a tuff cone are its main features. [25]

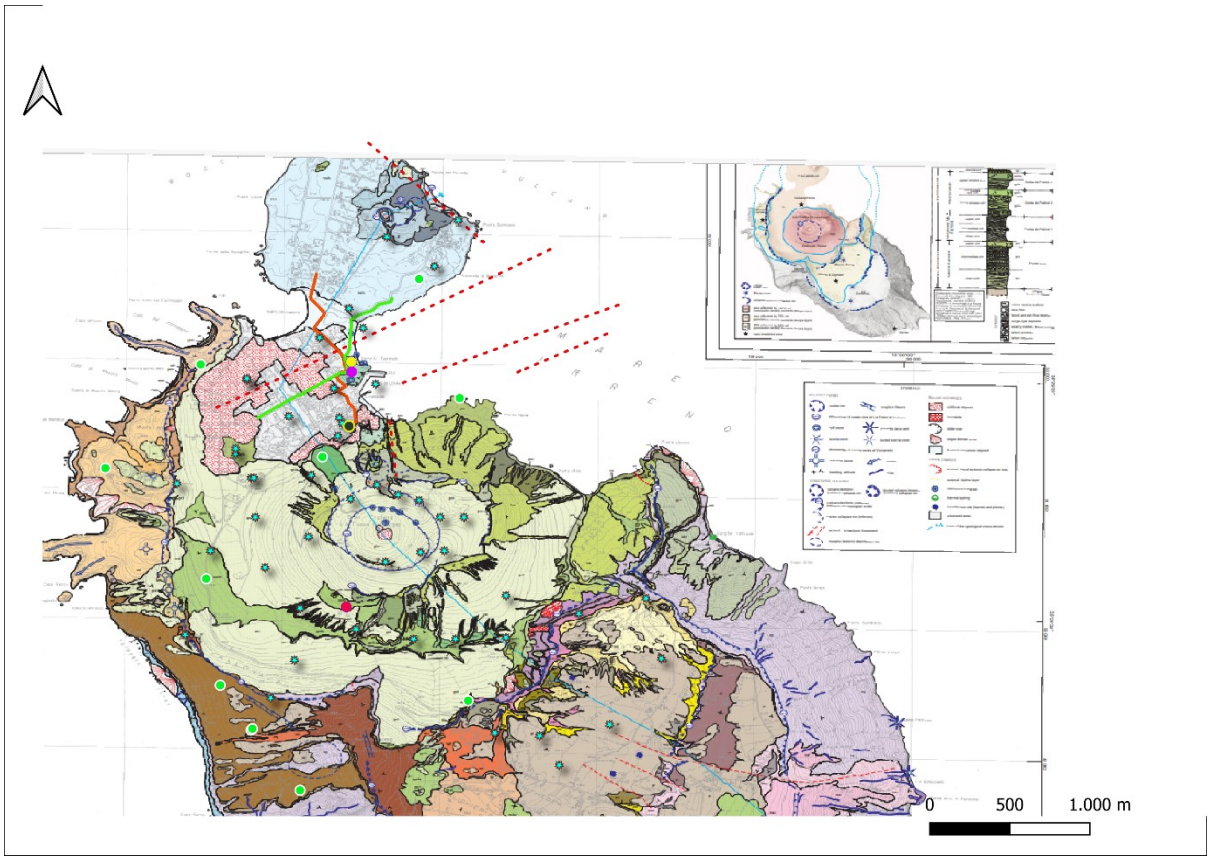

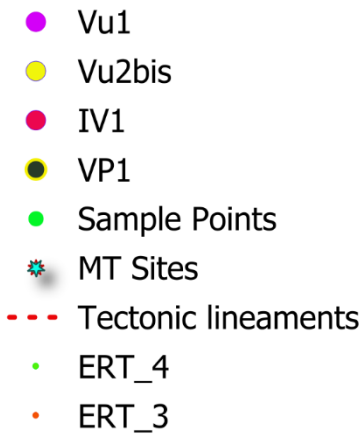

Fig5.1: ERT profiles, wellbores (Vu1, Vu2bis, IV1 and VP1), sample points, Magnetotelluric sites, and tectonic lineaments on the geological base map. The light blue color represents the Vulcanello 1b formation, the blue dotted pattern corresponds to the seashore deposits; while the Faraglione formation(fa) is in green, and the colluvial deposits in a red dotted pattern. (modified from Vulcano geological map [25])

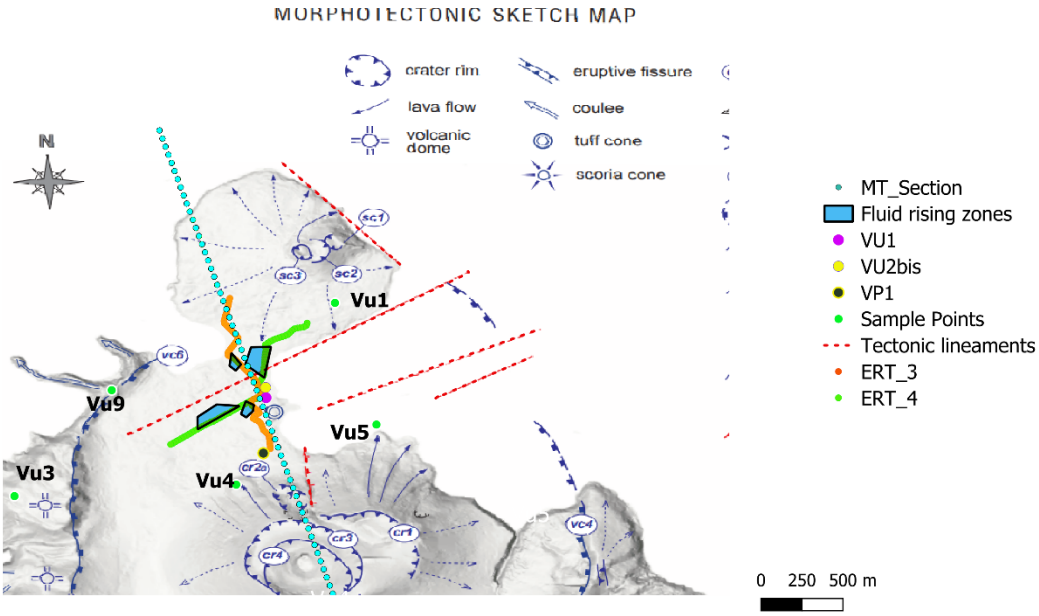

Fig5.2: Map showing the fluid upwelling intervals present on the ERT sections. (Morphotectonic sketch modified from [25])

5.1.1 ERT3 survey line:

Oriented N-W to S-E, this survey line starts in Vulcanello and starts going eastwards from Porto di Ponente up to the end, near Porto di Levante.

The first shallow interval shows low resistivities. Near the sea level, the conductivity starts to fade away, showing a quasi-continuous resistive body that got interrupted by a sub vertical conductive horizon as we move to the south. The conductive conduits seem to be starting from 400m up to 1000m of distance on the profile, raising to the surface in the respective intervals:400-600m, and 800-1000m. The last interval of the profile (1000-1200) shows higher resistivities compared to the first one between 0 and 400m

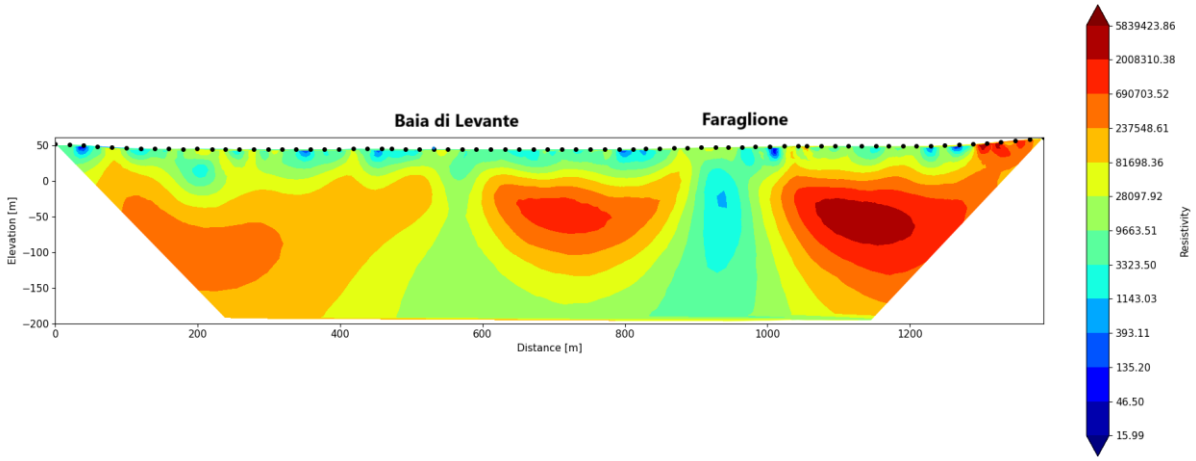

Fig5.3: ERT3 inverted section.

5.1.2 ERT4 survey line:

This ERT4 profile is a NE-SW oriented line that starts in the lower portion of Vulcanello, goes straight and then westwards, right after crossing the Baia di Levante and faraglione.

The inverted resistivity section presents from the deepest parts (about 200m) a resistive interval that is intercepted by subvertical conductive areas, separating it into three (3) resistive bodies among which, the most resistive one is located at the southernmost part between 1000 and 1200m along the profile. The subvertical conduits raise up to the surface between 300-600m and 850m to 1000m along the profile.

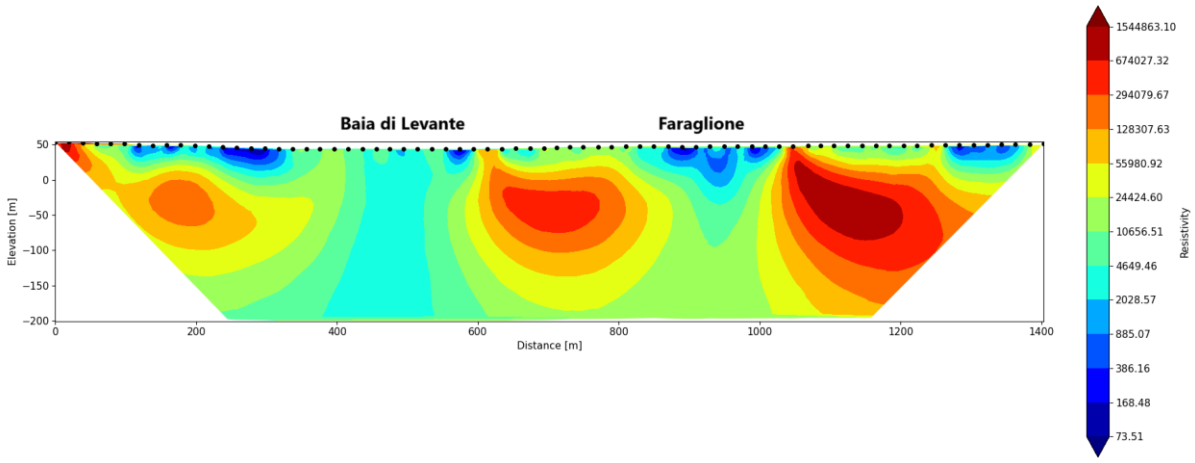

Fig5.4: ERT4 inverted section

5.2 Magnetotelluric data interpolation results:

The MT inverted section shown on fig (5.5), was gridded in Surfer 10, and the resulting image is shown below.

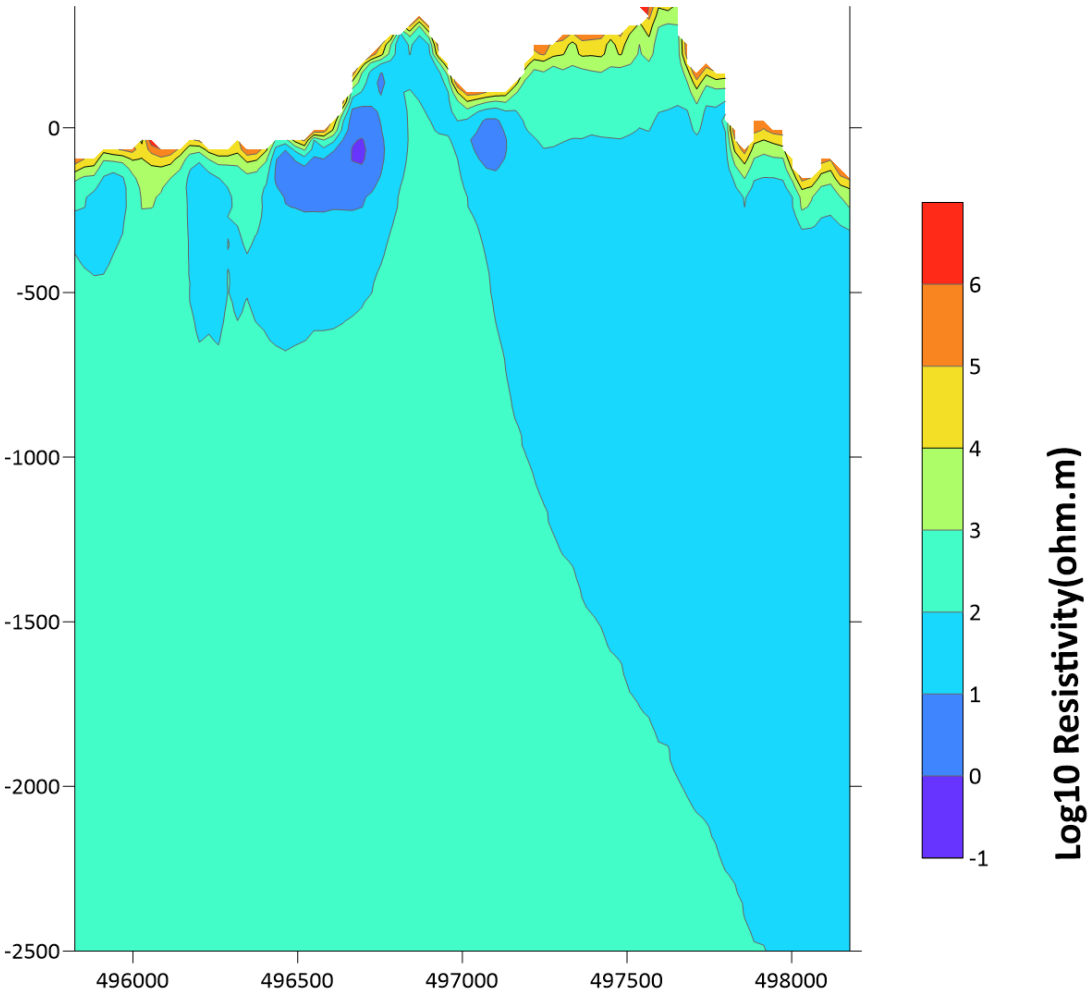

Fig5.5: MT section obtained by gridding in Surfer10. (X axis represents the easting UTM, WGS84 coordinates).

This figure represents the MT inverted section over 2500 m of depth and a distance of ~ 2400m. Coordinates on the horizontal axe is in UTM, separated by steps of 500m.

The two horizontal lines crossing the section corresponds to the in-depth dimensions of our ERT section.

Between 1000m and 1200m, a resistivity transition runs from the top of the interval corresponding to the ERT3 section (58 a.s.l to 200 b.s.l) to the bottom, going eastward. This line separates two zones of resistivity: the western side being more resistive, while the eastern part is more conductive.

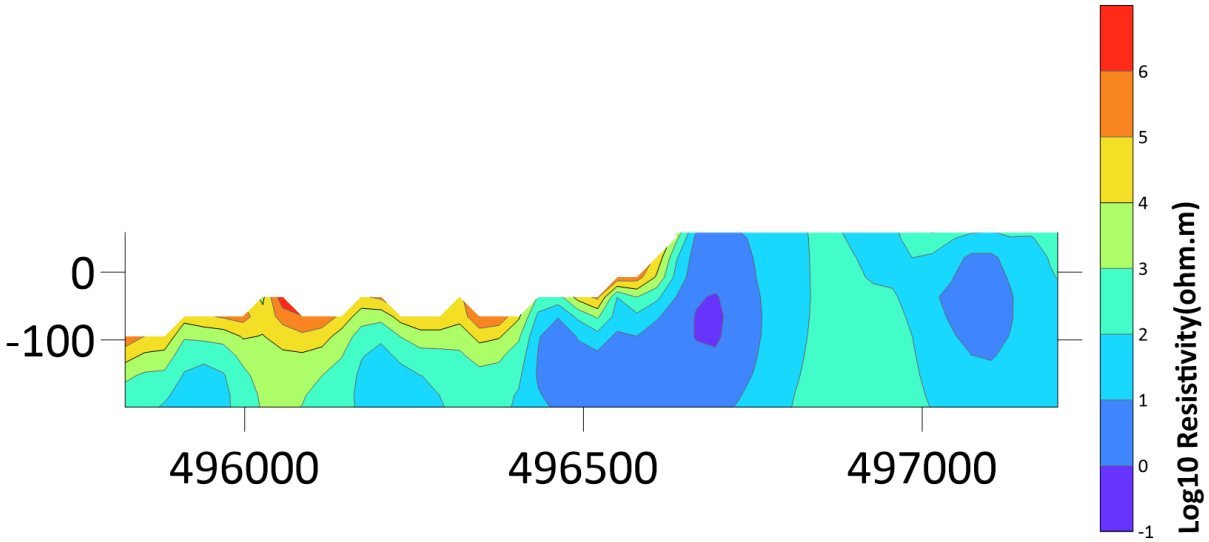

Fig5.6: MT section corresponding to the ERT3 dimensions.

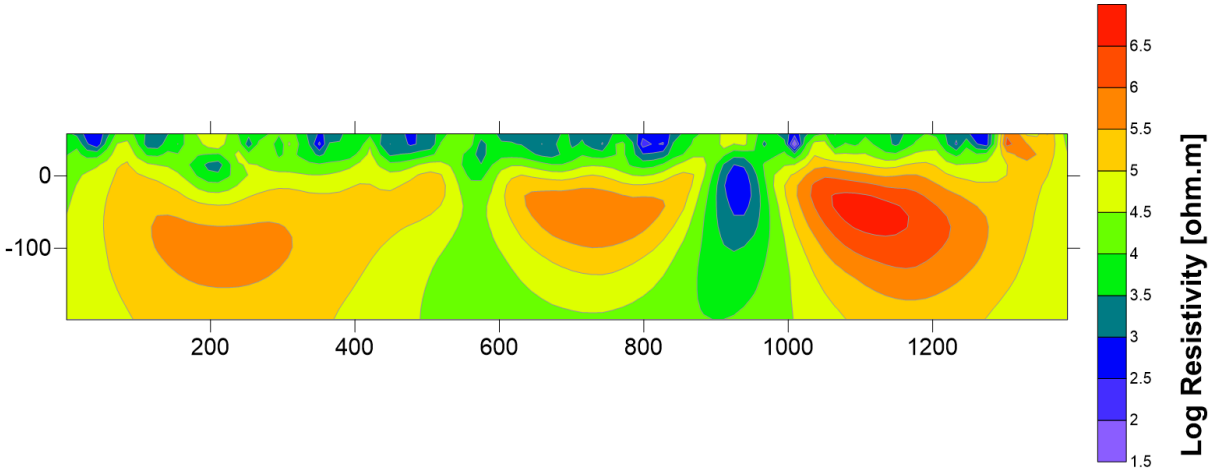

Fig 5.7: ERT3 section obtained by gridding the inversion data in Surfer 10.

On the MT section, between 1000m and 1200m, two distinct zones of resistivities are visible: the first one being of higher resistivity, and the second one in the eastern part, more conductive.

Examining both MT and ERT sections, we noticed two conductive areas, represented by a conduit-like structure, rising up to the surface: between 800m and 1000m; and between 400 and 600m.

Beyond 1000, the sections become more resistive. In the first interval, i.e., 0-500m, a relatively high resistive anomaly is seen on the ERT profile, from the sea level to greater depths, while the area above the sea level is more conductive unlike on the MT section where the opposite situation prevails. In fact, on the MT profile, a resistive anomaly lays from the top down to ~ 100m in depth and 800m horizontally. Beyond 800m of distance, a continuous conductive horizon that rises towards the surface is observed, being only interrupted in the last 400m by a higher resistive body.

5.3 Laboratory measurement results:

5.3.1 Thermal conductivities:

By examining the results, we note two distinct groups of conductivities: some with conductivities below unity (Vu2, Vu4, Vu5 and Vu7), and all the others, above.

The samples Vu8 and Vu10 revealed the highest thermal conductivity values, reaching respectively 2.44 and 2.42 in drained condition.

The most significant changes in the values in saturated condition were observed for the same samples that had low conductivities in drained condition; in most cases, the values increased up to twice compared to the initial values. (see fig 5.8)

A systematic rise in thermal conductivity values with pore saturation was observed for all the samples. However, slight variations in ambient temperatures led to a decrease in these values for consecutive measurements in some cases, leading us to consider the results for which the temperatures were the lowest possible.

Vu2 and vu7 are relatively close to the surface, and have primary porosity which is due to the nature of their granular texture while Vu4 is fractured. Vu5 is porous because of its vesicular texture, typical of scoriae.

Sample ID	Rock type	Well	Thermal conductivity range [W/mK]
Vu1	Latitic Hyaloclastites	VP1	1,4969 - 1,5110
Vu2	Pyroclastites	VP1	0,2789 - 0,3196
Vu3	Rhyolites	VP1	1,4886 - 1,5340
Vu4	Trachytes-latites	VP1	0,5754 - 0,6032
Vu5	Trachybasaltic Welded scoria	VP1	0,4028 - 0,4062
Vu6a	Trachybasaltic Welded scoria	IV1	1,2107- 1,4557
Vu6b	Trachybasaltic hydromagmatic tuffs	IV1	1,5138 - 1,6930
Vu7	Hyaloclastites	IV1	0,3229 - 0,3564
Vu8	Monzodioritic Intrusion	IV1	2,2062 - 2,4385
Vu9	Latitic Lava flows	VP1	1,3122 - 1,3318
Vu10	Trachybasaltic and trachyandesitic lava flow (primordial Vulcano)	IV1	2,3779 - 2,4216

Table 5.1: Samples measured thermal conductivities with C-therm in dry conditions.

The samples are taken from outcrops and correspond to lithologies of IV1 and VP1 wells.

Sample ID	Rock type	Well	Thermal conductivity range [W/mK]
Vu1	Latitic Hyaloclastites	VP1	1,5551-1,6221
Vu2	Pyroclastites	VP1	1,0469-1,0627
Vu3	Rhyolites	VP1	1,5477 - 1,5854
Vu4	Trachytes-latites	VP1	0,8742 - 0,8779
Vu5	Trachybasaltic Welded scoria	VP1	0,8414 - 0,8652
Vu6a	Trachybasaltic Welded scoria	IV1	1,4179 - 1,4346
Vu6b	Trachybasaltic hydromagmatic tuffs	IV1	1,5936 - 1,8389
Vu7	Hyaloclastites	IV1	0,6874 - 0,7035
Vu8	Monzodioritic Intrusion	IV1	2,4972 - 2,6251
Vu9	Latitic Lava flows	VP1	1,3813 - 1,3894
Vu10	Trachybasaltic and trachyandesitic lava flow (primordial Vulcano)	IV1	2,4865 - 2,5057

Table5.2 Thermal conductivities measured in saturated conditions (samples were submerged in water for 48h).

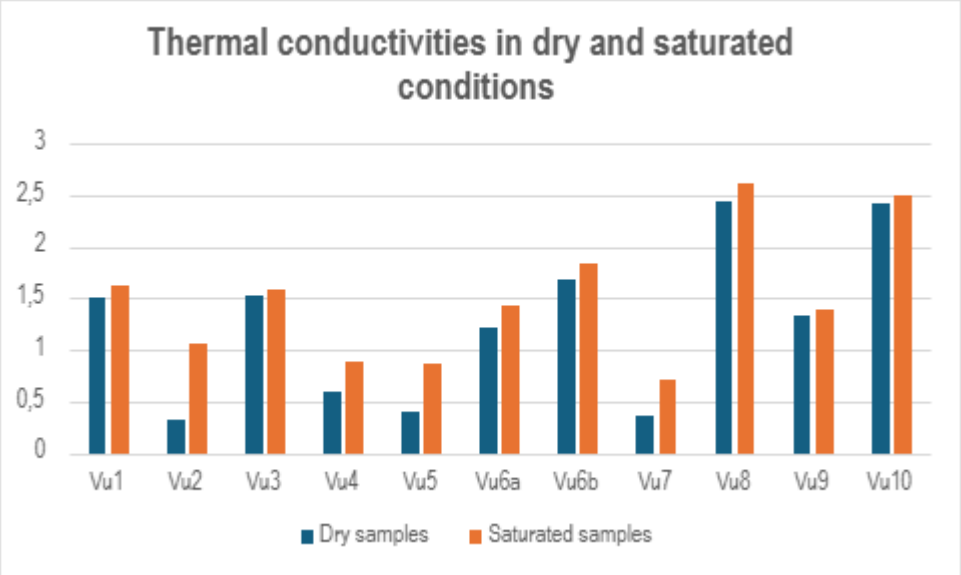

Fig5.8: Comparative diagram showing thermal conductivities on dry and saturated samples.

5.3.2 Elastic properties:

The calculated Vp, Vs and Vp/Vs ratios are reported in tables (5.3 and 5.4)

Samples	Tp [μs]	Ts [μs]	X [cm]	Vp[m/s]	Vs[m/s]	Vp/Vs
Vu1	10,80	21,50	3,70	3425,93	1720,93	1,990740741
Vu2	41,10	73,40	5,20	1265,21	708,45	1,785888078
Vu3	5,60	10,70	3,00	5357,14	2803,74	1,910714286
Vu4	12,20	29,20	4,40	3606,56	1506,85	2,393442623
Vu5	12,10	22,60	2,80	2314,05	1238,94	1,867768595
Vu6a	12,20	26,00	5,00	4098,36	1923,08	2,131147541
Vu6b	9,40	17,80	4,30	4574,47	2415,73	1,893617021
Vu7	29,00	51,70	4,00	1379,31	773,69	1,782758621
Vu8	5,10	9,00	2,00	3921,57	2222,22	1,764705882
Vu9	16,20	28,40	4,40	2716,05	1549,30	1,75308642
Vu10	7,40	14,60	4,50	6081,08	3082,19	1,972972973

Table5.3: Vp,Vs and Vp/Vs in drained condition. Tp is the P wave arrival time in microseconds ($\mu s = 10^{-6} s$), Ts is the S wave arrival time , X is the thickness of the sample in cm.

Samples	Tp [μs]	Ts [μs]	X [cm]	Vp[m/s] Sat	Vs[m/s] Sat	Vp/Vs
Vu1	10,00	20,80	3,70	3700,00	1778,85	2,08
Vu2	43,70	84,10	5,20	1189,93	618,31	1,924485126
Vu3	5,30	11,20	3,00	5660,38	2678,57	2,113207547
Vu4	11,40	23,60	4,40	3859,65	1864,41	2,070175439
Vu5	12,00	22,80	2,80	2333,33	1228,07	1,9
Vu6a	12,60	26,10	5,00	3968,25	1915,71	2,071428571
Vu6b	8,70	17,60	4,30	4942,53	2443,18	2,022988506
Vu7	30,10	63,80	4,00	1328,90	626,96	2,119601329
Vu8	3,80	5,20	2,00	5263,16	3846,15	1,368421053
Vu9	8,40	21,50	4,40	5238,10	2046,51	2,55952381
Vu10	7,30	14,80	4,50	6164,38	3040,54	2,02739726

Table5.4 : Vp,Vs and Vp/Vs in undrained condition. Tp is the P wave arrival time in microseconds (μs), Ts is the S wave arrival time, X is the thickness of the sample in cm.

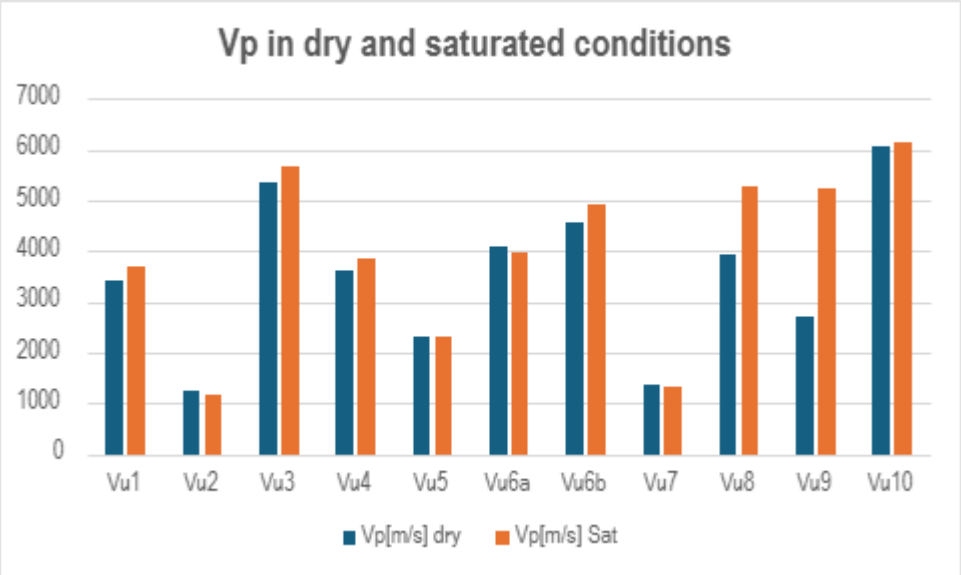

Fig 5.9: Vp in dry versus saturated conditions.

According to the tendancy of P waves velocities to increase or decrease from dry to saturated conditions, the samples maybe classified in two groups:

1.Those that showed an increase in Vp :Vu1, Vu3, Vu4, Vu5(very slight increase), Vu6b, Vu8, Vu9(almost double of the initial value in dry condition) and Vu10;

2. those that showed a decrease in Vp: Vu2,Vu6a and Vu7(slight decrease).

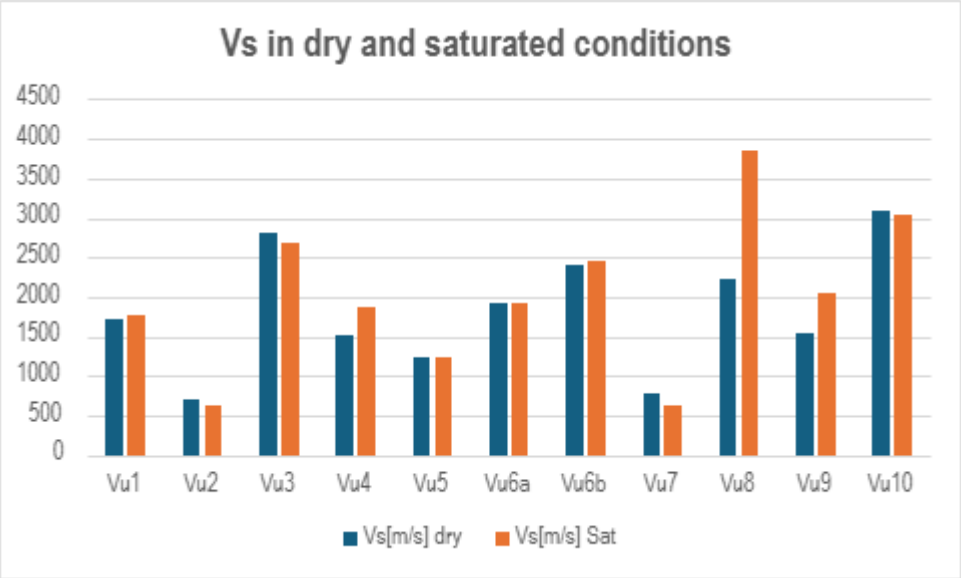

Fig5.10: Vs in dry and saturated conditions.

Like P wave velocities, S wave velocities either increased or decreased from dry to saturated conditions;
Those that decreased in saturated conditions are:
Vu2, Vu3,Vu5, Vu6a, Vu7 and Vu10.

And an increase of Vs in saturated conditions was observed for the following samples

Vu1, Vu4, Vu6b (slight increase),Vu8 (almost increased by double) and Vu9.

Thanks to the P and S waves velocities, the poisson's ratio were directly determined, followed by the shear, Young's and Bulk moduli.

ID	D[kg/m3]	Vp[m/s]	Vs[m/s]	Vp/Vs	ν	μ [Pa]	λ [pa]	E [Pa]	K [Pa]
Vu1	2164,56	3425,93	1720,93	1,99	0,33	6,41E+09	1,26E+10	1,71E+10	1,92E+09
Vu2	2272,15	1265,21	708,45	1,79	0,27	1,14E+09	1,36E+09	2,90E+09	4,42E+08
Vu3	1949,87	5357,14	2803,74	1,91	0,31	1,53E+10	2,53E+10	4,02E+10	5,06E+09
Vu4	2251,56	3606,56	1506,85	2,39	0,39	5,11E+09	1,91E+10	1,43E+10	1,00E+09
Vu5	1170,29	2314,05	1238,94	1,87	0,30	1,80E+09	2,67E+09	4,67E+09	6,25E+08
Vu6a	1665,37	4098,36	1923,08	2,13	0,36	6,16E+09	1,57E+10	1,67E+10	1,58E+09
Vu6b	2288,60	4574,47	2415,73	1,89	0,31	1,34E+10	2,12E+10	3,49E+10	4,50E+09
Vu7	2249,18	1379,31	773,69	1,78	0,27	1,35E+09	1,59E+09	3,42E+09	5,24E+08
Vu8	2456,22	3921,57	2222,22	1,76	0,26	1,21E+10	1,35E+10	3,07E+10	4,83E+09
Vu9	2623,40	2716,05	1549,30	1,75	0,26	6,30E+09	6,76E+09	1,59E+10	2,55E+09
Vu10	2806,31	6081,08	3082,19	1,97	0,33	2,67E+10	5,05E+10	7,08E+10	8,15E+09

Table 5.5: the samples density, Vp,Vs,Vp/Vs, the poisson's ratio ν , the shear modulus μ , the lamé's first parameter λ , the young's modulus E and the Bulk modulus K. given that the density was calculated on dry samples, the corresponding Vp,Vs and Vp/Vs were used for the calculations.

Among the calculated quantities, the Young's modulus is the most noticeable; with values reaching up to 7.08.10^10[Pa], followed by the shear and Bulk moduli.

The highest values of the Young's modulus are noticed respectively for the following samples: Vu10, Vu3, Vu6b and Vu8.

Similarly, the same samples (Vu10, Vu3, Vu6b and Vu8) showed the highest shear moduli.

Concerning the bulk moduli, the same samples listed above displayed the highest values, except that Vu8 sample had a higher value than Vu6b.

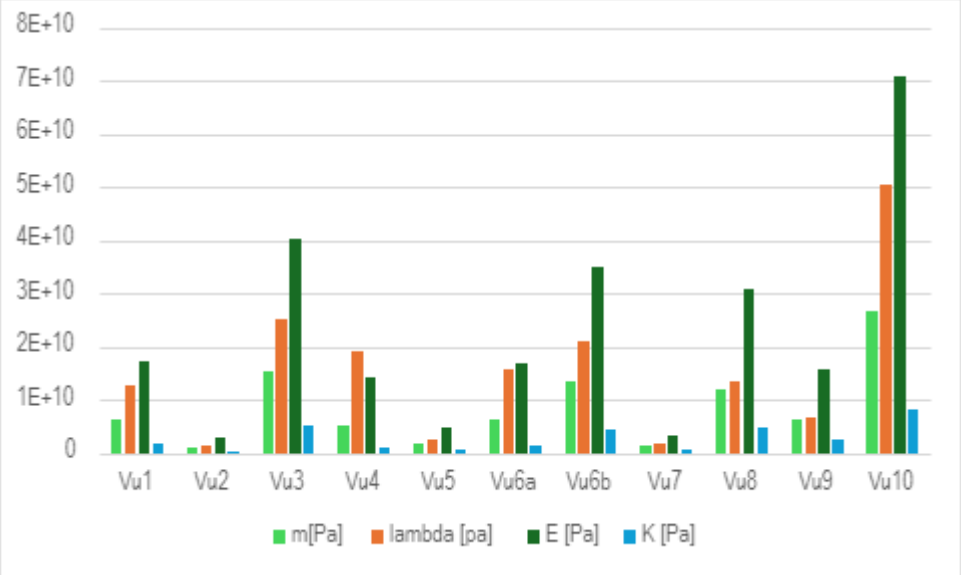

Fig5.11: Comparative graph of shear(m), Lamé's first parameter(lambda), Young's(E) and Bulk(K) moduli.

Considering the opposite trend, i.e. the lowest values,they were recorded for the samples Vu2, Vu7 and Vu5 in terms of young's and shear moduli.

Moreover, we were able to observe a similar tendancy between lamé's first parameter and the bulk moduli, although in most cases, they present differences of an order of magnitude in their quantities. However, the bulk modulus is not only dependent on lamé's first parameter but also on the shear modulus as seen in this relationship:

$K = \lambda + \frac{2}{3}\mu$.

Furthermore, a proportionality between Vp/Vs ratios and the poisson's ratio was noted.

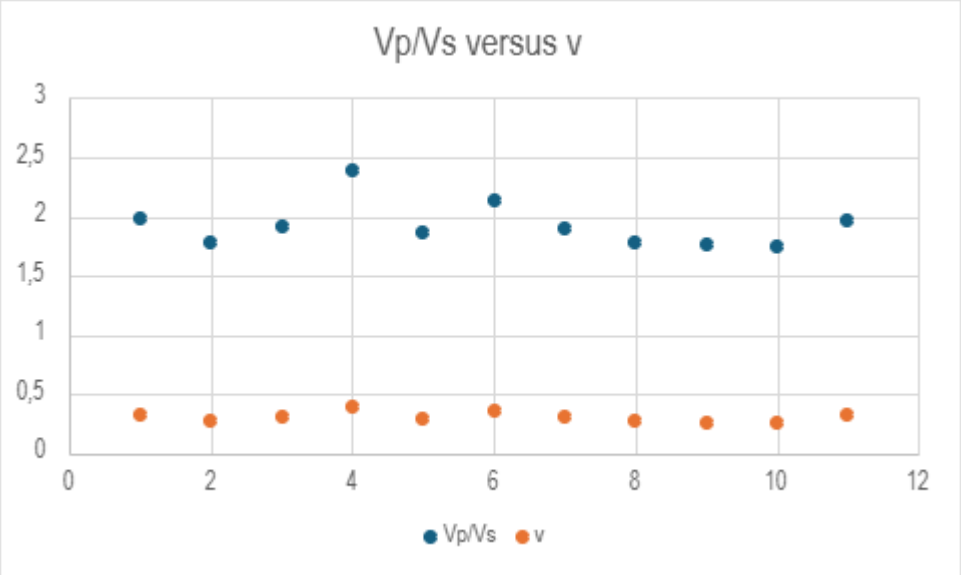

Fig5.12: Figure showing the relationship between Vp/Vs and v the poisson's ratio.

5.3.3 Electrical Resistivities:

The calculated resistivities are reported in table 5.6

Sample ID	Resistance [ohm]	Area [· $10^{-4}\ m^2$]	length [· $10^{-2}\ m$]	Resistivity[ohm.m]
Vu1	14060700	21,35	2,33	1288394,614
Vu2	15969,7	286,8	2,87	15958,57129
Vu3	562307	48,71	1,83	149671,9889
Vu4	18565300	190,7	2,77	12781237,22
Vu5	1246140	91,52	1,733	658088,4755
Vu6a	4383,94	282	2,67	4630,228764
Vu6b	8984,12	202	3	6049,307467
Vu7	39475,7	56,745	3,233	6928,699649
Vu8	41818,2	135,28	2,533	22333,85747
Vu9	696197	167,02	3,1	375092,9772
Vu10	7092,4	31,2	2,167	1021,1485

Table 5.6: Resistances, areas, lengths and resistivities in [ohm.m] of the eleven samples.

From all resistivity values, the sample Vu4 the highest, followed by Vu1 and Vu5.

Conversely, the most conductive samples are: Vu10, Vu6a, Vu6b and Vu7.

5.4 Discussions:

The main conductive conduits on both profile lines ERT3 and ERT4 are located between Baia di Levante and Vulcano Porto where there are fumarolic manifestations. These conductive conduits are undoubtedly the hydrothermal fluids rising towards the surface through fractures or faults triggered by tectonic movements along the NNE-SSW tectonic lineament that crosses the two survey lines. The magnetotelluric results reinforce this hypothesis, not only highlighting a fault that certainly serves as an ascension path for hydrothermal fluids, but also indicates conductive conduits corresponding to those encountered on the ERT sections.

In view of the results, we consider the central part of our investigation zone to be the most suitable for geothermal wells. The choice of this zone is based on 3 main criteria: the underlying formations, their physical properties, and the integrity of the drilling installations.

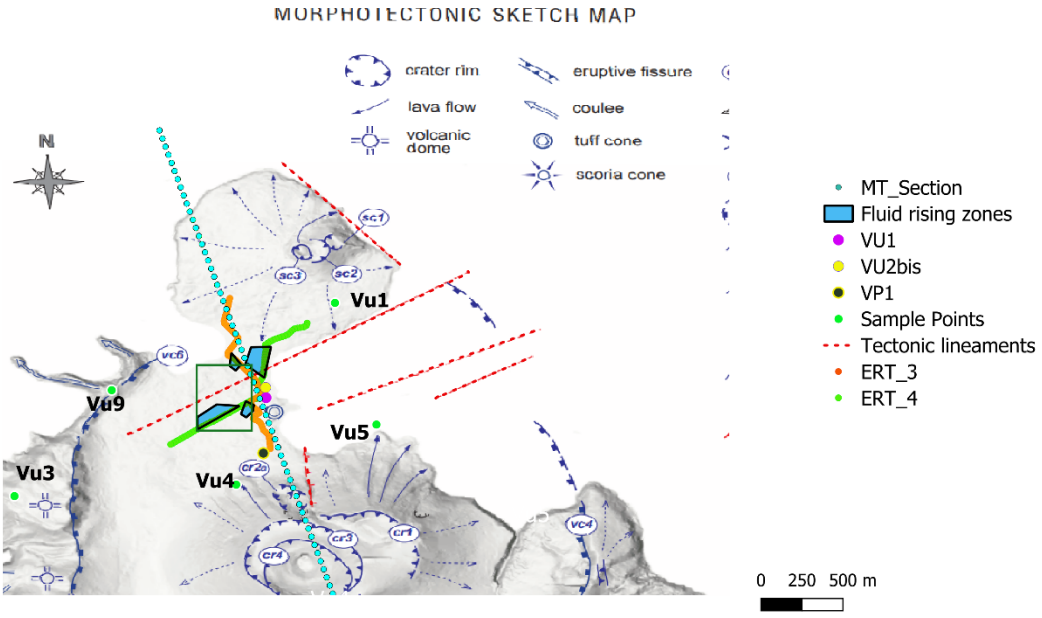

Fig5.13: Survey map with the preferential drilling zone squared in green.

The presence of resistive bodies immediately near the sea level could be interpreted as pyroclasts underlying seashore deposits. This resistivity distribution aligns with the encounter of a hard formation that was found around 10 m of depth, during the VU2 drilling operations, leading to its interruption and drilling of VU2bis.[2] The seashore deposits emerge from Porto di ponente and continue towards Porto di Levante , [25] up to twenty metres above sea level. This would explain the thin conductive layer on the top of the two sections. The southern parts

of the sections (SE on ERT3 and SW on ERT4) with higher resistivities could be explained by nearby lava flows from the crater of la Fossa: the Punte Nere formation (Pn2).

The Punte Nere formation 2 (Pn2) is part of the lower portion of the gran Cratere formation. It consists of a succession of thick to medium bedded pyroclastites (up to 100m of depth), composed of dense and oxidised lapilli whose composition ranges from latites to trachytes. It also presents eruption fallout blocks layered with planar to cross-laminated coarse to fine ash deposits. The pn2 formation starts below Porto di Ponente and gets thicker as we move towards Porto di Levante and beyond. [25]

It should be noted that the tortuosity of the acquisition profiles affects not only the acquired data quality, but also the resistivity model resulting from the inversion process, for which the algorithms are based on straight lines.

The ERT3 survey line is apparently close to the VP1 well location, whose lithology shows pyroclastic succession in the first 300m.

The stratigraphic columns from VU1, VU2bis, and IV1 also show overall pyroclastic deposits more or less in the first 300m. The asheous lapillis in VU2 bis around 100m could be related to the Pn2 formation that also extends up to a depth of 100m of depth. (see figures 2.1 and 2.2)

The fact that the fluid upwelling zones are roughly aligned, implies that the fractures that allow them to rise are on the same plane.

The ERT4 resistivity profile, shows similar features to the ERT3 profile; some resistive blocks, present at the top can be assimilated to concreate from the urbanised area and colluvial deposits. The Pn2 formation is seemingly associated to the resistive body present on this resistivity section as well.

The vapor manifestations noticed at various levels of the VU1 and VU2 bis could have contributed to the increase in resistivity right below the sea level as seen on the ERT profiles [25] [5]. This shallow high resistive distribution aligns with the one detected on the MT sections. [33]

Usually, in volcanic environment, the low resistivity anomalies are associated with hydrothermal alteration zones, i.e. clay cap. In our case, the low resistivities could not only be associated with hydrothermal alteration, but also fluid upwelling, because the structure that apparently represents the clay cap according to the 3D MT model [33], is fractured as to allow fumarolic vents right below la fossa, at Baia di Levante and Faraglione where there are also seawater and meteorologic water inputs. Furthermore, hydrothermal fluid circulation was confirmed by the petrographic studies of the wells (Barbieri,1984), whereby mineral veins were noticed below la Fossa around 300 m of depth.[5]

The magnetotelluric section shows a fault running from the top to the bottom, going eastwards. The transition in resistivity from resistive in the west to conductive in the east, attest of either one or a combination of these factors: hydrothermal fluid upwelling, hydrothermal alteration, and seawater input. This conductive zone corresponds to the fumarolic vents at Baia di Levante and Faraglione. The fault continuing beyond 2 km of depth, suggests that magmatic fluids from the Fossa magmatic chamber rise through it towards the surface, before being mixed with sea and meteorologic water.

Under saturated conditions, the thermal conductivity increased in the first place because of air in the pores being replaced by water which is more conductive than air. However, at a porosity of 50% and beyond, the rocks' bulk conductivity starts to decrease as the contact between solid particles decreases. [54]

There is no significant change in thermal conductivity values from dry to saturated state, except for the most porous samples Vu2, Vu4, Vu5 and Vu7 which are respectively pyroclastites, trachyte-latites, trachybasaltic welded scoria and hyaloclastites.

Vu2 (0-36m) and vu7(50-150m) being relatively close to the surface should have a significant porosity which is also due to the nature of their material (granulous and brittle) while Vu4 is fractured. Vu5 is porous because of its vesicular texture, typical of scoriae.

Pore fluid saturation significantly affects the Vp and Vs and consequently their ratio Vp/Vs.

In general, the results of ultrasonic velocity measurements showed an increase in Vp and the ratio Vp/Vs in saturated conditions. This is due to the increase in bulk compressibility, which makes the rock stiffer, hence P waves travel faster through the rock [55]

Conversely, saturation of rock pores leads to a decrease in the propagation velocity of S-waves within them, due to the increase in density. However, in some cases, these velocities actually increased, as in the case of samples Vu1, Vu4, Vu6b (slight increase), Vu8 (increased by double) and Vu9.This could be due to the fact that the presence of fluids can increase the effective stress of the rock matrix, leading to a more pronounced rigidity, and consequently the increase of Vs. On the other hand, fluids can act as a kind of cement that would cause a better cohesion between the rock grains, which would lead to the same result, i.e. the increase of Vs. An heterogeneous fluid distribution within the pores is also a factor to consider.[50]

As reported in fig (5.9), the P waves propagation velocities for some samples slightly declined in undrained conditions. This could be explained by the presence or predominance of gas filling the pores or by the shape of pores, notably spherical, polygonal, elongated or tube-like pores, thin cracks being less affected. Vp/Vs decreases with increasing fluid content, notably for gas-saturated cracks and for texturally equilibrated water-saturated inclusions [56]

This was true for the samples Vu8, Vu6a and Vu4, the Vp/Vs ratios of which declined once saturated with water. The decline in Vu8 would be explained by its equilibrated texture (monzodiorite) , while the decline in Vu6a (trachybasaltic welded scoria) and Vu4(trachytes-latites) would be explained by the texture but also by their gas content. (See tables 5.3 and 5.4)

The poisson's ratio is directly relatable to the Vp/Vs ratio and water content; the poisson's ratio of liquids tends to 0.5 ($Vp/Vs \rightarrow +\infty$) as porosity tends to 1 (i.e. when the material is effectively just a fluid). [57]

One should therefore expect porous materials to display high values of poisson's ratio.

Independently of mineralogical constraints, low effective pressure (quasi-lithostatic pore fluid pressure) in a highly microfractured medium can lead to anomalously high Poisson's ratio values of 0.4 and above (i.e., Vp/ Vs = 2.69). Another hypothesis for high poisson's ratios is partial melting, anisotropy and depletion in quartz.[57]

The highest poisson’s ratio, were displayed by: Vu4 (0.39), Vu6a (0.36), Vu1 (0.33), reflecting their high porosity. They are followed by Vu10 (0.32) and Vu3 (0.31) that apparently are not that much porous. These results would therefore be better explained by the hypothesis of partial melting, anisotropy and depletion in quartz.[57]

The samples Vu10, Vu3, Vu6b and Vu8 with the highest young's and shear moduli, would be the most resistant to uniaxial compression (or tension) and shearing.

Likewise, the bulk moduli of these samples (Vu10, Vu3, Vu6b and Vu8) prove their resistance, this time, to uniform compression; with the sole difference that Vu8 had a higher bulk modulus than Vu6b, attributable to the more compact aspect of Vu8.

Moreover, lame's first parameters align with the other elastic moduli, in the fact that Vu10, Vu3 and Vu6b had highest values, except for Vu4 that appeared high for lamé’s first parameter, and Vu8 that was not in the top highest values.

Concerning the lowest elastic moduli: young’s, shear, bulk and Lamé, the samples Vu2, Vu7 and Vu5 appeared every time.

However, differences remain; some samples, notably the Vu4, appear to have a low bulk modulus, and a relatively high lamé’s first parameter. This could only be due to the fractures present on this sample, which are even visible to the naked eye. The Vu6a sample also displays a relatively low bulk modulus.

With the exception of Vu4, which had both a low thermal conductivity and a debatable mechanical strength due to its fractures, samples with low thermal conductivities also had the lowest mechanical strengths (Vu2, Vu7, Vu5).

The findings indicate that rocks with a strong mechanical strength also seem to conduct heat the best. Specifically, the Vu8 and Vu10 samples, that had the highest thermal conductivity values, most likely as a result of the strong bonds within the grains which fosters heat conduction.

High resistivity values observed for Vu4, Vu1 and Vu5 could be related to their mineralogy, porosity and their pore fluid content.

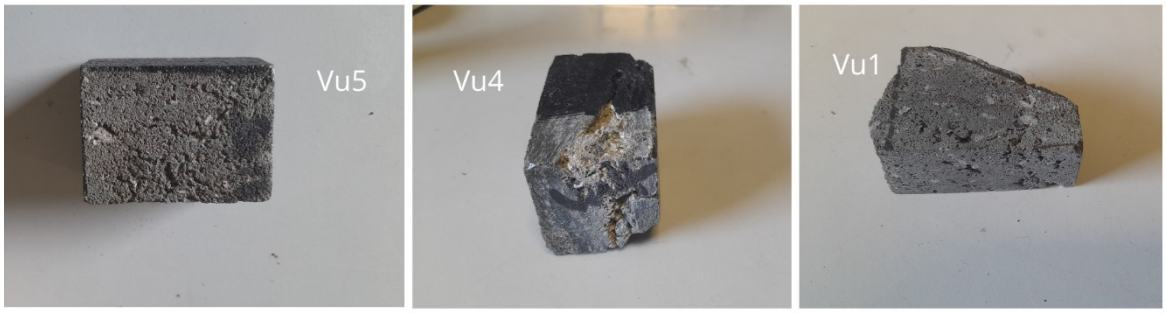

Fig5.14 : Samples Vu5, Vu4 and Vu1.

Vu4 has an intermediate composition standing between trachytes and latites; and is fractured, which contributes to its high resistivity.

The sample Vu1, is a latitic hyaloclastite, which present some irregular pore geometries, and could possibly contain some glass fragments. All these factors could have increased the resistivity.

The texture, the nature of the fluid contained in the pores of the trachybasaltic welded scoria sample (Vu5), are some elements that could have contributed to raising its electrical resistivity.

concerning the most conductive samples, can be found on the list Vu10(trachybasaltic/trachyandesitic lava flow), Vu6a(trachybasaltic welded scoria), Vu6b (trachybasaltic hydromagmatic tuff), Vu7 (hyaloclastites); this could be largely attributed to their porosity, mineralogy, fluid content,etc.

In the literature, a range of resistivities is reported for frequently studied rocks (~ 1- 10^6), such as granites, basalts, syenites, etc. It is therefore not very common to find resistivity data for specific rocks with varying compositions.[52]

In our case, the results fall within this range, although some samples exceed the 10^6.

ID	Well	Depth [m]	ν	μ [GPa]	λ [GPa]	E [GPa]	K [GPa]	Th.c [W/m°K]	ρ [ohm.m]
Vu1	VP1	115-225	0,331	6,41	12,6	17,1	1,92	1,511	1288394,6
Vu9	VP1	225-615	0,258	6,3	6,76	15,9	2,55	1,3318	375092,97
Vu5	VP1	615-655	0,299	1,8	2,67	4,67	0,625	0,4062	658088,47
Vu4	VP1	730-840	0,394	5,11	19	14,3	1	0,6032	12781237,2

Table5.7 Physical properties of the closest samples to our study area, (th.c are the thermal conductivities in drained conditions).

Based on the stratigraphy analysis of the wells, VU1, VU2bis, VP1 and IV1, the reading of the geological map and in particular the geological section, examination of sample Vu9 and of the ERT sections, we have come to the conclusion that in our area of investigation, beyond the depth of ~ 200m, lava flows exist with temperatures approaching 200°C.

Vu9 is the only lava sample fairly close to our study area whose lateral and in-depth continuity from a depth of 100m and beyond, has been supported by well stratigraphy and geophysical data. For instance, already in the first 200m of VP1, the stratigraphic column shows us the Vu9 sample, which extends to a depth of 615 m. Similarly, on the stratigraphic columns of wells VU1 and VU2bis, lavas of unspecified nature are present. The resistive bodies on the resistivity profiles also point to the presence of lavas already at shallow depths and well beyond 200m of depth.

In addition, the Vu9 has modest physical properties whose requirements should not complicate the selection of drilling and geothermal resource exploitation techniques, given that rocks with mechanical properties close to extremes (either weak or strong), are prone to create instability around the borehole, thus presenting significant environmental (blowouts) and economic (equipment failure) risks.

Lastly, the proximity for some samples (Vu1 and Vu5) to the fumarolic vents increasing phreatic eruption risks, their irregular pore geometry, the depth at which they lay (Vu5, Vu4, Vu3, beyond 600m), the insufficient data allowing to ascertain their spatial continuity, simply presented the central zone as optimal location for a geothermal wellbore.

Although the central question of locating the hydrothermal fluid ascension paths, hence suitable wellbore targets has been addressed, for an optimized geothermal resource exploitation, a more detailed investigation is necessary.

Therefore, we recommend the realization of in-situ tests: temperature logs, resistivity logs, borehole imaging, flow rate and pressure measurements, sampling and laboratory analysis of hydrothermal fluids and rocks,etc.

5.5 Proposed solution for energy production:

In order to gain access to the hydrothermal fluids whose pathways to the surface have been identified, drilling remains an imperative that also will improve our knowledge of the reservoir. Given the very high cost of drilling operations, it would be wise to adapt techniques and tools to local conditions.

Therefore, we would like to propose a broad outline of an operating scheme that we believe will ensure optimum productivity for Vulcano's reservoir, while remaining as environmentally friendly as possible.

5.5.1 Thermal power Conversion:

Electricity generation from thermal heat requires steam to run the turbines that in their turn power an electric generator. The conversion from heat to energy is done through a working fluid that undergoes a thermodynamic closed cycle called the *Carnot cycle*.

The Carnot cycle represents ideal conditions for a thermodynamic conversion between two extreme temperatures. It can be summarized in these 4 steps: compression, heating, expansion and cooling.

In practice, carrying out compression and expansion of steam-liquid fluids can cause some technical problems such as corrosion and scaling; to overcome this, compression is done in the liquid phase and expansion in the steam phase. This way of operating is referred to as Rankine cycle. For low temperature heat sources, Organic Rankine Cycle (ORC) is used.

[7] [39]

In the case of high temperature(>150°C) geothermal power plants, liquid dominant fluids are separated into a steam and liquid fractions. The steam fraction drives the turbines and is then transformed into a condensate which is injected together with the liquid fraction into the injection well. This kind of use is referred to as general use, implying the direct contact of the geothermal fluid with the turbine.

For low temperature resources, a common technique is to use a binary cycle power plant. In this case, a secondary fluid, usually an organic fluid of lower boiling point compared to water is used to generate the required steam. The operating scheme can be summarized as follows:

1. The geothermal fluid is extracted from the well and arrives in a heat exchanger where it yields its heat to a secondary working fluid,
2. The secondary working fluid vaporizes in the turbine,
3. This vapor runs the generator and produces electricity
4. The vapor condensates by cooling and is injected together with the geothermal fluid in the injection well.

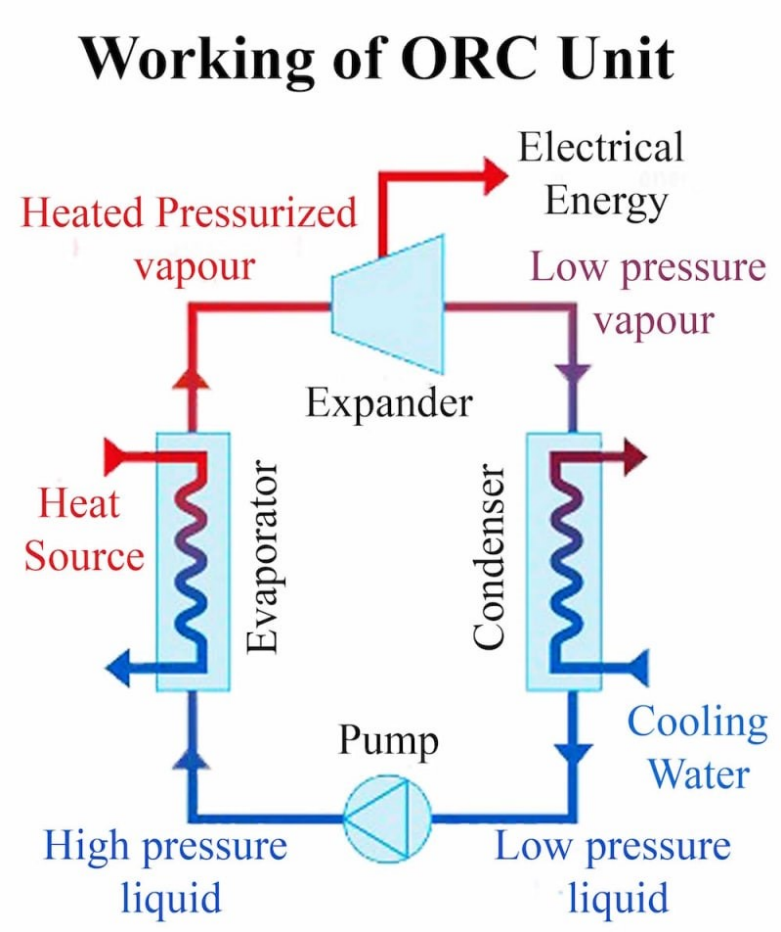

Fig5.15: Schematic representation of an organic Rankine cycle. (Organic Rankine cycle - Energy Education)

Binary systems, as well as making it possible to exploit low-enthalpy resources, also solve the problems of corrosion and scaling seen in the direct cycle, due to contact between the turbine and the hydrothermal fluids. [7]

5.5.2 Power Plant design

To access hot fluids and extract the heat, extraction wells are built in which pipes are inserted. The size, shape, casing, grout and material of the piping have to be selected carefully. The high temperatures, the chemical composition of fluids, the local geology and physical properties, the geomechanical conditions in the geothermal reservoir are some factors that must be taken into account. [58]

There are several pipe configurations, in the case of Vulcano, we suggest the following parameters reported in the table.

Piping

Configuration	Coaxial
Material	Inner: Polytetrafluoroethylene (PTFE), Outer: mainly steel
Dimensions (diameter)	25cm, 35 cm, or 45cm, depending on the budget
Working fluid	Water
Grout	cement incorporated with steel fibers
Heat exchange process	Conduction and convection

Table5.8: Some characteristics of the recommended piping system.

Polytetrafluoroethylene is an insulating material able to resist high temperatures and reduce the risk of thermal short-circuiting between the flowing fluid and the inner pipe.

Cement and incorporated steel fibers are intended to enhance the thermal conductivity between the outer pipe and the surrounding soil.

The heat exchange process involving the pipe and soil will be done by conduction, while convection will ensure heat transfer from the coaxial pipe wall to the flowing fluid.

Water is the carrier fluid that will absorb heat from hot fluids in the borehole, by flowing through the coaxial pipe. Because of its high specific heat capacity and harmlessness to the environment, water is preferable to an organic fluid that is expensive and polluting if leakage occurs.

Other aspects such as the system's efficiency, performance and maintenance, detailed installation design, they should be addressed after final decisions on the project, in line with regulations, available finances, the terrain's thermophysical parameters, have been made.

It should be noted, however, that these proposals for the heat exchange system are made on the basis of the current knowledge available to us, and must be carefully studied by professionals who will be able to improve them as knowledge of the site deepens.

Conclusions:

This work focused on the study of the geothermal system of Vulcano through the integration of Electrical Resistivity Tomography and Magnetotelluric data, supported by laboratory measurements of the thermal, electrical and elastic properties of outcropping rock samples, representing the stratigraphy of local wells.

Thanks to this approach, hydrothermal fluid ascension paths have been localized in the investigated area, corresponding to the most suitable drilling targets.

On the one hand, geophysical methods pointed out resistivity contrasts that allowed the identification of formations and structures making up the northern part of Vulcano.

On the other hand, laboratory analyses helped in determining rocks properties, especially the lava flows that were evidenced by the examination of geological and geophysical data to be the most likely to have significant spatial coverage despite having modest physical properties.

The knowledge of these mechanical properties is essential for planning the next stages of Vulcano's electrification and seawater desalination project. They can help to mitigate, or even avoid, major environmental and economic risks such as blowouts, subsidence, and equipment failure.

They will serve as a benchmark for the selection of drilling equipment compatible with the thermal conductivity and strength of the targeted formation. This will ensure the stability and longevity of the installations.

Their judicious use can also help minimize changes in the reservoir's geomechanical conditions, due to: stress redistribution, thermal expansion and thermal contraction, associated with the hot and cold cycles to which rocks in heat exchange systems are subjected.

The results align with previous studies by confirming hypotheses on the structure of Vulcano's geothermal system from Cioni and D'Amore (1980-1984), Picot and Valette (1981), and the 3D Magnetotellurics (2021).

All these theories stand in favor of a geothermal dry model in which the heat source is a volume of a degassing hot rock laying at over 2 km of depth, whose magmatic fluids escape through faults, and are subsequently mixed with seawater, discontinuous aquifers and meteorological waters.

The hypothesis of hot fluid upwelling paths between Baia di Levante and Faraglione, crossed by the tectonic lineament NNE-SSW, has been confirmed by our findings.

Furthermore, the laboratory tests depict the sensitivity of rocks thermal conductivity, electrical resistivity and elastic moduli to porosity, fluid content, pore shape and pore heterogeneity. The variation of these thermophysical parameters could also be related to pore pressure, effective stress, heterogeneous fluid saturation and the mineralogical content of rocks.

The integrated analysis of these data represents a major step forward in our knowledge of Vulcano's geothermal system in terms of structure and physical properties, important in planning drilling operations, and predicting the reservoir's response to subsequent changes in volume and pressure.

Addressing the thorny question of identifying hydrothermal fluid ascension paths toward the surface, raises the question of the analyzed samples' representativeness of terrain conditions.

In-situ conditions are subject to changes, unlike laboratory conditions; this invites to the realization of well logs along which temperature, pressure, flow rate and electrical resistivity, will be recorded. Borehole imaging for a precise identification of lithologies, their bedding, fractures, as well as fluid and rock sampling for further laboratory analyses should be considered.

In addition, we recommend mineralogical analysis of the samples to get new insights into their porosity, and in the ways in which partial melting and fractional crystallization affect the physical properties of volcanic rocks in subduction zones.

REFERENCES

[1] Aggiornamento del piano energetico ambientale della regione Siciliana (PEARS 2030)

[2] Sommaruga, C. *Le Ricerche Geotermiche Svolte a Vulcano Negli Anni 50*. *Rendiconti Della Società Italiana Di Mineralogia E Petrologia* (1984).

[3] Pietro Francesco Andaloro, A., Salomone, R., Andaloro, L., Briguglio, N. & Sparacia, S. Alternative energy scenarios for small islands: A case study from Salina Island (Aeolian Islands, Southern Italy). *Renewable Energy* **47**, 135–146 (2012).

[4] Madonia, P. *et al.* Hydrogeological and geochemical characteristics of the coastal aquifer of Stromboli Volcanic Island (Italy). *Water* **13**, 417 (2021).

[5] *Sintesi Geomineraria Finale*. *Rapporto Interno N°472, AGIP SPA-EMS-ENEL* (1987).

[6] 30 Years of Tongonan-1 (Leyte, Philippines) Sustained Production (geothermal-energy.org)

[7] *Electricity Production from Renewable Energies*. *Wiley eBooks* (2012). doi:10.1002/9781118562611.

[8] Banks, D. *An Introduction to Thermogeology: Ground Source Heating and Cooling*. (John Wiley & Sons, 2012).

[9] Clauser, C. Heat transport processes in the Earth's crust. *Surveys in Geophysics* **30**, 163–191 (2009).

[10] Suart F Simmons. Encyclopedia of Geology. in *geothermal resources* (Academic Press, 2020).

[11] Zarrouk, S. J. & McLean, K. Geothermal systems. in *Elsevier eBooks* 13–38 (2019). doi:10.1016/b978-0-12-814946-1.00002-5.

[12] Di Renzoni, N. A., Levi, N. S. T., Renzulli, N. A., Rosi, N. M. & Yoon, N. D. Should I stay or should I go? 6000 years of human presence and abandonments at Stromboli volcano and an overview on the whole Aeolian Archipelago (Southern Tyrrhenian Sea, Italy). *Annals of Geophysics* **64**, VO545 (2021).

[13] Ventura, G. Chapter 2 Kinematics of the Aeolian volcanism (Southern Tyrrhenian Sea) from geophysical and geological data. *Geological Society London Memoirs* **37**, 3–11 (2013).

[14] Bortoluzzi, G. *et al.* Multidisciplinary Investigations at Panarea (Aeolian Islands) after the Exhalative Crisis of 2002. in *Multidisciplinary Investigations at Panarea (Aeolian Islands) after the Exhalative Crisis* (2011).

[15] Soldati, M. & Marchetti, M. Volcanic landforms and landscapes of the Aeolian Islands (Southern Tyrrhenian Sea, Sicily): Implications for hazard evaluation. in *World geomorphological landscapes* (2017). doi:10.1007/978-3-319-26194-2.

[16] FavalliM, M., Karátson, D., Mazzuoli, R., Pareschi, M. T. & Ventura, G. Volcanic geomorphology and tectonics of the Aeolian archipelago (Southern Italy) based on integrated DEM data. *Bulletin of Volcanology* **68**, 157–170 (2005).

[17] Ventura, G., Vilardo, G., Milano, G. & Pino, N. A. Relationships among crustal structure, volcanism and strike–slip tectonics in the Lipari–Vulcano Volcanic Complex (Aeolian Islands, Southern Tyrrhenian Sea, Italy). *Physics of the Earth and Planetary Interiors* **116**, 31–52 (1999).

[18] Monaco, C., Tortorici, L., Nicolich, R., Cernobori, L. & Costa, M. From collisional to rifted basins: an example from the southern Calabrian arc (Italy). *Tectonophysics* **266**, 233–249 (1996).

[19] Peccerillo, A., De Astis, G., Faraone, D., Forni, F. & Frezzotti, M. L. Chapter 15 Compositional variations of magmas in the Aeolian arc: implications for petrogenesis and geodynamics. *Geological Society London Memoirs* **37**, 491–510 (2013).

[20] Romagnoli, C. *et al.* Chapter 4 Bathy-morphological setting of the Aeolian Islands. *Geological Society London Memoirs* **37**, 27–36 (2013).

[21] Forni, F. *et al.* Chapter 10 Stratigraphy and geological evolution of the Lipari volcanic complex (central Aeolian archipelago). *Geological Society London Memoirs* **37**, 213–279 (2013).

[22] Billi, A. *et al.* Tectonics and seismicity of the Tindari Fault System, southern Italy: Crustal deformations at the transition between ongoing contractional and extensional domains located above the edge of a subducting slab. *Tectonics* **25**, (2006).

[23] Rossi, S. *et al.* Role of magma mixing in the pre-eruptive dynamics of the Aeolian Islands volcanoes (Southern Tyrrhenian Sea, Italy). *Lithos* **324–325**, 165–179 (2019).

[24] Lucchi, F., Keller, J., De Astis, G., Francalanci, L. & Tranne, C. A. Geological map of Stromboli, scale 1:10 000 (Aeolian archipelago). *Aeolian Archipelago* (2013).

[25] De Astis, G., Dellino, P., La Volpe, L., Lucchi, F. & Tranne, C. A. Geological map of the island of Vulcano, scale 1:10 000(Aeolian archipelago). *Aeolian Archipelago* (2013).

[26] Lucchi, F., Tranne, C. A., Forni, F. & Rossi, P. L. *Geological Map of the Island of Lipari (Aeolian Archipelago)*. *INGV* (2013).

[27] Lucchi, F. *et al. Geological Map of the Island of Salina (Aeolian Archipelago)*. *INGV,Università Degli Studi Di Bologna, Keele University* (2013).

[28] Lucchi, F., Tranne, C. A. & Rossi, P. L. *Geological Map of the Island of Filicudi (Aeolian Archipelago)*. *Università Di Bologna* (2013).

[29] Lucchi, F., Tranne, C. A., Keller, J. & Rossi, P. L. *Geological Map of the Island of Panarea, Aeolian Archipelago*. *Università Di Bologna* (2013).

[30] Lucchi, F., Tranne, C. A., Pecerillo, A. & Rossi, P. L. *Geological Map of the Island of Alicudi, Aeolian Archipelago*. *Università Di Bologna,Università Di Perugia* (2013).

[31] Italiano, F., Valenza, M. & Nuccio, P. M. Geothermal energy and mass release at Vulcano,Aeolian Islands,Italy. *Researchgate* (1987).

[32] Todesco, M. Modeling of the Geothermal Activity at Vulcano (Aeolian Islands,Italy). *Dipartimento Di Scienze Della Terra ,Universita' Degli Studi Di Pisa*.

[33] Di Giuseppe, M. G., Isaia, R. & Troiano, A. Three-dimensional magnetotelluric modeling of Vulcano Island (Eolie, Italy) and its implications for understanding recent volcanic unrest. *Scientific Reports* **13**, (2023).

[34] Bruno, P. P. G., Paoletti, V., Grimaldi, M. & Rapolla, A. Geophysical exploration for geothermal low enthalpy resources in Lipari Island, Italy. *Journal of Volcanology and Geothermal Research* **98**, 173–188 (2000).

[35] De Ritis, R., Ventura, G. & Chiappini, M. Aeromagnetic anomalies reveal hidden tectonic and volcanic structures in the central sector of the Aeolian Islands, southern Tyrrhenian Sea, Italy. *Journal of Geophysical Research Atmospheres* **112**, (2007).

[36] Esposito, A. *et al.* Modeling ground deformations of Panarea volcano hydrothermal/geothermal system (Aeolian Islands, Italy) from GPS data. *Bulletin of Volcanology* **72**, 609–621 (2010).

[37] Revil, A., Finizola, A., Sortino, F. & Ripepe, M. Geophysical investigations at Stromboli volcano, Italy: implications for ground water flow and paroxysmal activity. *Geophysical Journal International* **157**, 426–440 (2004).

[38] Patanè, D. *et al.* The shallow magma chamber of Stromboli Volcano (Italy). *Geophysical Research Letters* **44**, 6589–6596 (2017).

[39] Huenges, E. & Ledru, P. *Geothermal Energy Systems: Exploration, Development, and Utilization*. (John Wiley & Sons, 2011).

[40] *Best Practices Guide for Geothermal Exploration*. (2014).

[41] Simpson, F. & Bahr, K. *Practical Magnetotellurics*. (2005). doi:10.1017/cbo9780511614095.

[42] Telford, W. M., Geldart, L. P. & Sheriff, R. E. *Applied Geophysics*. (Cambridge University Press, 1990).

[43] Reynolds, J. M. *An Introduction to Applied and Environmental Geophysics*. (John Wiley & Sons, 2011).

[44] Fabriol, H. & Debeglia, N. *Méthodes Géophysiques Appliquées à l'exploration Géothermique En Contexte Insulaire Volcanique Synthèse Bibliographique*. *BRGM/RP-53137-FR* (2004).

[45] Casagrande, M. F. S., Furlan, L. M., Moreira, C. A., Rosa, F. T. G. & Rosolen, V. Non-invasive methods in the identification of hydrological ecosystem services of a tropical isolated wetland (Brazilian study case). *Environmental Challenges* **5**, 100233 (2021).

[46] Balasco, M., Lapenna, V., Rizzo, E. & Telesca, L. Deep Electrical Resistivity Tomography for geophysical Investigations: the state of the art and future directions. *Geosciences* **12**, 438 (2022).

[47] Cassiani,G.,Course material of geophysics for cultural heritage and civil engineering, academic year (2021-2022), Department of Geosciences,University of Padua.

[48] Marco A.Pérez,. Dipole-Dipole resistivity imaging of the Ahuachapan-Chipilapa Geothermal Field,El Salvador. *Elsevier Science* **vol 26, No. 576,pp,657-680**, (1997).

[49] Blanchy, G., Saneiyan, S., Boyd, J., McLachlan, P. & Binley, A. ResIPy, an intuitive open source software for complex geoelectrical inversion/modeling. *Computers & Geosciences* **137**, 104423 (2020).

[50] Guéguen, Y. & Palciauskas, V. *Introduction to the Physics of Rocks*. (Princeton University Press, 1994).

[51] Greaves, G. N., Greer, A. L., Lakes, R. S. & Rouxel, T. Poisson's ratio and modern materials. *Nature Materials* **10**, 823–837 (2011).

[52] Di Sipio, E.,Course material of petrophysics, academic year 2022-2023), Department of Geosciences,University of Padua.

[53] Ji, S., Sun, S., Wang, Q. & Marcotte, D. Lamé parameters of common rocks in the Earth's crust and upper mantle. *Journal of Geophysical Research Atmospheres* **115**, (2010).

[54] Cermak, V.and Rybach.,1982. Thermal properties: Thermal conductivity and specific heat of minerals and rocks. In: G.Angeneister(Ed.),Landolt-B"rnstein Zahlenwerte and Funktionen aus Naturwissenschaften und Technik, Neue Serie, Physikalische Eigenschaften der Gesteine. Springer Verlag,Berlin,Heidelberg and New York,V/1a,305-343.

[55] Rojas, E., Davis, T. L., Batzle, M., Prasad, M. & Michelena, R. J. V p - V s ratio sensitivity to pressure, fluid, and lithology changes in tight gas sandstones. (2005) doi:10.1190/1.2147950.

[56] Brantut, N. & David, E. C. Influence of fluids on VP/VS ratio: increase or decrease? *Geophysical Journal International* **216**, 2037–2043 (2018).

[57] Pimienta, L. *et al.* Anomalous VP/VS ratios at seismic frequencies might evidence highly damaged rocks in subduction zones. *Geophysical Research Letters* **45**, (2018).

[58] Galgaro,A.,Course material of Geothermics ,academic year (2022-2023), Department of geosciences, University of Padua.